IN-SITU REGENERATION OF GRANULAR ACTIVATED CARBON (GAC) USING FENTON'S REAGENTS

by

Carla Linette De Las Casas

A Dissertation Submitted to the Faculty of the

DEPARTMENT OF CHEMICAL AND ENVIRONMENTAL ENGINEERING

In Partial Fulfillment of the Requirements
For the Degree of

DOCTOR OF PHILOSOPHY
WITH A MAJOR IN ENVIRONMENTAL ENGINEERING

In the Graduate College

THE UNIVERSITY OF ARIZONA

2006

THE UNIVERSITY OF ARIZONA
GRADUATE COLLEGE

As members of the Dissertation Committee, we certity that we have read the dissertation

prepared by Carla Linette De Las Casas

entitled In-situ Regeneration of Granular Activated Carbon (GAC) Using Fenton's Reagents

and recommend that it be accepted as fulfilling the dissertation requirement for the

Degree of Doctor of Philosophy

_____Date: 11/15/16
Wendell P. Ela

_____Date: 11/15/06
A. Eduardo Sáez

_____Date: 11/15/06
Robert G. Arnold

Final approval and acceptance of this dissertation is contingent upon the candidate's submission of the final copies of the dissertation to the Graduate College.

I hereby certify that I have read this dissertation prepared under my direction and recommend that it be accepted as fulfilling the dissertation requirement.

_____Date: 11/15/06
Dissertation Director: Wendell P. Ela

STATEMENT BY AUTHOR

This dissertation has been submitted in partial fulfillment of requirements for an advanced degree at the University of Arizona and is deposited in the University Library to be made available to borrowers under rules of the Library.

Brief quotations from this dissertation are allowable without special permission, provided that accurate acknowledgment of source is made. Requests for permission for extended quotation from or reproduction of this manuscript in whole or in part may be granted by the head of the major department or the Dean of the Graduate College when in his or her judgment the proposed use of the material is in the interests of scholarship. In all other instances, however, permission must be obtained from the author.

SIGNED: Carla Linette De Las Casas

ACKNOWLEDGMENTS

First of all, I would like to thank God for blessing me in so many ways and for giving me the strength and health to overcome every challenge in my life.

I owe a great debt to my advisors Drs. Wendell Ela, Robert Arnold, and Eduardo Sáez, whose questions, suggestions, encouragement, and friendship helped me make an ambitious project manageable. I admire them as professors and individuals. They have gone beyond their duty to help me in my academic and personal life. I appreciate deeply Dr. Ela's motivational support, impelling me to keep working through rough times.

Thanks to my colleagues in the Fenton research project, who collaborated with me and contributed to the success of the overall project. They are Lisa Bercik, Kurt Bishop, Dongxu Yan, Mike Johnson, and Matthew Potzler. I would like to acknowledge the use of Yan's experimental data in the modeling efforts. A warm thank you goes to my friend, Lisa, who shared the challenges of getting this research started. I also appreciate the support of Scott Huling at EPA for all his contributions, suggestions, and comments.

Most of all, I would like to thank my family, friends and staff. I am grateful to my family in Panama for their love and support. Thanks to my brothers José, who suggested me to explore the environmental field, and Juan for their solidarity. My friends and staff members have blessed me with their kindness. They include Claudia, Erik, Katia, Donna, Danielle, Sahar, Lauren, Cary, Otak, Erica, Jeremy, Jenny, Sandy, Norma, Ozer, Heng, Xiumin, Jilei, Hao, Dhananjay, Junior, Amlan, Sri, Loraine, Jacky, Nadi, Maylin, Ron, Brian, Rose, Arla, Jo, Judee, Genine, and Eric. I am especially grateful to Umur Yenal whose support, inspiration, friendship, and love made gradschool a wonderful experience.

DEDICATION

To my parents, Zoila and Víctor, who taught me the value of good ethics, honesty, responsibility and hard work. They have always encouraged me to achieve my goals and pursue my dreams.

TABLE OF CONTENTS

TABLE OF CONTENTS - *Continued*

TABLE OF CONTENTS - *Continued*

TABLE OF CONTENTS - *Continued*

TABLE OF CONTENTS - *Continued*

LIST OF FIGURES

LIST OF FIGURES - *Continued*

LIST OF FIGURES - *Continued*

LIST OF FIGURES - *Continued*

LIST OF TABLES

LIST OF TABLES-*Continued*

ABSTRACT

Fenton-dependent recovery of carbon initially saturated with one of several chlorinated aliphatic contaminants was studied in batch and continuous-flow reactors. A specialty carbon, URV-MOD 1 (Calgon) was employed to minimize non-productive H_2O_2 demand – that which does not yield hydroxyl or superoxide radicals.

Enhancement of PCE degradation kinetics by ferric iron addition is limited by iron solubility, even at relatively low pH. Quinone addition increased the pseudo-first-order rate constant for PCE loss temporarily. Only copper addition sustainably enhanced the specific rate of PCE loss. For copper-to-iron molar ratios of 0.25 to 5, the pseudo-first-order rate constant for PCE transformation was increased by a factor of 3.5. It is apparent that the effect of copper addition on Fenton-dependent reaction rates is complex, and involves a shift in chemical mechanism, as indicated by the differing slopes in the Arrhenius plot (with and without copper).

A mathematical model was developed to evaluate the effect of operational parameters ($[Fe(III)]_{T:}[H_2O_2]_o$ ratio and pH) on degradation kinetics and optimize the PCE degradation process in homogeneous reaction mixtures. The model simulated experimental degradation of the organic target in a homogeneous Fenton-reaction system. The model requires further refinement to simulate Fenton's systems in which ions in solution (such as sulfate and chloride) play significant roles.

In continuous-flow reactors, Fenton's reagents were cycled through spent GAC in columns to degrade one of seven chlorinated compounds tested. The contaminant with the weakest adsorption characteristics, methylene chloride, was 99% lost from the carbon

surface during a 14-hour regeneration period. At the field site, the GAC was saturated with gases containing TCE and PCE from a soil vapor extraction (SVE) system. In the field, up to 95% of the sorbed TCE was removed from GAC during regeneration periods of 50-60 hours. Recovery of PCE-loaded GAC was significantly slower. Column experiments show that there is minimal loss of carbon adsorption capacity during Fenton treatment and that the rate of GAC regeneration is compound specific. Scoping-level cost estimates indicated that field use of Fenton regeneration is not cost effective without optimization and/or iron surface amendments, except in the case of the most soluble VOCs.

1. BACKGROUND

Ten of the 25 most frequently detected hazardous contaminants at National Priority List (Superfund) sites are chlorinated volatile organic compounds (CVOCs) (NRC, 1994). CVOCs are commonly recovered from contaminated groundwater or soils using pump-and-treat, air stripping, and soil vapor extraction (SVE) methods. After the contaminated fluid is extracted from the subsurface, granular activated carbon (GAC) adsorption is often used to separate VOCs from liquid and gas streams derived from these recovery techniques. When the carbon is loaded to capacity, it must be regenerated or replaced. Advanced oxidation processes (AOPs) also can be employed for the remediation of fluid stream derived from extraction processes (Kommineni et al., 2003; Prousek, 1995; and Zoh, 2002). AOPs can destroy VOC contaminants, leaving only mineralized products, but AOPs are relatively expensive for treatment of low-concentration pollutants.

In this project, we explore the feasibility of using Fenton's reaction for regeneration of spent GAC that has been used to collect and concentrate VOCs. Fenton's reaction is an AOP process in which reaction of hydrogen peroxide (H_2O_2) with iron (Fe), generates two radical species (•OH, and HO_2•/O_2•$^-$). A very broad range of organics, including a variety of prominent contaminants, are oxidized by hydroxyl radicals, which are among the strongest and least specific oxidants known (Table 1-1; Gallard and De Laat, 2000; Huling et al., 2000; Duesterberg et al., 2005; Chen et al., 2001). Fenton-dependent processes can mineralize even heavily halogenated targets such as PCE and TCE (Teel et

al., 2001). Rate limitations, potential rate acceleration strategies and process feasibility of Fenton-dependent regeneration of CVOC-loaded GAC were investigated in a series of bench-scale experiments. Field-scale process feasibility was also examined at an Arizona State Superfund site, where GAC is being used to separate chlorinated VOCs and volatile hydrocarbons from a SVE gas stream. Carbon recoveries at bench and field scales were compared and evaluated.

Table 1-1. Hydroxyl radical (•OH) reactivity with organic compounds

Target Compound	$k_{\bullet OH,R}$ (M^{-1} s^{-1})[a]
Trichloroethylene	2.90E+09
	(3.3-4.3) E+09[b]
Tetrachloroethylene	2.00E+09
1,1-Dichloroethane	7.90E+08
1,1,1-Trichloroethane	1.00E+08
1,1,2-Trichloroethane	3.00E+08[c]
Chloroform	5.00E+07[c]
Methylene Choride	9.00E+07[c]
Carbon Tetrachloride	<1e6[c]
	1.90E+09[d]
1,4-Benzoquinone	1.2 E+09
Isopropanol	1.90E+09[d]
Atrazine	(1.2-3) E+09[e]
Formic Acid	6.50E+08[f]
H_2O_2	3.3 E+07[g]

NOTE: $k_{\bullet OH,R}$ is the second-order rate constant for the reaction of hydroxyl radical with the target organic compound.
SOURCE: [a]Radiation Chemistry Data Center of the Notre Dame Radiation Laboratory, URL http://www.rcdc.nd.edu/ (Aug 2005) except [b]Trichloroethylene (Chen et al, 2001); [c]1,1,2-Trichloroethane, Chloroform, Methylene Chloride and CT (Haag and Yao, 1992); [d]CT and Isopropanol (Buxton et al., 1988); [e]Atrazine (Gallard and De Laat, 2000); [f]Formic Acid (Duesterberg, et al., 2005); [g]Hydrogen peroxide (De Laat and Gallard, 1999).

The field site selected was the Park-Euclid (Tucson, Arizona) State Superfund site, where the primary vadose zone contaminants are PCE, TCE, dichloroethene isomers, and volatile components of diesel fuel. A SVE system with GAC treatment of the off-gas was installed at the site as an interim remediation scheme while the state Remedial

Investigation at the Park-Euclid site was underway. There are four distinct zones of contamination -- the upper vadose zone, perched aquifer, lower vadose zone, and regional aquifer (Figure 1-1). Both the upper and lower vadose zones contain dry-cleaning-related contaminants (i.e. PCE, TCE, DCE isomers). The Park-Euclid SVE system draws gases from the upper vadose zone. Chlorinated solvents (primarily PCE) are present in both free product (diesel fuel atop the perched aquifer (Figure 1-1)) and perched groundwater. The regional aquifer begins at about 200 ft below land surface. Diesel fuel has not contaminated the regional aquifer. However, a PCE plume with concentrations from 1-100 ppb extends more than 1,300 feet north-northeast from the origin of contamination, a well serving a former on-site dry cleaner (Miller Brooks, 2004). TCE and degradation by-products such as *cis*-1,2-dichloroethene are also present in the plume. Although there are no production wells in the immediate vicinity, the regional aquifer is relied upon to provide potable water within the Tucson basin. Maximum aqueous-phase contaminant concentrations in the regional aquifer are on the order of 10 and 100 ppb for TCE and PCE, respectively (Miller Brooks, 2004).

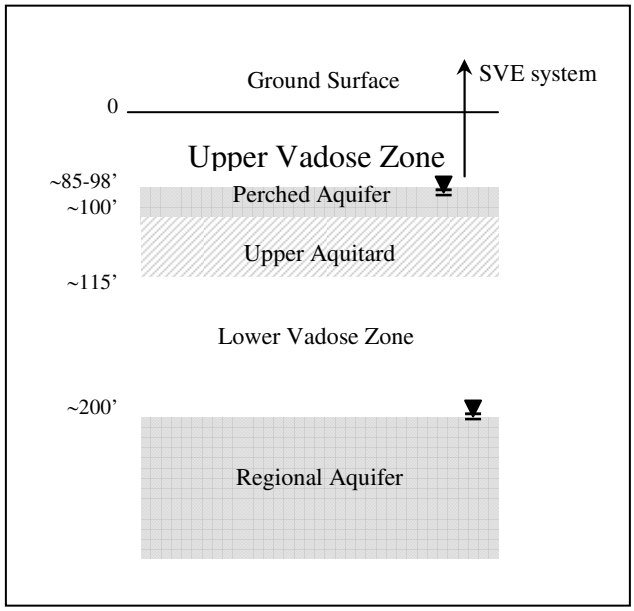

Figure 1-1. Cross-section of the Park-Euclid Arizona state Superfund site. PCE and TCE contamination is observed in the regional and perched aquifers and in both the lower and upper vadose zones. SVE gases are extracted from the upper vadose zone.

1.1 Fenton's Mechanism

In Fenton's mechanism, iron cycles between the Fe(II) and Fe(III) oxidation states due to reaction with H_2O_2. The oxidation of Fe(II) produces a highly aggressive hydroxyl radical $(\cdot OH)$ that is relied upon to attack organic environmental contaminants (Huling et al., 2000; Teel et al., 2000). Reduction of Fe(III) to Fe(II) limits the overall rate of radical production under most circumstances (Chen and Pignatello, 1997; De Laat and Gallard, 1999; Teruya, 2000). Thus, iron speciation is a strong determinant of Fenton's kinetics (Gallard et al., 1999; De Laat and Gallard, 1999). The distribution of Fe(III) among free ferric ion and hydroxylated forms (predominantly Fe^{3+}, $FeOH^{2+}$, $Fe(OH)_2^{+}$, $Fe_2(OH)_2^{4+}$) depends primarily on solution pH. Furthermore, the insolubility of $Fe(OH)_3$ (s) (pK_{so} for $Fe(OH)_3$ (s, amorph) = 38.7; Stumm and Morgan, 1981) is

expected to limit total iron solubility at all but very low pH values. At pH ≤ 2, the free ferric ion is the predominant Fe(III) species. Changes in iron speciation in the low pH range, however, can account for the dependence of Fenton reaction kinetics on pH. Fe(III)-hydroperoxyl complexation reactions are fast, and equilibrium conditions are generally satisfied on the time scale of Fenton applications. Complexation with peroxide ion precedes Fe(III) reductions.

The following mechanism for organic contaminant destruction is simplified from a more detailed Fenton's scheme proposed by De Laat and Gallard (1999)—see Chapter 4.0:

Initiation reactions:

$$Fe(III) + H_2O_2 \rightarrow Fe(II) + HO_2\bullet + H^+ \quad [1.1\text{-}1]$$

$$Fe(II) + H_2O_2 \rightarrow Fe(III) + \bullet OH + OH^- \quad [1.1\text{-}2]$$

$$\bullet OH + R \rightarrow OH^- + \bullet R \quad [1.1\text{-}3]$$

Chain propagation:

$$HO_2\bullet + Fe(III) \rightarrow Fe(II) + O_2 + H^+ \quad [1.1\text{-}4a]$$

$$\bullet R + Fe(III) \rightarrow R^+ + Fe(II) \quad [1.1\text{-}4b]$$

(where Fe (II) reacts again with H_2O_2 to yield another hydroxyl radical)

The organic cation is consumed through a highly exothermic reaction as follows:

$$R^+ + H_2O \rightarrow ROH + H^+ \quad [1.1\text{-}5]$$

The dominant chain termination steps are:

$$\bullet R + \bullet R \rightarrow R\text{-}R \quad [1.1\text{-}6]$$

$$\bullet R + Fe(II) \rightarrow Fe(III) + R^- \quad [1.1\text{-}7]$$

$$\bullet OH + O_2\bullet^- \rightarrow O_2 + OH^- \quad [1.1\text{-}8]$$

$$\bullet OH + HO_2\bullet \rightarrow O_2 + H_2O \quad [1.1\text{-}9]$$

The overall rate is limited normally by the rate of reduction of Fe(III) to Fe(II) by H_2O_2 (reaction 1.1-1). The hydroxyl radical produced from reaction 1.1-2 can oxidize the target organic compound (R), producing an organic radical (•R). These organic radicals can reduce Fe(III) to Fe(II), propagating the chain reaction. The chain reaction is terminated by radical dimerization, as in reaction 1.1-6, by reaction of the organic radical with Fe(II) or radical-radical reactions (1.1.8 and 1.1.9). The same radical terminating reactions have been used to explain various inhibition effects (Walling and Kato, 1971).

In homogeneous batch systems, contaminant reaction kinetics follow the second-order rate equation,

$$\frac{d[R]}{dt} = -k_{\bullet OH,R}[R][\bullet OH] \quad [1.1\text{-}10]$$

where $k_{\bullet OH,R}$ is the compound-specific reaction rate constant for reaction of the target compound with •OH. It is assumed that upon initiation of the Fenton's reaction, the concentration of •OH rises quickly and stabilizes at a near-steady concentration within a very short period of time (seconds or less). A steady-state approximation for •OH concentration is frequently assumed for kinetic analyses so that short-term pseudo-first-order decay kinetics are often the basis of kinetic analyses of contaminant destruction:

$$\frac{d[R]}{dt} = -k'[R] \quad [1.1\text{-}11]$$

where *k'* is defined as

$$k' = k_{\bullet OH,R}[\bullet OH]_{ss} \qquad [1.1\text{-}12]$$

Pseudo-first-order kinetics are only expected, however, if the hydroxyl radical concentration is essentially constant. Furthermore, it is expected that $[\bullet OH]_{ss}$ will depend on total iron, H_2O_2 concentration, pH, and temperature. At a constant total iron concentration, the near-steady •OH concentration may be fairly insensitive to H_2O_2 concentration (Huling et al., 2000). If H_2O_2 concentration is low, for example, the Fenton's mechanism slowes, which limits the rate of production of radicals. However, the overall rate of •OH scavenging may also be relatively low. If, on the other hand, excess H_2O_2 is present, it acts as both a source of radicals and a scavenger for •OH.

$$\bullet OH + H_2O_2 \rightarrow HO_2\bullet + H_2O \qquad [1.1\text{-}13]$$

Therefore, small fluctuations in H_2O_2 have little effect on the observed pseudo-first-order rate constant for contaminant destruction via oxidation with •OH in homogeneous Fenton systems.

1.2 Copper as a Fenton Metal

There is considerable debate regarding the status of copper as a Fenton metal. Although copper cycles between the Cu(I) and Cu(II) oxidation states via reaction with H_2O_2, hydroxyl radicals are not generally produced (Masarwa et al., 1988). Nevertheless, the reaction of the cuprous ion and hydrogen peroxide (reaction 1.2-1) results in the formation of a copper complex, $(H_2O)_m Cu^{+}\bullet O_2H^{-}$ that may react with organics present in solution. In acidic solution and in the absence of organics, the copper complex

decomposes into free cupric ion and hydroxyl radicals (reaction 1.2-2) (Masarwa et al., 1988).

$$Cu^{+} + H_2O_2 \rightarrow Cu^{+}\bullet O_2H^{-} + H^{+} \quad [1.2\text{-}1]$$

$$(H_2O)Cu^{+}\bullet O_2H^{-} \rightarrow Cu^{2+} + \bullet OH + 2OH^{-} \quad [1.2\text{-}2]$$

Cupric copper can also react with organic radicals (reaction 1.2-3). The Cu(I) product of reaction 1.2-3 can either react with Fe(III) to regenerate Fe(II) or with H_2O_2 to produce cuprous ions (Walling and Kato, 1971). Since an array of unidentified organic radicals may be produced during Fenton-driven decomposition of target contaminants (particularly in the presence of non-target organics), this pathway may be of practical importance in environmental applications. The reaction of Cu(II) with R• is comparable to Fe(III) reduction (reaction 1.1-4). The reduction of Fe(III) by Cu(I) (reaction 1.2-4) and subsequent reaction of Fe(II) with H_2O_2 would increase the overall rate of •OH generation (Walling and Kato, 1971).

$$R\bullet + Cu(II) \rightarrow Cu\ (I) + \text{products} \quad [1.2\text{-}3]$$

$$Cu(I) + Fe(III) \leftrightarrow Fe(II) + Cu(II) \quad [1.2\text{-}4]$$

Walling and Kato (1971) indicated that iron undergoes electron-transfer during reaction with R•, whereas the copper reaction can involve either complexation (reaction 1.2-5) or reduction via formation of an organo-copper intermediate (reactions 1.2-5 and 1.2-6).

$$R\bullet + Cu^{2+}(H_2O)_n \rightarrow RCu^{2+}(H_2O)_n \quad [1.2\text{-}5]$$

$$RCu^{2+}(H_2O)_n \rightarrow ROH + Cu^{+}(H_2O)_{n-1} + H^{+} \quad [1.2\text{-}6]$$

Furthermore, they found evidence that organic radicals with strong electron withdrawing groups (e.g. Cl^-) are preferentially reduced by ferrous iron. Trichloroethene radical, for example, would satisfy requirements for such a reaction.

Cu(II) is a weaker oxidizing agent than Fe(III), and therefore less capable of oxidizing R• (as in reaction 1.1-4) by outer-sphere electron transfer. Instead, the reaction involves formation of an organo-copper intermediate (Walling, 1975). Comparison of oxidation rates attributable to Cu(II) and Fe(III) indicated that Cu(II) oxidations were slower, but that ligand-Cu(II) exchanges were fast (Walling, 1975).

Cu(II) and Cu(s) are thermodynamically favored over Cu(I) as shown by the following reactions (Holleman and Wiberg, 2001; Cotton et al., 1999):

$$Cu^+ + e^- \leftrightarrow Cu\ (s) \qquad E^o = 0.52\ V \qquad [1.2\text{-}7]$$

$$Cu^+ \leftrightarrow Cu^{2+} + e^- \qquad E_H{}^o = -0.16\ V \qquad [1.2\text{-}8]$$

$$2Cu^+ \leftrightarrow Cu\ (s) + Cu^{2+} \qquad \Delta E^o = 0.36\ V \qquad [1.2\text{-}9]$$

At equilibrium, only low concentrations of Cu(I) ($<10^{-2}$ M) can exist in aqueous solutions (Cotton et al., 1999). Stability differences arise in part because the energy of hydration of Cu^{2+} is much higher than that of Cu^+ (2100 vs. 582 kJ/mol), all of which helps to explain why Cu(I) does not normally exist in aqueous solution, but rather disproportionates to Cu and Cu(II) (Heslop and Robinson, 1967):

$$K = \frac{\left[Cu^{2+}\right]}{\left[Cu^{+}\right]^2} \approx 10^6 \qquad [1.2\text{-}10]$$

However, Cu^{2+} is favored with anions unable to make covalent bonds or bridging groups (e.g. SO_4^{2-}) (Cotton et al., 1999). Copper participates in outer sphere electron transfers as opposed to inner sphere electron transfers in which the transfer of electrons occurs through a chemical bridge. The ligand covalently links the two metal redox centers and typically has more than one lone electron pair, serving as an electron donor to both the reductant and the oxidant (www.wikipedia.com). The coordination chemistry of the Cu^{2+} ion is dominated by nitrogen- and oxygen-donating ligands followed by chloride and sulfur-containing groups (King, 2006).

1.3 Fenton-driven GAC regeneration

1.3.1 Contaminant Removal and Destruction Mechanisms

Removal of adsorbates from GAC particles may be kinetically limited by any of four distinct steps (Figure 1.3.1-1): desorption from the GAC surface, "1"; pore and surface diffusion, "2"; film transport outside the particle, "3", in which the film thickness (δ) is inversely related to the local bulk velocity; and removal of reactant from bulk aqueous phase, "4", due to reaction and advective transport. In most cases, intraparticle effects (pore diffusion-"2" and/or desorption-"1") control the observed rate of transfer from the particle to the bulk aqueous phase (Crittenden, 1987).

Figure 1.3.1-1 illustrates the possible sources of rate limitation experienced by a desorbing species. Partitioning between the solid and liquid within a pore is governed by the surface desorption rate or equilibrium condition "1". Once the contaminant is in the liquid within a pore, intraparticle transport "2" is largely governed by molecular

diffusion. At the surface of the particle, transport into the bulk aqueous phase can be limited by molecular diffusion across a mass transfer boundary layer. Removal from the bulk aqueous phase relies on a mixture of convection and (in the presence of Fenton's reagents) reaction.

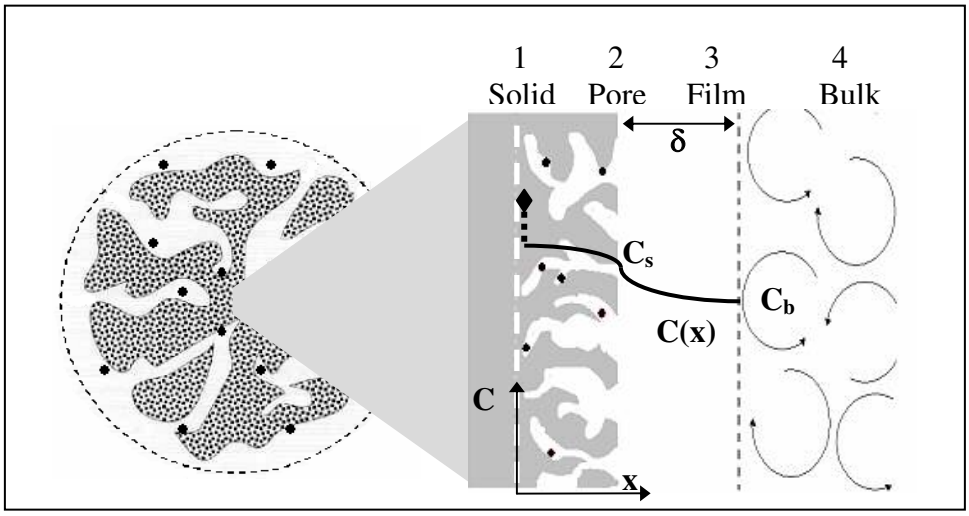

Figure 1.3.1-1. Potential sources of rate limitation for desorption of adsorbate from the GAC (solid) to the bulk fluid. 1.Desorption from solid to liquid phase. 2.Diffusive transport within the pores (pore or surface diffusion). 3.Diffusive transport through a quiescent film surrounding the particle. 4.Convective transport or reaction in bulk fluid.

Because hydroxyl radicals are extremely reactive and short-lived, they do not persist any significant distance beyond the point where they are generated. Thus, if the Fenton's reagents are primarily present in the bulk phase (as opposed to in the pore volume of the GAC), it is reasonable to hypothesize that the reaction of the target compound with hydroxyl radicals will occur mainly in the bulk aqueous phase. This physical model represents a hypothesis to be tested using experimental carbon recovery data.

In the general case, it is possible that carbon recovery kinetics are limited by either the rate of reaction of target contaminants with Fenton-dependent radicals, by the rate of

desorption of contaminants from the particle surface or by a combination of pore and surface diffusion. This physical description provides a starting point for data analysis.

1.3.2 Theoretical Considerations – Fenton's Treatment for GAC Regeneration

This section discusses possible scenarios and theoretical considerations that may take place in heterogeneous systems. It should be clear to the reader that the discussion encompasses theoretical speculations as opposed to a supportable set of hypothesis related to the physical-chemical events in these experiments.

In heterogeneous systems, there exist a variety of scenarios in which pseudo-first-order recovery kinetics could be expected. Similar to homogeneous reaction kinetics, Fenton-dependent recovery rates in expanded-bed heterogeneous trials may be limited by the bulk-phase reaction of the target with the •OH. Since the overall rate of contaminant loss is related to the •OH concentration present in the bulk, a steady state approximation for •OH would lead to pseudo-first-order kinetics. Under these circumstances, the bulk liquid-phase concentration of contaminant must be in approximate equilibrium with its adsorbed concentration throughout the recovery period. Therefore, an approximately linear adsorption isotherm would be an additional, necessary condition for first-order kinetics. In such a case, the observed recovery rate would be directly related to the second-order rate constant for the aqueous-phase reaction.

Alternatively, it is possible that the reaction rate of the •OH with the adsorbed contaminant limits overall recovery kinetics. In these circumstances, the bulk aqueous-phase concentrations of H_2O_2, total iron and (therefore) •OH would seemingly extend to

the carbon surface, where the reaction rate would depend on the abundance of adsorbed contaminant (Figure 1.3.2-1). The bulk aqueous-phase contaminant concentration would be essentially zero, or at least much less than the equilibrium aqueous-phase concentration. If the concentration of the aqueous-phase radical is steady, the rate of target destruction will be proportional to the adsorbed concentration under surface-reaction limited conditions.

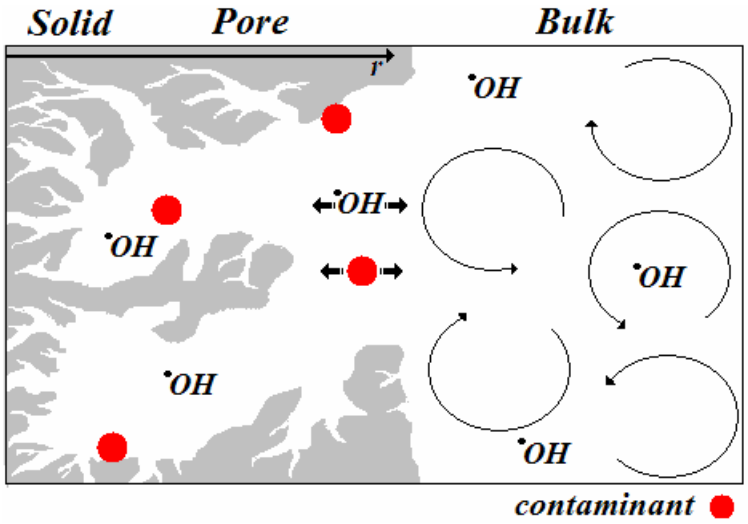

Figure 1.3.2-1. Intraparticle porous transport of hydroxyl radical to GAC particle surface.

Intraparticle transport mechanisms, such as pore and surface diffusion and surface desorption may also limit carbon recovery in heterogeneous systems (Figure 1.3.2-2). If the overall rate of contaminant destruction were limited by the rate of chemical desorption from the carbon surface, first-order kinetics would be expected. That is, the overall desorption rate of compound disappearance would be proportional to the adsorbed concentration. There are, however, some underlying assumptions here, such as the equivalence of adsorption sites on the carbon surface. Thermodynamic equivalence must

exist among the carbon adsorption sites, so that rapid desorption from less energetically favorable sites does not result in recovery rates that are initially faster, and subsequently slower, than predicted from a single first-order kinetic relationship.

Finally, first-order recovery kinetics might be expected if the overall rate of compound disappearance were controlled by intraparticle diffusive transport to the bulk solution (Figure 1.3.2-2). No fraction of the carbon surface, however, could be kinetically inaccessible relative to the remainder of the surface. This restriction seems unlikely considering that relatively small pores within the particle interior typically dominate carbon surface area. Therefore, kinetic equivalence of adsorption sites in the particle interior and those at the surface, in terms of accessibility to the bulk solution, seems improbable. The loss of contaminant from the carbon surface would, under those circumstances, be proportional to the aqueous-phase concentration in equilibrium with the sorbed concentration of contaminant. The diffusion coefficient for intraparticle transport is related to a geometric tortuosity factor, τ, and reflects, at least to a degree, the physical characteristics of the adsorbent.

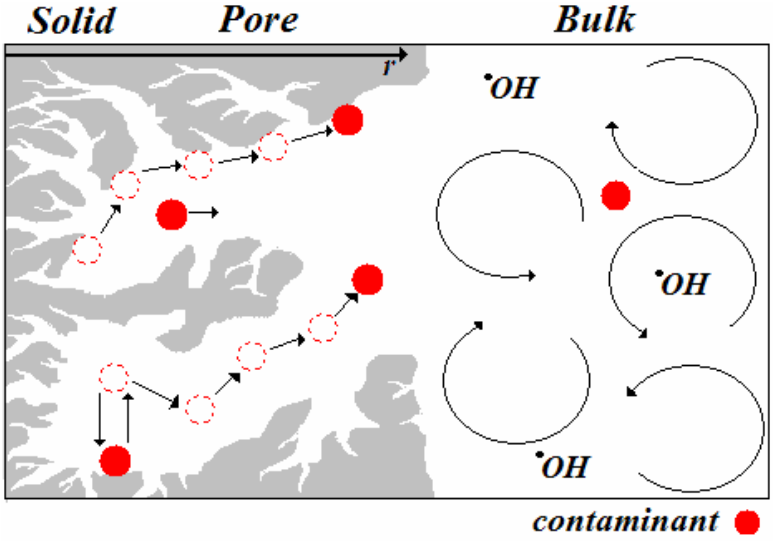

Figure 1.3.2-2. Pore and surface diffusion, and surface desorption of contaminant within a GAC particle pore.

In summary, the rate of disappearance of initially adsorbed contaminants can be proportional to the mass of target in the heterogeneous system under a variety of circumstances. Chemical contaminants that react slowly with •OH may accumulate in the bulk liquid-phase reflecting a reaction-limited rate of chemical destruction. Chemicals that are insoluble or show a very high affinity for solid surfaces (e.g. carbon) may experience overall rates of Fenton-driven transformation that are limited by pore and surface diffusion or by the rate of desorption from the surface. Each situation could yield pseudo-first-order recovery kinetics.

1.4 Project Objectives

The project seeks to increase the knowledge and applicability of an innovative means of destroying GAC-sorbed VOCs without the need to remove the sorbent from the

adsorption reactor. The project focuses on laboratory bench-scale experimentation, evaluation and modeling combined with limited pilot-scale field testing.

The specific laboratory objectives were:

- Investigate the use of reductants and electron shuttles, other than hydrogen peroxide to accelerate the Fenton-driven process for organics degradation.
- Evaluate the effect of chloride build-up in the Fenton reagent regenerant solution during chlorinated organic degradation.
- Establish the relative merits of regenerant liquid amended versus surface precipitated iron for catalyzing Fenton's reaction.
- Identify the mechanism and rate limiting step(s) for Fenton reagent destruction for a range of chlorinated organics.
- Evaluate the dependence of reaction kinetics and efficiency on solution pH.
- Provide a scoping level evaluation of the relative economics of Fenton reagent regeneration of VOC-bearing GAC versus conventional off-site thermal regeneration or hazardous waste disposal.

The specific field testing objectives were:

- Provide proof of concept of Fenton-driven, in-place regeneration of VOC-laden GAC.
- Establish basic performance characteristics and challenges for field use of Fenton's reagents for GAC regeneration.

- Establish the effect on GAC adsorption capacity of multiple regenerations by Fenton's reagents.
- Establish a scoping level estimate of field scale economics of the process.

2. MATERIALS AND METHODS

2.1 Chemicals

Purified water (Milli-Q^{TM} Water System by Millipore) was used in all experiments. The following chemicals were obtained from Sigma-Aldrich: carbon tetrachloride, CT (99.9% HPLC grade), 1,1,1-trichloroethane, TCA (>99%), hexachloroethane, HCA, ferric sulfate [$Fe_2(SO_4)_3$•5.6H_2O], cupric sulfate pentahydrate ($CuSO_4$•5H_2O), hydroxylamine hydrochloride (H_3NO•HCl; minimum 99%), copper (I) chloride (CuCl; 97%), 1,4-benzoquinone (1,4-BQ; 98%), hydroquinone (HQ; 99%), 9,10-anthraquinone 2,6-disulfonic acid disodium salt (> 98%). Hydrogen peroxide (30%, reagent grade) and methanol (HPLC grade) were from Fischer Scientific. Ultra resi-analyzed tetrachloroethylene (PCE), methylene chloride (CH_2Cl_2), trichloroethylene (TCE), chloroform (CF), *n*-heptane, 1,10-phenanthroline monohydrate, ferrous sulfate hepta hydrate ($FeSO_4$•7H_2O), and hydrochloric acid were from J.T. Baker. Titanium sulfate solution was obtained from Pfaltz and Bauer, and sulfuric acid, ethyl acetate, ammonium acetate, and 1,2-dichloroethane (DCA) were from EM Science. Potassium permanganate and isopropyl alcohol were obtained from EMD Pharmaceuticals, and ferrous ammonium sulfate [$FeSO_4(NH_4)_2SO_4$•6H_2O] from Spectrum Chemical Mfg. Corporation. All chemicals were reagent grade or better and were used as obtained.

2.2 Analytical

2.2.1 Target Organic Compounds

The target VOCs (methylene chloride, chloroform, carbon tetrachloride, 1,2-dichloroethane, 1,1,1-trichloroethane, trichloroethylene, tetrachloroethylene) were analyzed using a modified version of the EPA method 551.1, "Determination of Chlorinated Solvents by Liquid-Liquid Extraction and Gas Chromatography with Electron-Capture Detection." Samples were prepared for analysis by placing a 20-μL (15-μL in some experiments) in a 2-mL glass crimp-top vial containing 1 mL of heptane. Using an auto sampler 1 μL of the extract was injected into a Hewlett Packard 5890 Gas Chromatograph (GC, Palo Alto, CA) equipped with a DB-624 fused silica capillary column (J & W Scientific, Fulsom, CA; 0.53 mm ID, 30 m in length). The GC used an electron-capture detector (ECD) for quantification of chlorinated compounds. Nitrogen and helium were used as the make-up and carrier gases. The gas flow rate was 26 mL/min. The temperatures of the detector and inlet were 275°C, and 150°C, respectively. The oven temperatures ranged from 35°C to 100°C and the sample run times were 5-20 minutes, depending on the compound analyzed. A chlorinated compound (e.g. carbon tetrachloride) was added to each sample as an internal standard to adjust for instrument error and sample size inaccuracy. A response factor was obtained from the calibration curve relating the response of the analyte to that of the internal standard. This factor was then used to determine the analyte concentrations. A calibration curve was run prior to all analysis; samples were diluted as needed. To ensure proper results and monitor instrument performance, a check standard was run every tenth sample. The percent

deviation between check standards was no larger than 5%, indicating proper operation of the GC.

2.2.2 Hydrogen Peroxide

Hydrogen peroxide was analyzed using a peroxytitanic acid colorimetric method (Boltz and Holwell, 1978), as modified by Teruya (2000). The procedure was as follows. The sample (50 μL) and 50 μL of titanium sulfate (Pfaltz and Bauer, Inc., Waterbury, CT) solution were added to 4.9 mL of deionized water. Titanium sulfate was provided in stoichiometric excess to react with H_2O_2 leading to color development and quenching the Fenton reaction. After 1 hour, color development was measured at a wavelength of 407 nm using a Hitachi U-2000 doubled-beamed spectrophotometer (Hitachi Corporation, Schaumburg, IL). Samples were diluted with deionized water as necessary to fall within the range of the standards.

2.2.3 pH

A Hach One pH/ISE meter (Hach Company, Loveland, CO) was used to monitor the pH of the solution containing Fenton's reagents. The meter was calibrated using standard pH calibrating buffers (pH 2 and 4) from VWR (Aurora, CO).

2.2.4 Iron

Total iron content of all the samples was analyzed using the phenanthroline method (Standard Methods for the Examination of Water and Wastewater, 1995).

2.3 Quality Assurance

The utmost care was taken to assure the quality of laboratory work. In accordance with the Quality Assurance Project Plan (QAPP), the lab maintained logbooks, internal standards, proper storage of samples, and check standards. The Quality Assurance Officer specified all analytical methods, evaluated analysts for competency to perform the analyses, and monitored all phases from sample collection to disposal. The project was subject to audit by EPA and quarterly audits by the Quality Assurance Officer. These audits consisted of reviews of analytical methods, analyst familiarity with methods, reviews of standard solution quality, reviews of calculations, and instrument performance.

2.4 Experimental

2.4.1 General

Experiments were conducted in either batch or column reactors. In general, batch reactors were used to investigate homogeneous Fenton reaction kinetics. However, a set of heterogeneous batch experiments was used to explore the pH dependence of the system with and without organic present. Experiments in bench-scale column reactors were designed to examine the role of mass transfer limitations to Fenton-driven carbon recovery rates and to expose key operational characteristics of the Fenton-dependent carbon regeneration mechanism. It is not known with certainty, for example, whether compound desorption must precede reaction with Fenton-derived free radicals and (consequently) whether desorption rates control overall process kinetics. Column

reactors were also designed and tested at the field-scale. Isotherms for target compounds were developed by varying the mass of carbon in a series of batch reactors that contained identical masses of the target contaminant. Masses of carbon and contaminant were estimated in advance to provide a broad range of aqueous-phase concentrations following attainment of equilibrium.

2.4.2 Homogeneous Batch Kinetic Experiments

Reaction vessels consisted of 65-mL glass vials, capped with mini-inert valves. Chemicals in the reaction mixtures always included PCE or CT (the target compounds in these experiments), ferric iron (added from a pH-adjusted solution of ferric sulfate), and H_2O_2 (added to achieve target initial concentrations from a 30% stock solution). Depending on experimental objectives, one of several quinones, copper, or radical ($\bullet OH/O_2\bullet^-$) scavengers were at times part of the reacting mixture. Reactors were filled to near capacity and placed in an Orbit Shaker Bath for temperature control. In a subset of the experiments, H_2O_2 and/or PCE were periodically replenished. Both PCE and CT degradation were studied in the presence of radical scavengers in Fenton's reaction. In these experiments, the same 65-mL vials were utilized but with 5 mL headspace.

Experiments with 0.5 mM total iron were run at room temperature (22-24°C). When total iron was 0.1 mM, the temperature was maintained at 30-31°C. Experiments involving quinones were conducted at room temperature (22-24°C). Experiments studying the effect of pH, Cl^- accumulation and radical scavengers in Fenton's reaction were at 32°C. Temperatures in the range 8.8-54.4°C were also explored in the

experiments designed to establish the effect of copper addition on Fenton's (iron based) reaction for PCE decomposition.

2.4.3 Adsorption Isotherms

Isotherms were obtained for each of seven chlorinated target compounds (Table 2.4.3-1). For each compound, five 160-mL glass serum bottles containing varying masses of carbon (1-6 grams) were filled with water containing the respective target chemical and crimp sealed. A blank (compound solution with no carbon) was utilized when running all isotherms. The measurement of this blank was used as the C_o (initial concentration).

Water at near-saturation levels with contaminant was used to initially load the target CVOC into the serum bottle to avoid co-solvent effects and/or adsorption of neat-phase contaminant directly onto the carbon. The serum bottles were placed in a temperature-controlled water bath (32°C) equipped with a shaker element. The bottles were allowed to equilibrate for at least 36 hours. The liquid phase was then sampled and analyzed for the contaminant by GC-ECD. The mass adsorbed on the carbon was determined from the difference between the initial (saturated water) concentration and the liquid concentration following adsorption. Isotherm data were fitted using a Freundlich model ($S=KC_{eq}^{1/n}$). Model parameters were determined via simple linear regression analysis of the log-transformed data.

Table 2.4.3-1. Chemical Properties of the Organic Compounds Studied

Name	*Formula*	*Log K_{ow}*[a]	*$k_{\bullet OH,R}$ (M^{-1} s^{-1})*[b]	*Diffusivity (cm^2/s)*[c]	*Freundlich Parameters*[d] *K (mg/g)(L/mg)$^{1/n}$*	*1/n*
Methylene Chloride (MC)	CH_2Cl_2	1.15	9.00E+07	1.21E-05	0.07	1.06
1,2-DCA	$C_2H_4Cl_2$	1.47	7.90E+08	1.01E-05	0.04	1.33
1,1,1-TCA	$C_2H_3Cl_3$	2.48	1.00E+08	9.24E-06	0.65	0.87
Chloroform (CF)	$CHCl_3$	1.93	5.00E+07	1.04E-05	1.48	0.77
Carbon Tetrachloride (CT)	CCl_4	2.73	2.00E+06	9.27E-06	12.30	0.59
TCE	C_2HCl_3	2.42	2.90E+09	9.45E-06	5.82	0.70
PCE	C_2Cl_4	2.88	2.00E+09	8.54E-06	45.66	0.56

NOTE: $k_{\bullet OH,R}$ is the second-order rate constant for the reaction of hydroxyl radical with the target organic compound.
SOURCE: [a]Swarzenbach et al., 1993; [b]www.rcdc.nd.edu, except carbon tetrachloride (Haag and Yao, 1992); [c]calculated from Wilke-Chang equation (Logan, 1999); [d]From isotherm data obtained in this lab at 32ºC.

2.4.4 Column Experiments

2.4.4.1 GAC Selection and Preparation

Granular activated carbon (URV-MOD 1, Calgon Corporation, Pittsburgh, PA) was used in all trials. This experimental-type carbon was selected because of its relatively high iron and low manganese contents. The GAC was steam-activated to minimize reactivity with H_2O_2 (Huling et al., 2005a). It is a bituminous coal, 8 x 30 mesh (effective size 0.6-2.4 mm), with a specific surface area of 1290 m^2/g and pore volume of 0.64 mL/g (Huling et al., 2005a). Physical properties of this experimental carbon provided by the Calgon Corporation are summarized in Table 2.4.4.1-1. The 8×30 mesh size fraction

was used in expanded-bed column and isotherm adsorption experiments. In fixed-bed studies, sieve-sorted particle distributions of 1.0-1.18 mm, 1.4-1.7 mm, and 2.0-2.38 mm were used. Calgon URV-MOD 1 carbon was sieve sorted using USA Standard test sieves with ASTM-11 specification.

Table 2.4.4.1-1 - Physical Properties of Calgon URV-MOD 1

Property	Value
BET Surface Area (95% CI)	1290 m^2/g ± (1260-1330 m^2/g)
Total Pore Volume (95% CI)	0.643 mL/g ± (.613-.673 mL/g)
Micropore	0.386 mL/g
Meso & Macropore	0.257 mL/g
Porosity	0.592

SOURCE: Huling et al., 2005a.

Prior to use in experiments, GAC was dried overnight at 103°C to obtain the dry weight. Dried carbon was cooled in a vacuum dessicator, and then wetted with de-ionized water from a Milli-Q-water system. To guarantee a fully hydrated surface, the suspended carbon was shaken at room temperature for 24 hours prior to contaminant loading. Loading of a target contaminant onto the carbon was done in an aqueous-phase suspension to avoid co-solvent effects, and the adsorbed mass was determined by GC-ECD analysis, and verified by determining the difference between pre- and post-adsorption liquid-phase concentrations. Pre-loading of carbon for bench-scale experiments was accomplished by placing 12-16 g of GAC into 1.00 L of water containing the experiment-specific target contaminant. Normally, the water was nearly saturated with the target at room temperature prior to the introduction of carbon. The 1-L batch reactors with negligible headspace were then sealed and tumbled for approximately

60 hours (room temperature) for attainment of equilibrium between the dissolved and adsorbed chemical. Final (measured) adsorbed concentrations are provided in Table 2.4.3-1.

2.4.4.2 Iron-amended GAC Preparation

In one set of trials, iron was precipitated on the GAC surface to evaluate the effectiveness of using iron-amended GAC versus providing iron in the bulk solution. These trials were conducted in bench-scale column reactors using GAC loaded with either TCE or PCE as the target VOCs.

To precipitate iron on the surface of the carbon, an iron solution was equilibrated with the carbon for approximately 4 days. The iron loading was based on a critical iron loading on GAC particles that was established by Huling et al. (2005c). The critical loading was established as the GAC-bound level that maximized the rate of H_2O_2 consumption for the iron-amended GAC in water plus H_2O_2. To prepare the iron solution, $FeSO_4 \bullet 7H_2O$ was dissolved in water to obtain 2.2 g/L Fe (0.039 M Fe). Ten grams of dry GAC were placed in each vial with 30 mL of the iron solution. Sulfuric acid was added as necessary to maintain the pH of the iron-GAC solution near 2.5 during the equilibrium process (~4 days). After 4 days, the pH was increased to 3.0 using a solution of NaOH. The liquid was analyzed for total iron using the phenanthroline method. Subsequently, the iron-amended GAC from each vial was combined in a beaker, dried, weighed and utilized in the column experiments. For analysis of the iron content on the carbon, 5 g of iron-amended and background (clean) GAC were crushed to homogenize the samples.

Replicates of the crushed GAC samples were analyzed by Shaw Environmental, Inc., under EPA direction. Samples were prepared by microwave extraction and filtration and analyzed by ICP-OES (Perkin Elmer Optima 3300DV ICP). A standard operating procedure for determination of total nitric acid extractable metals from solids and sludges was used.

2.4.4.3 Heterogeneous Batch Kinetic Experiments

2.4.4.3.1 pH dependence on H_2O_2 degradation

The degradation of hydrogen peroxide was evaluated in water, and in the presence of background (unamended) GAC and iron-amended GAC in the pH range 3 to 7. In these trials 12 g of GAC (when used) and 100 mLs mQ-water were placed in a beaker and pH adjusted using either a diluted solution of NaOH or H_2SO_4. The beaker and its contents were placed in a waterbath for temperature control (Figure 2.4.4.3.1-1). All experiments described in this section were performed at 32°C. A pH probe was used to monitor pH variations throughout the course of the experiment. An overhead mixed was utilized to stir the solution. To start the reaction, 1 mL 50% H_2O_2 was added to the reaction mixture. Hydrogen peroxide samples were taken from the solution and measured as described previously.

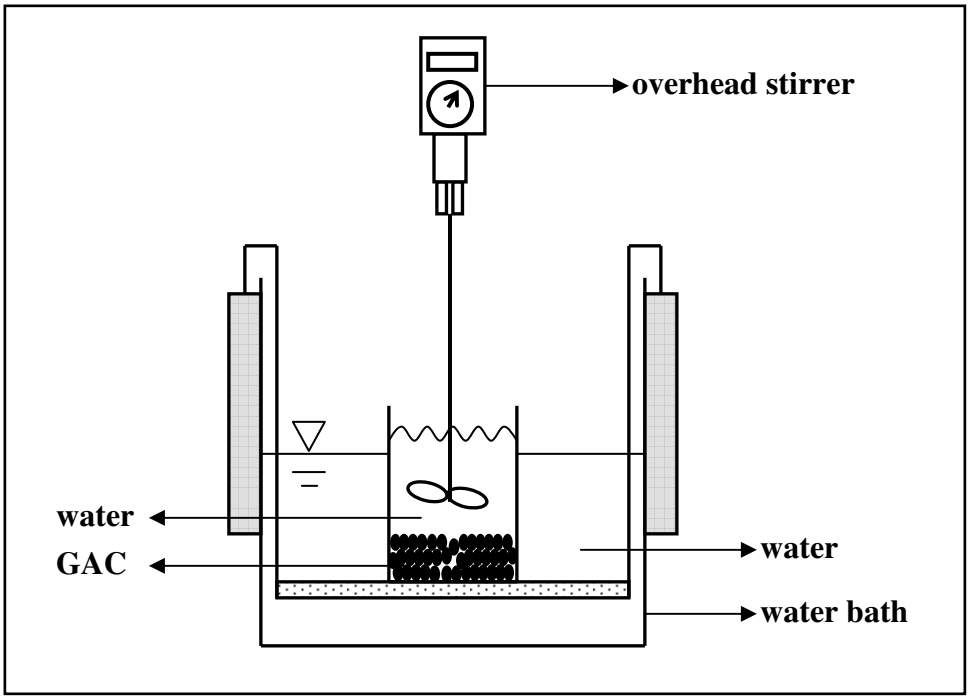

Figure 2.4.4.3.1-1. Diagram for the set up used for studying the pH dependence on H_2O_2 degradation with an overhead mixer.

2.4.4.3.2 pH dependence on H_2O_2 degradation in the presence of TCE

Kinetics of hydrogen peroxide degradation was studied at pH 3 and 7 for three types of GAC. In these trials background (clean), iron-amended and SolmeteX GAC were utilized. The iron content on these carbons is approximately 2, 7, and 57 mgFe/gGAC, respectively. Reaction vessels consisted of 160-mL glass serum bottles sealed with a crimped top. At pH 7, each vessel contained 2 g GAC (background, iron-amended or SolmeteX), hydrated prior to use. To load the GAC, 150 mLs of a water- TCE saturated solution was added and let it to equilibrate for at least 5 days. Following the equilibration period, the solution was pH adjusted with either a diluted solution of NaOH or H_2SO_4. The pH was monitored by using pH strips. To start the reaction 1 mL of 50% H_2O_2 was added. A needle was placed on the septa to release the pressure buildup overtime. Liquid

samples were obtained for the analysis of hydrogen peroxide and TCE from the reacting solution. Reactors were sacrificed at different times. The liquid was then decanted from each reactor and the pH was measured with a pH meter. To extract the TCE from the GAC, 30 mLs ethyl acetate were added to the reactor vessel with the wet GAC and analyzed after 12 hours. GAC samples were analyzed using the GC-ECD as described previously.

At pH 3, the reactors were prepared by using 5 g GAC and adjusting the pH prior to loading the GAC with the TCE solution. In these trials, 70 mLs of mQ-water were added to the GAC containing reactors, pH adjusted and then loaded with 70 mLs of TCE-water saturated solution. The pH was checked after the equilibrium period to readjust it, if necessary. All samples were analyzed in an analogous way.

2.4.4.4 Extraction of VOCs from GAC

Bercik (2003) evaluated four organic solvents in terms of their ability to extract PCE from activated carbon. The extracting solvents analyzed were heptane, pentane, ethanol, and ethyl acetate, and the target organic compound was tetrachloroethylene (PCE). Of the four solvents, ethyl acetate provided the highest extraction efficiency (≥93%) after 12 hours (Bercik, 2003). Based on these results, all extractions of chlorinated solvents from GAC used ethyl acetate solvent and a 12-hour extraction period.

2.4.4.5 Sample Analysis

In all column experiments, representative volumes of carbon (0.5-0.7 g) were withdrawn from the reactor, weighed, and extracted in ethyl acetate in crimp sealed vials. After the 12-hour extraction period, samples were prepared for analysis by withdrawing a 20-µL sample of ethyl acetate from the crimped carbon vials, and injecting it into a 2-mL glass crimp top vial containing 1 mL of heptane. The mass of VOC in the heptane was subsequently quantified by GC-ECD (see earlier description). Liquid samples from the reactor bulk fluid were collected at the same time as the GAC samples to measure contaminant desorption rates and to complete a mass balance. Liquid-phase contaminant levels were monitored in the bulk aqueous-phase by placing samples from the reservoir (Figure 2.4.4.5-1) in 1-mL crimp sealed vials. Dilutions were performed in heptane as needed, and 1.00 µL was then injected in the GC-ECD. An internal standard, appropriate for each compound, was added to each sample to analyze and adjust for instrumentation inconsistencies. Analyte-specific internal standards were selected based on GC peak retention times, to produce sufficient separation between the target and the internal standard. The oven temperature and run time were also selected based on chromatographic peak analysis. Oven temperatures ranged from 60°C-100°C (inlet temperature: 200°C, detector temperature: 275°C) with run times of 4-9 minutes, depending on the compound being analyzed. A calibration curve was established prior to all analyses.

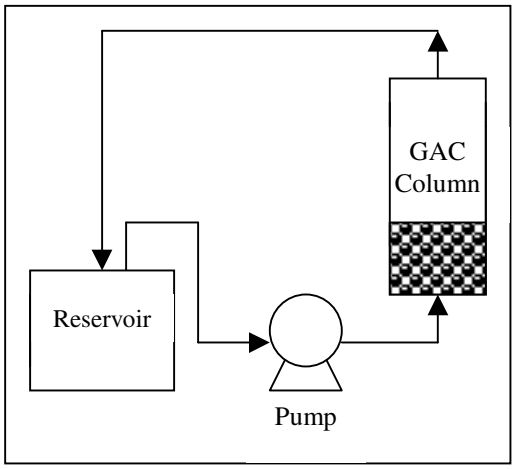

Figure 2.4.4.5-1. Expanded Bed Desorber Set Up

2.4.4.6 Desorption Rate Experiments

Expanded-bed column experiments were performed at a temperature of 32°C (± 2°C) using a Chromaflex® borosilicate glass chromatography column with a 2.5-cm inner diameter and 15-cm length (obtained from VWR). In these experiments, the temperature was controlled by means of a water bath.

The column was fitted with 2.5-cm inner diameter PTFE frits tapped with 5/8-inch Swagelok stainless steel fittings that fed to 5/8-inch Teflon tubing. A 6-600 rpm Masterflex® peristaltic pump transported the bulk liquid in an up-flow mode through the column at a flow rate of 950 mL per minute, a volume flow-rate sufficient to expand the carbon bed and ensure proper mixing. To improve hydrodynamic mixing, a 5-cm Chromaflex® extension packed with 3-mm glass beads was added to the column influent (Figure 2.4.4.5-1).

Desorption rates were measured by circulating clean (contaminant free) water through the column. That is, elution water did not contain Fenton's reagents. In these trials, the

water was recirculated through the reservoir (T = 32ºC) and the contaminant was stripped from the reservoir using a bubbler. MC, CF and TCE were used in these trials. Water was passed through the pre-loaded columns at rates designed to minimize aqueous-phase contaminant concentrations at the column exit, so that rates of mass transport from the carbon surface to bulk solution were not affected by the bulk liquid-phase concentration. In this manner, contaminant transport kinetics from surface to bulk could be established directly. Desorption kinetics were established by periodically measuring both residual contaminants on carbon samples and the contaminant concentration in the liquid exiting the column.

2.4.4.7 Regeneration Rate Experiments

Regeneration kinetics were first studied by circulating Fenton's reagents through a fluidized bed of pre-loaded GAC as described for the desorption rate experiments above. Column recovery was monitored by periodically withdrawing carbon samples and extracting residual contaminants for analysis (see earlier descriptions). Preliminary experiments of this type were conducted at room temperature. When it became apparent that room temperature was subject to significant uncontrolled changes, temperature was controlled at 32ºC in subsequent experiments. In the initial bench-scale column experiments, VOC-loaded carbon was packed into a Chromaflex® borosilicate glass chromatography column, I.D.=2.5 cm, L=15 cm, V=85 mL (Ace Glass, Inc., Louisville, KY). Fenton's reagents were prepared on the day of use. During regeneration, a 10 mM Fe (ferric sulfate) solution was recirculated in up-flow mode through the column at a rate

sufficient to expand the carbon bed by approximately 50%. To initiate recovery, 0.2 M H_2O_2 was added to the recirculating fluid. At 10-60 minute intervals, sufficient H_2O_2 was added to restore the original concentration. This generally produced an H_2O_2 concentration that differed from the original concentration by less than 50% (data not shown). Periodically the reagent circulation was stopped, while carbon samples were withdrawn from the top and bottom of the column for extraction and analysis of the target compound. Extraction periods were of at least 12 hours in ethyl acetate on a shaker table. Extracts were analyzed using GC-ECD with the methods described below. Carbon samples were then dried at 103°C and weighed. Data are reported as the mean results of the values for samples from the top and bottom (one each) of the fluidized bed. Aqueous-phase samples were taken from the recirculation reservoir for analysis of the target compound, reaction by-products and residual hydrogen peroxide.

In iron-amended GAC trials, the reservoir contained water (no iron solution). A smaller reservoir size was utilized in these experiments (approx. 400 mL). Hydrogen peroxide was added using a peristaltic pump (as described previously), but the rate of addition necessary to maintain a constant H_2O_2 concentration was relatively low (see discussion). In these experiments, the pH was uncontrolled, but monitored.

2.4.4.8 Field-scale Column Experiments

Fenton-driven carbon regeneration was applied to soil vapor extraction (SVE) gas at the Park-Euclid (Arizona) State Superfund site, in which the primary contaminants are perchloroethene, trichloroethene, dichloroethene isomers, and the volatile hydrocarbon

components of diesel fuel. Local groundwater and soil gases have been studied intensively so that the extent and severity of pollution are well characterized. A side stream was taken off the full-scale SVE system at the field site to provide a source of SVE gases (containing mainly TCE and PCE) to the project's GAC column. The carbon was packed into a borosilicate glass chromatography column, I.D.=5.00 cm, L=30.0 cm, V=600.0 mL. The gas flow rate passing through the column was 4.0 cfm. Column effluent was returned to the SVE system. The carbon was typically loaded for approximately 72 hours. After loading, the carbon was regenerated in place via Fenton's reaction, reloaded with contaminant, and re-regenerated to study process feasibility (see Figure 2.4.4.8-1). During regeneration, solid and aqueous-phase samples were withdrawn and extracted as in the bench-scale experiments (see Figure 2.4.4.8-2). Initially, hydrogen peroxide was added to the 7-liter reservoir to maintain a near-constant concentration (0.2 M) throughout the regeneration period. Less frequent pulse additions of H_2O_2 were later used as a strategy to reduce H_2O_2 utilization during carbon recovery.

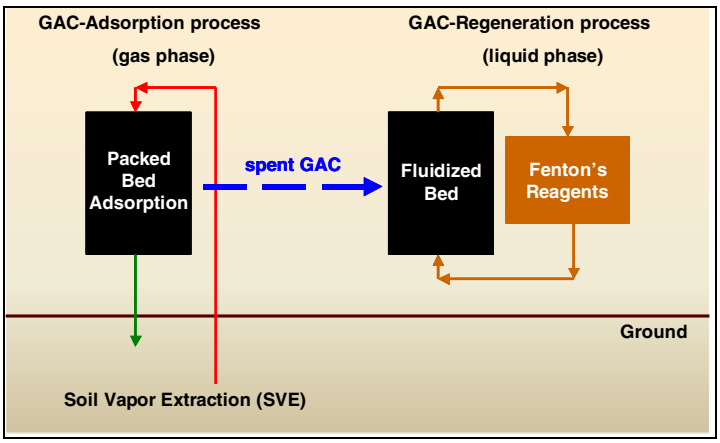

Figure 2.4.4.8-1. SVE-GAC system at field site.

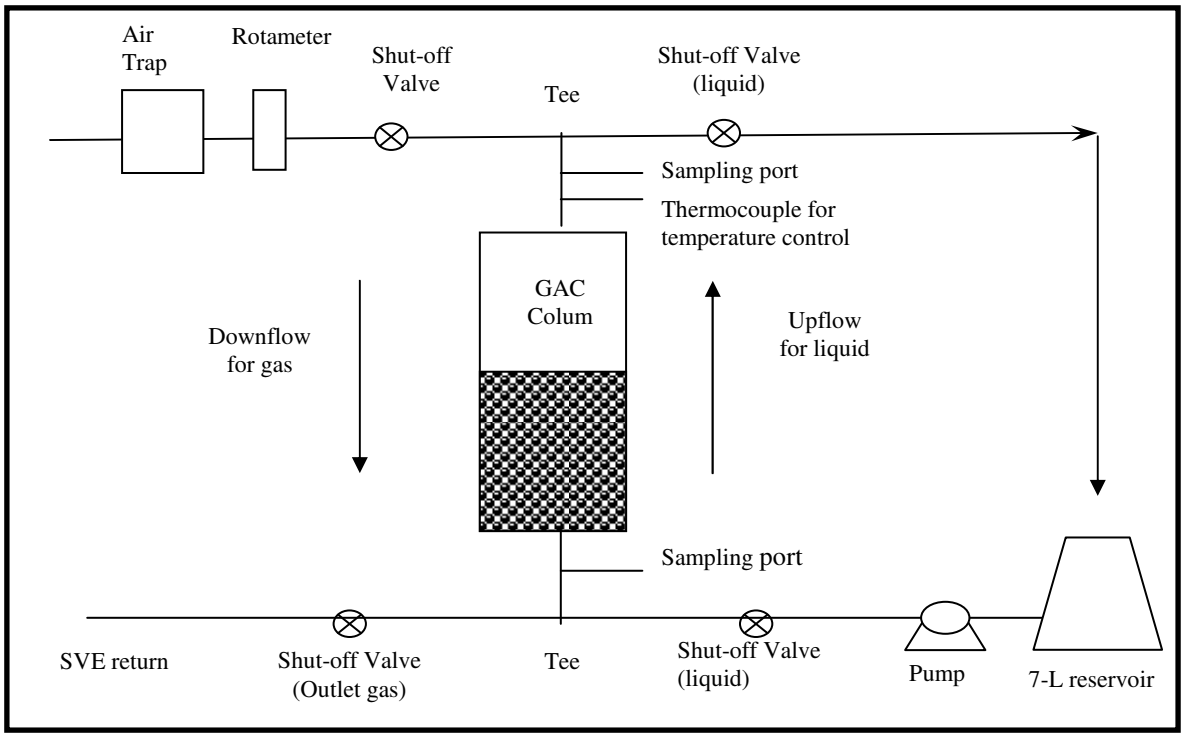

Figure 2.4.4.8-2. Diagram of the field experimental set-up for GAC-regeneration experiments. The carbon was loaded in a down flow mode and regenerated in an up flow mode. Column ID = 50 mm, L = 300 mm, 0.60 L, HRT (column) = 2 s., HRT (reservoir) = 0.9 min, pH = 2.0, $[Fe(III)]_T$ = 10 mM, and $[H_2O_2]_o$ =0.38M.

3. PCE DEGRADATION RATE ENHANCEMENT IN A HOMOGENEOUS SYSTEM

3.1 Dependence of PCE Reduction Kinetics on Total Iron Concentration

Preliminary experiments were carried out at initial concentrations of 0.10 M H_2O_2, pH 2.0, and either 0.1, 0.5 or 2.0mM Fe_T (added as Fe(III)). Starting PCE concentrations were 50 μM. PCE disappearance obeyed apparent first order kinetics (Figure 3.1-1) even though there was no attempt to maintain H_2O_2 at a constant level over the 2-hour experiments. The magnitude of the first order rate constant varied with total iron concentration. At the highest total iron concentration (2.0 mM), the half time for PCE disappearance was 19 minutes. The reaction proceeded with essentially no lag following the addition of H_2O_2, indicating that near steady concentrations of iron species and hydroxyl radical were established quickly.

The pseudo-first-order rate constant for PCE disappearance in the experiment with a total iron concentration of 2.0 mM was about 20 times that of the experiment with $[Fe]_T = 10^{-4}$ M. However, the rate constant for PCE destruction at $[Fe]_T = 5 \times 10^{-4}$ M was unexpectedly low. There is no convincing explanation for the seeming inconsistency.

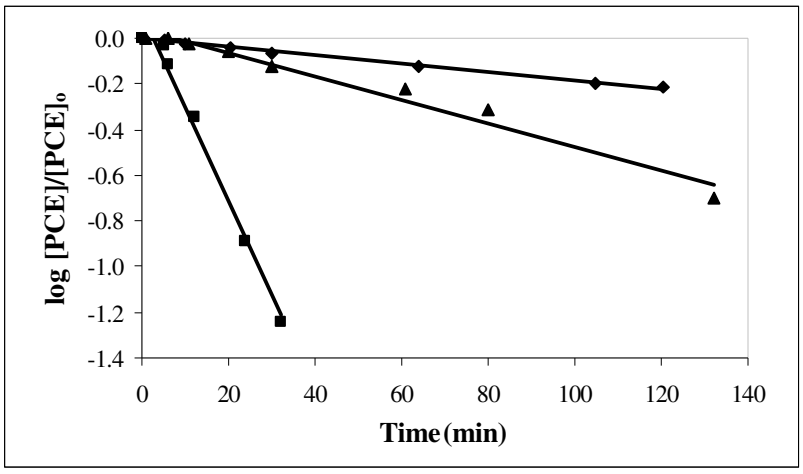

Figure 3.1-1. Effect of iron concentration on PCE disappearance at a fixed initial hydrogen peroxide concentration of 0.10 M. Total iron concentrations were 0.1 mM(♦), 0.5 mM (▲), and 2.0 mM (■). The data yield pseudo-first-order rate constants k_1 of 0.0018 min^{-1} (♦), 0.0047 min^{-1} (▲), and 0.0366 min^{-1} (■), respectively.

3.2 Rate Enhancement via Chemical Addition

Many investigators have shown that Fenton-driven reaction rates are initially very fast but subsequently decelerate rapidly when iron is provided as Fe(II) (Chen and Pignatello, 1997; Gallard and De Laat, 2000; Poppe, 2001). The observation directly supports assertions that Fe(III) reduction limits the overall rate of radical generation and, in these cases, contaminant destruction. On this basis, it was hypothesized that chemical reductants that convert Fe(III) to Fe(II) faster than the reaction of Fe(III) with H_2O_2 would increase the overall rate of hydroxyl radical formation and the rate of PCE disappearance. Several chemical additives were tested as potential means to circumvent or accelerate this rate limiting step in the simple Fenton's reagent system. Work by Bercik (2003) shows that addition of hydroxylamine initially accelerates the destruction of PCE many fold, but the effect of NH_2OH addition is rapidly lost.

3.2.1 Quinone Addition

Quinone addition was investigated as a means for accelerating the rate limiting step, Fe(III) reduction, in the Fenton's mechanism. Quinones are effective agents for facilitating electron transfer to Fe(III) (Fredrickson, 2000). The mechanism involves a series of 1-electron transfers that yield a semiquinone radical intermediate (Chen and Pignatello, 1997). The initial reductant in this reaction series is thought to be the superoxide radical produced via Fenton's mechanism (Figure 3.2.1-1). These experiments do not distinguish between superoxide or hydroxyl radicals as participants in PCE transformation. Later experiments using isopropanol (IP) as an •OH radical scavenger, however, suggest that •OH is the primary reactant with PCE (see later section on superoxide radical effects). Three different quinones were tested in these experiments (Figure 3.2.1-2). It was hypothesized that the more complex structure of 9,10-anthraquinone-2,6-disulfonic acid (AQDS) might protect the molecule against radical attack, preserving or extending its ability to shuttle electrons to the Fe(III) target.

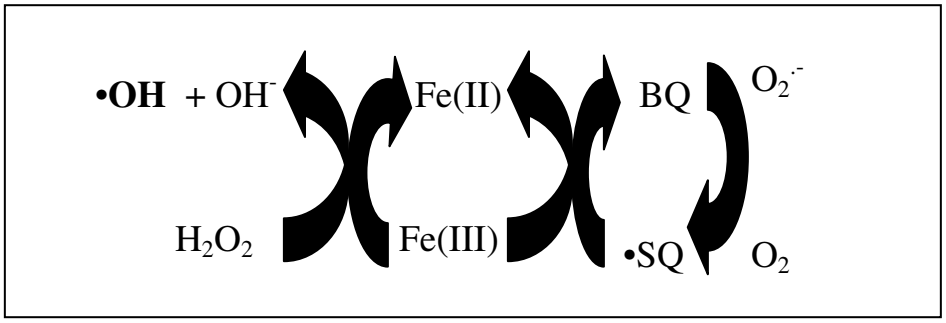

Figure 3.2.1-1. Simplified quinone mechanism (adapted from Chen and Pignatello, 1997). •SQ stands for semiquinone radical, and $O_2•^-$ for superoxide radical.

Quinones were tested by adding them at concentrations up to 5×10^{-4} M to Fenton reagents consisting initially of 5×10^{-4} M Fe_T (initially as Fe(III)), 0.10 M H_2O_2, pH 2.0 and 70 μM PCE. All experiments were at room temperature (22-24ºC). Initial PCE conversion rates increased monotonically with increasing initial quinone concentration (Figure 3.2.1-3). Addition of 5×10^{-5} M hydroquinone, for example, doubled the initial rate of PCE disappearance. An additional 10-fold increase in the hydroquinone concentration, to 5×10^{-4} M, increased the initial rate constant of PCE disappearance by another factor of two. It is apparent that for periods approaching an hour hydroquinone addition increased the overall rate of Fe(III) reduction and, consequently, the concentration of hydroxyl radicals in these experiments.

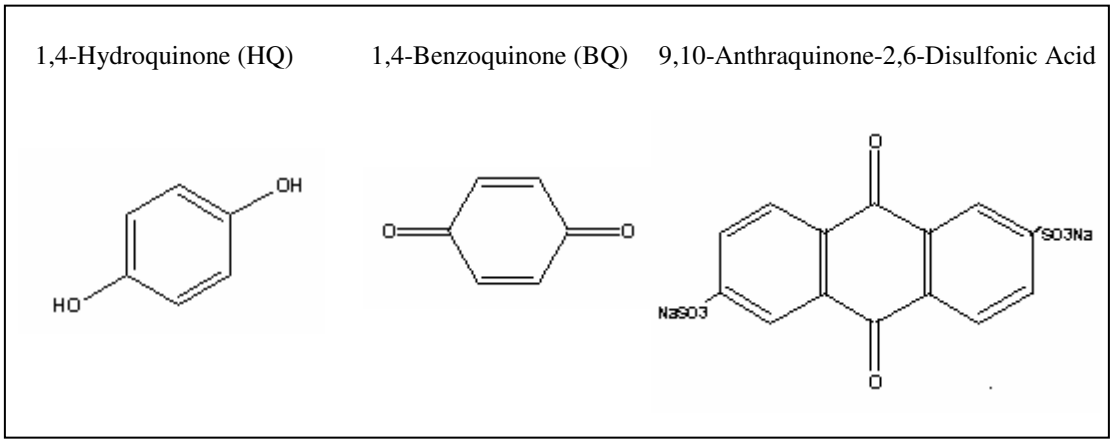

Figure 3.2.1-2. Structures of quinones investigated as agents for enhancing Fe(III) reduction rates in Fenton's mechanism.

A summary of quinone-dependent first-order rate constants is provided as Table 3.2.1-1. First-order rate constants represent reaction kinetics at the outset of the experiment, before the specific rates of PCE disappearance decreased as a consequence of quinone destruction or accumulation of reaction intermediates. Initial rates of PCE disappearance are plotted as a function of the hydroquinone addition in Figure 3.2.1-4. A linear relationship between the specific rate of PCE loss and the initial hydroquinone concentration is evident.

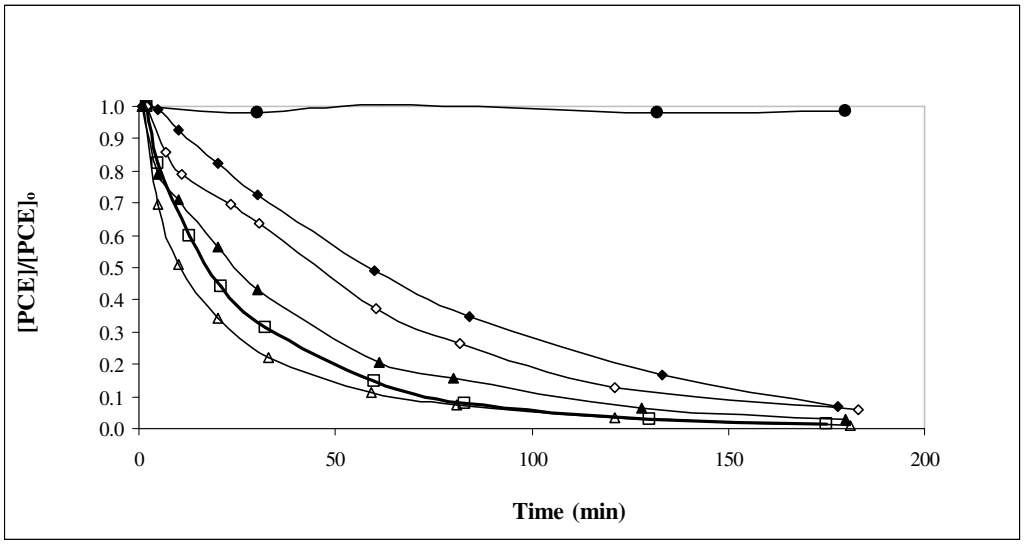

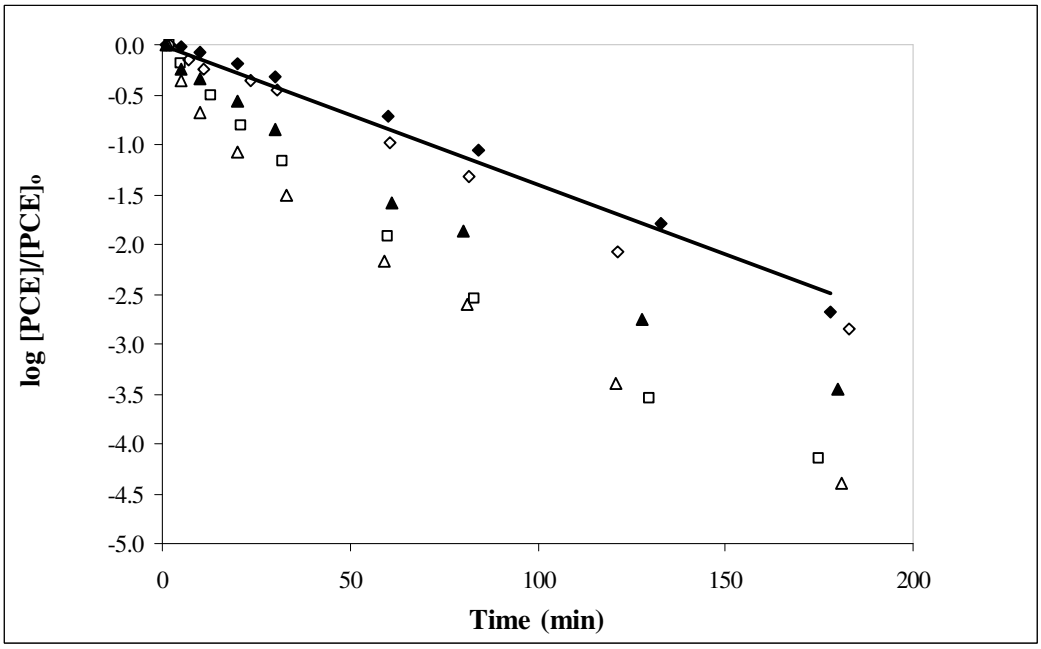

Figure 3.2.1-3. PCE degradation as a function of 1,4-hydroquinone added. Initial conditions: $[Fe(III)]_T = 0.5$ mM @ pH = 2.06, $[H_2O_2]_o = 0.10$ M, $[PCE]_o = 4E\text{-}5M$, room temperature. Legend: no H_2O_2 (●), 0 mM HQ (♦), 0.01 mM HQ (◊), 0.05 mM HQ(▲), 0.2 mM HQ(□), 0.5 mM HQ(Δ)

Table 3.2.1-1. First-order rate constants for PCE disappearance as a function of the initial hydroquinone concentration.

HQ (mM)	k_1(min^{-1})	R^2
0.5	1.89E-02	0.946
0.4	1.59E-02	0.947
0.3	1.41E-02	0.972
0.2	1.28E-02	0.979
0.05	8.30E-03	0.996
0.01	6.90E-03	0.998
0.005	6.60E-03	0.989
0	4.45E-03	0.990

NOTE: Values were derived via linear regression using the (semi-log) transformed data from Figure 3.2.1-3. In general, only the first 4-5 data points (first 30-min) from each experiment were used. R^2 values are included to illustrate goodness of fit.

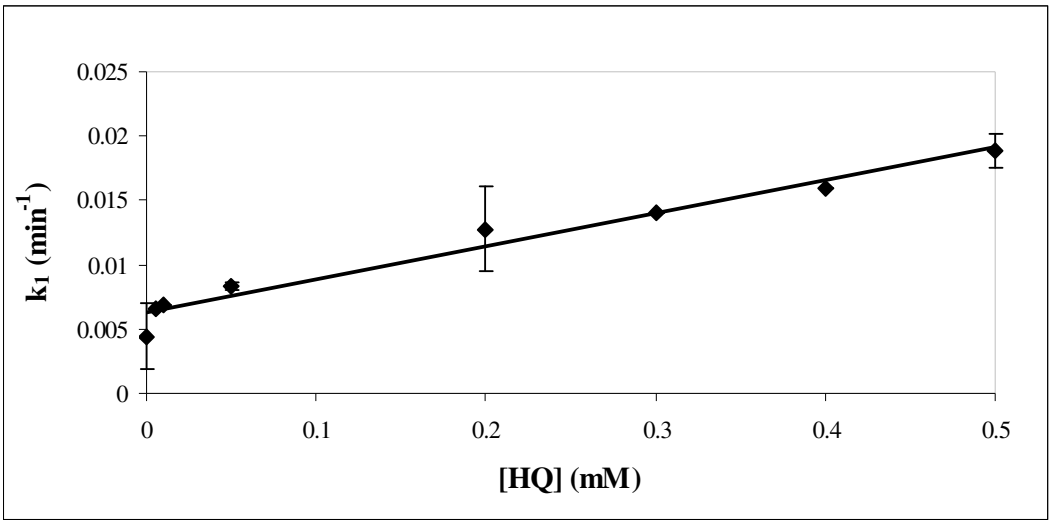

Figure 3.2.1-4. Initial first order rate constants for different hydroquinones concentrations. When two or more experiments were run at a single HQ concentration, symbols indicate average values. Error bars represent ± 1 standard deviation (n=3).

Inspection of the Figure 3.2.1-3 data indicates that, in the presence of hydroquinone, the specific rate of PCE conversion decreased continuously during the course of each three-hour experiment. It was therefore posited that Fenton-derived radicals gradually destroy HQ. To test this hypothesis, the reaction time for PCE destruction was extended by renewing the PCE and H_2O_2 concentrations in both the HQ-free control and the reactor

initially amended with 0.5 mM HQ (Figure 3.2.1-5). The kinetic advantage initially afforded by HQ addition was completely absent in the second half of the experiment. Results strongly suggest that HQ no longer served as an electron shuttle after the first three-hour period of the experiment. Others have noted that quinone function is rapidly lost in the presence of reactions that yield hydroxyl radicals (Chen and Pignatello, 1997). The practical implication of these results is that hydroquinone addition can accelerate Fenton-driven conversions only briefly unless the quinone concentration is periodically renewed. Practical and economic considerations probably dictate against this.

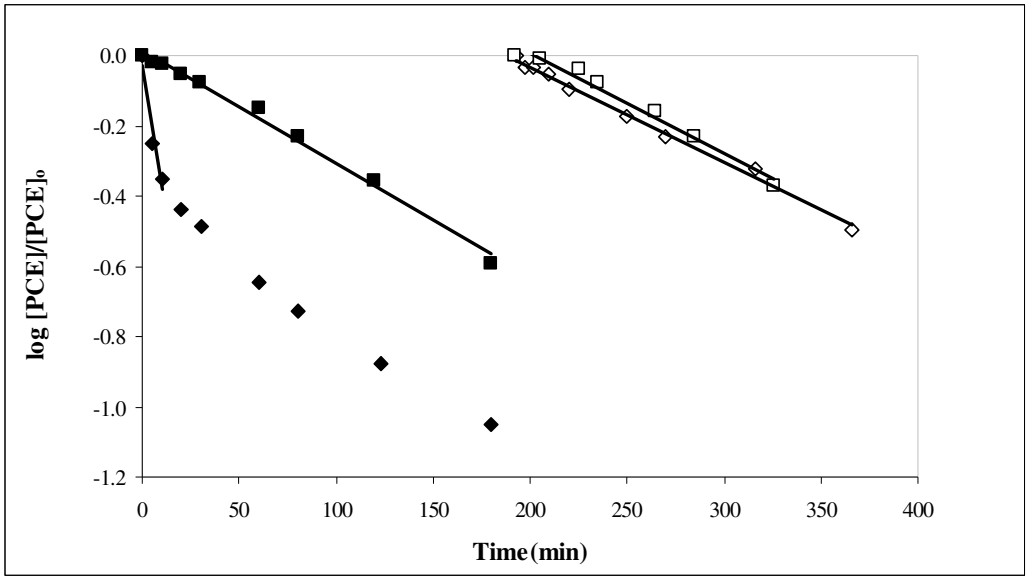

Figure 3.2.1-5. Two-period hydroquinone addition experiment comparing the performances of Fenton's mechanism for PCE destruction, with (♦/◊) and without (■/□) 5×10^{-4} M hydroquinone addition. The second period of the experiment involved reestablishment of initial conditions via PCE and H_2O_2 addition after the first three hours of the experiment. Initial conditions: $[Fe(III)]_T = 0.5$ mM, $[H_2O_2] = 0.10$ M, $[PCE] = 7.26\times10^{-5}$ M, pH=2.0, room temperature.

Experiments with 1,4-benzoquinone (BQ) were parallel in design and similar in result to those involving HQ. Reactors, reaction mixtures and physical conditions of the

experiments were identical to those described for HQ. The initial BQ concentration was varied from 0.0 to 0.5 mM. Initially, the specific rates of PCE disappearance were significantly enhanced by addition of BQ (Figure 3.2.1-6), although a saturation effect was apparent: BQ concentrations ≥ 0.3 mM all produced approximately the same effect on reaction kinetics (Figures 3.2.1-6 and 3.2.1-7). PCE disappearance was initially 7 times faster in the reactor amended with 0.3 mM BQ than in the BQ-free reactor. However, prior to the end of the first 5-hour phase of the experiment, the kinetic advantage offered by BQ addition was entirely lost and likely reversed. After 5 hours, H_2O_2 and PCE concentrations were restored to their original levels in the reactors that initially contained 0.0 or 0.3 mM BQ. The BQ-free control clearly outperformed the BQ-amended reactor at that point (Figure 3.2.1-8). It is hypothesized, but not verified, that organic residuals derived from the destruction of quinones served as radical scavengers, thus depleting the •OH radical pool available for PCE depletion.

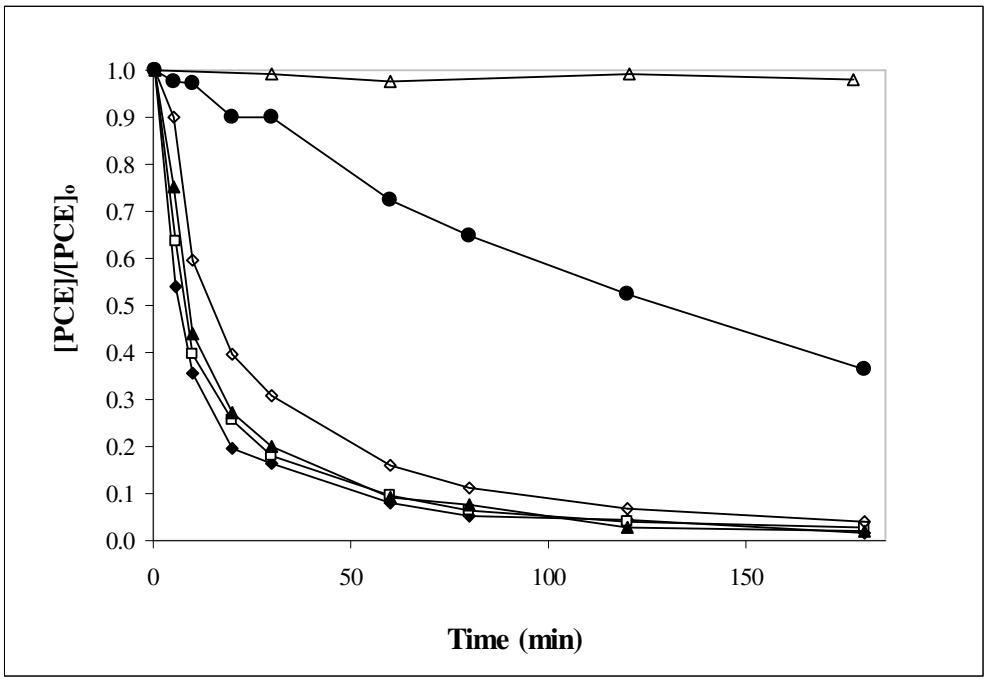

Figure 3.2.1-6. Effect of initial benzoquinone concentration on the Fenton-dependent rate of degradation of PCE. Initial conditions: $[Fe(III)]_T$ = 0.5 mM, pH = 2.0, $[H_2O_2]$ = 0.10 M, [PCE] = 8E-5 M. The control had no H_2O_2. Legend: control (Δ), 0 mM BQ (●), 0.2 mM BQ (◊), 0.3 mM BQ(▲), 0.4 mM BQ(□), 0.5 mM BQ(♦).

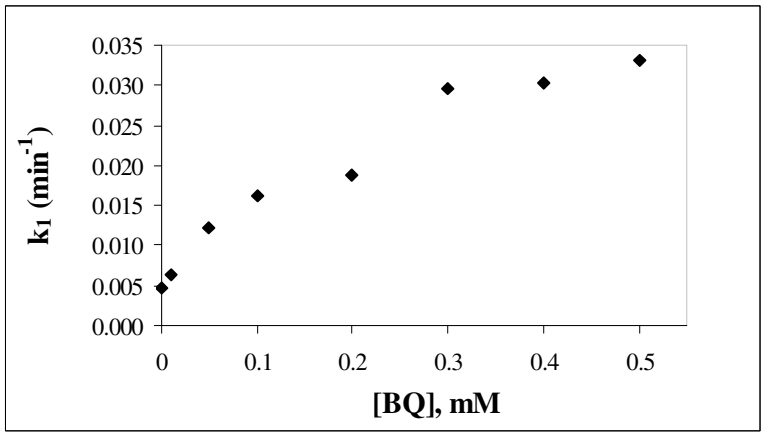

Figure 3.2.1-7. Effect of initial benzoquinone concentration on the observed first-order rate constant for Fenton-dependent PCE disappearance. Initial conditions are given in Figure 3.2.6.

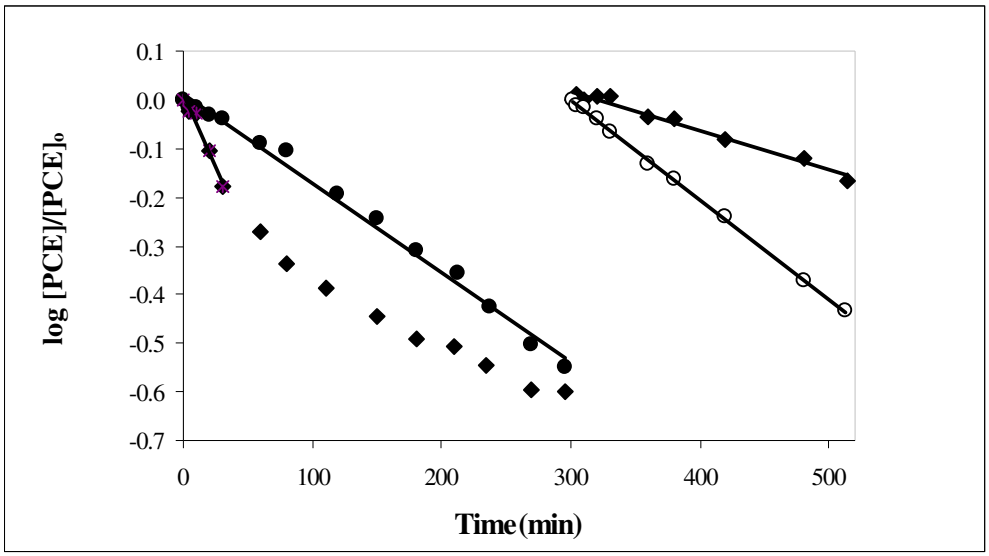

Figure 3.2.1-8. Effect of 0.3 mM BQ addition on the (log transformed) PCE concentration. Initial conditions: $[Fe(III)]_T$= 0.5 mM, $[PCE]_o$ = 1E-4 M, $[H_2O_2]_o$ = 0.10 M, pH = 2.0. PCE and H_2O_2 concentrations were restored to original levels after 300 minutes. The slopes for the segments of straight lines are 0.0018 min^{-1}(●) and 0.0020 min^{-1}(○) for the BQ-free reactors and 0.0055 min^{-1}(♦) and 0.0008 min^{-1}(◊) for BQ-amended reactors. Closed symbols indicate the original reactors.

Experiments with 9,10-anthraquinone-2,6-disulfonic acid (AQDS) produced similar results to the BQ and HQ trials. That is, the initial catalytic effect was quickly lost, and the AQDS-free control outperformed the amended reactor in the second phase of the experiment (Figure 3.2.1-9). It is apparent that addition of functional groups to the quinone did not enhance quinone longevity. Neither did the added functional groups make organic by-products from quinone destruction less effective radical scavengers. Again, the experiment highlights the practical limitations of quinone addition for enhancement of Fenton-driven destruction of hazardous organic compounds.

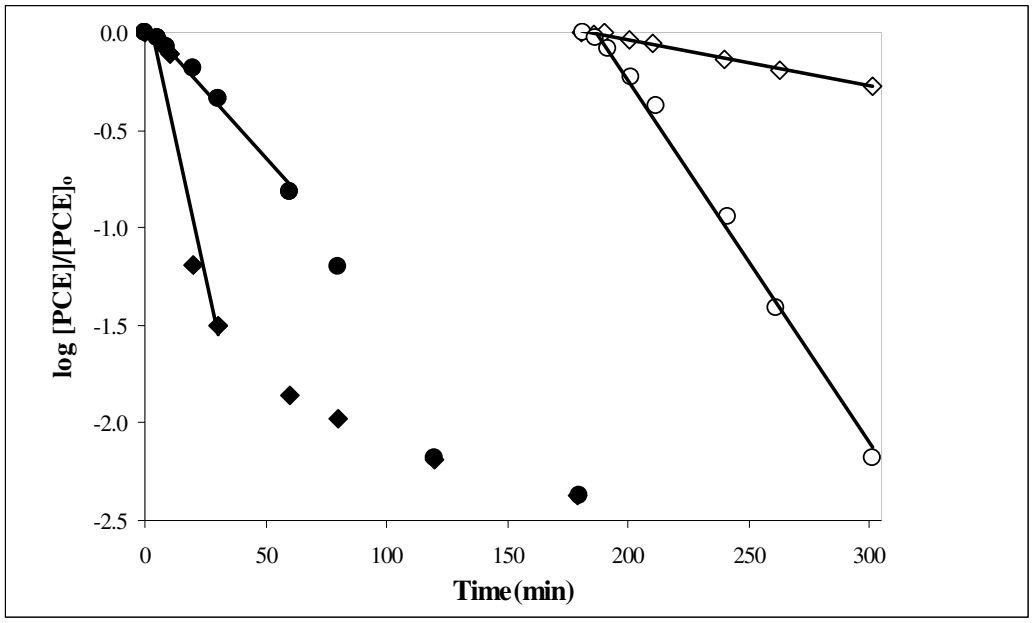

Figure 3.2.1-9. Effect of 0.5 mM AQDS addition to Fenton's reagents for PCE transformation. Log-transformed PCE data are on the ordinate. Initial conditions: $[Fe(III)]_T$=0.05 mM, $[H_2O_2]$=0.10 M, [PCE]=9.9×10^{-5} M, pH= 2.1. Initial PCE and H_2O_2 levels were restored after 180 minutes. The slopes for the segments of straight lines are 0.0126 min^{-1}(●) and 0.0186 min^{-1}(○) for the AQDS-free reactors and 0.0492 min^{-1}(♦) and 0.0024 min^{-1}(◊) for AQDS-amended reactors. Closed symbols indicate the original reactors.

3.2.2 Copper Effects

Based on the findings of Walling and Kato (1971), it was hypothesized that the presence of copper in solution can propagate hydroxyl radical chain reactions, possibly enhancing the rate of PCE destruction in homogeneous experiments. To test this hypothesis, initial experiments were conducted in which 0.0 or 4×10^{-3} M Cu(II) (Figure 3.2.2-1) was added to the aqueous-phase system that consisted of 5×10^{-4} M Fe(III), 0.10 M H_2O_2 and 10^{-4} M PCE. The initial pH was 2.1, and the experiment was conducted at room temperature. Negative controls contained 4×10^{-3} M Cu(II), but lacked either iron or

H_2O_2. In both controls, the loss of PCE was negligible over the 5-hour experiments. Rate dependence on copper concentration proved to be complex.

Unlike the quinone and hydroxylamine trials, PCE conversion kinetics remained first order throughout each experiment since copper was conserved during the radical generation and reaction process. Presumably the concentrations of copper species changed little over the course of the experiment, following establishment of near-steady conditions in the first minutes of each experiment.

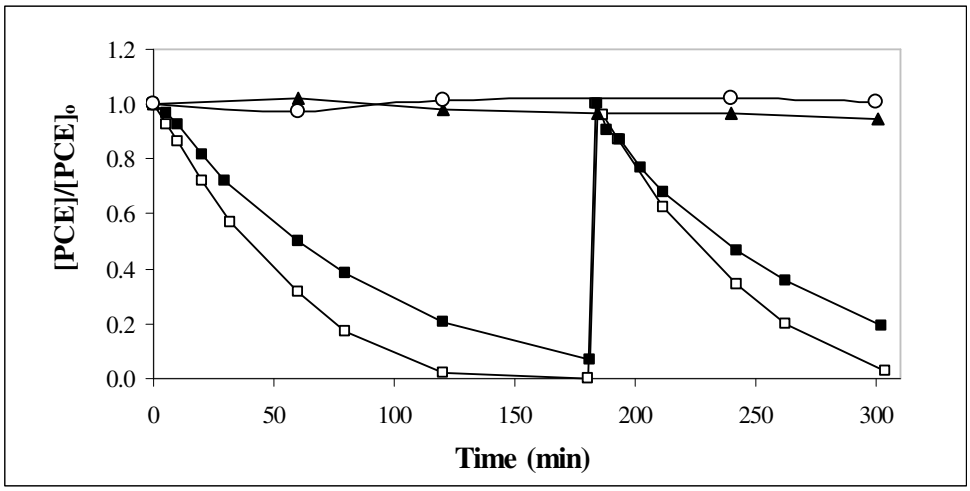

Figure 3.2.2-1. Effect of 4×10^{-3} M Cu(II) addition on the Fenton-driven rate of PCE destruction. Initial conditions: $[Fe(III)]_T$ = 0.5 mM, $[H_2O_2]_o$ = 0.10 M, [PCE] = 10^{-4} M, pH = 2.1, room temperature. At 180 minutes, PCE and H_2O_2 were added to the system to reestablish their initial conditions. Legend: no H2O2 (○), no iron (▲), no copper (■), copper and iron (□).

To evaluate the effect of copper as a possible Fenton metal another set of experiments was designed in which hydroxylamine was used to reduce Cu(II) to Cu(I). In these trials all reactors started with 30mM Cu(II) and $6x10^{-5}$ M PCE. To initiate the reaction, 60mM H_2O_2 was added to solution. Hydroxylamine was added 20 minutes after the H_2O_2. Negative controls contained Cu(II) but lacked either NH_2OH or H_2O_2. Neither PCE nor H_2O_2 was degraded in the control reactors. Complete PCE and H_2O_2 degradation was only observed in reactors that contained NH_2OH (Figure 3.2.2-2). Results suggest that Cu(II) does not react with H_2O_2 or that this reaction occurs very slowly, and that Cu(I) can react with H_2O_2 to produce •OH as indicated by PCE degradation data. Work by Yan (2006) shows that when isopropanol, an •OH scavenger, is added to a Fenton reaction mixture, PCE is not degraded suggesting that PCE reacts mainly with •OH in Fenton-driven systems.

The effect of varying Cu(II) concentrations on Fenton's reaction to degrade PCE was studied by adding 0 to 0.5mM Cu(II) to reactors containing 0.1 mM Fe(III), $10x10^{-5}$ M PCE and 0.10 M H_2O_2. The initial pH was 2.0 and the temperature was maintained at 30°C throughout the course of the experiment. At Cu/Fe molar ratios from 0.25-5, rates of PCE degradation were enhanced by copper addition. Process kinetics remained first-order in PCE, but the apparent first-order rate constant was increased nearly 3.5 times in reactors that contained Cu(II) at all concentrations except 0.075 mM Cu(II). At 0.075 mM Cu(II), the rate of PCE loss was approximately 3 times faster than that of the 0 M Cu(II) controls (Figure 3.2.2-3). Enhancement of the rate of PCE decomposition by

addition of Cu(II) was observed even at the lowest Cu(II) concentration tested (0.025mM).

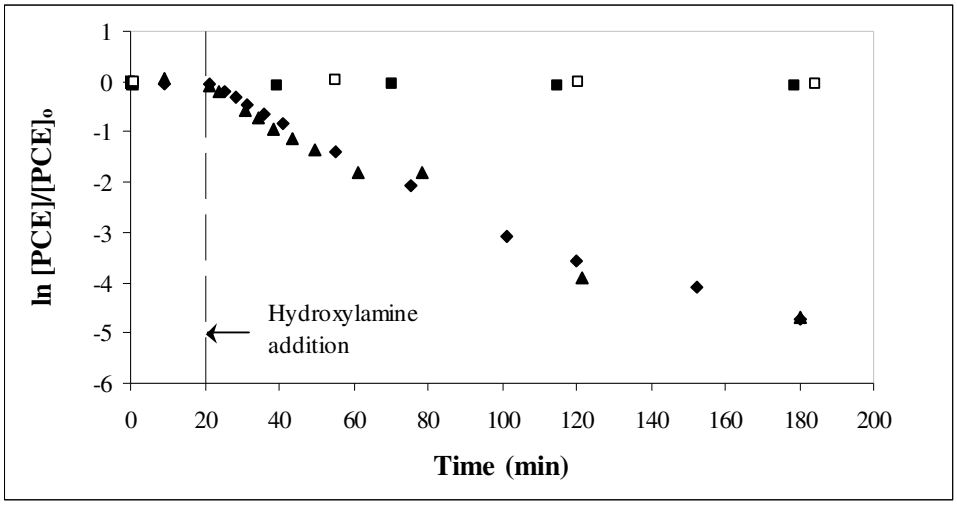

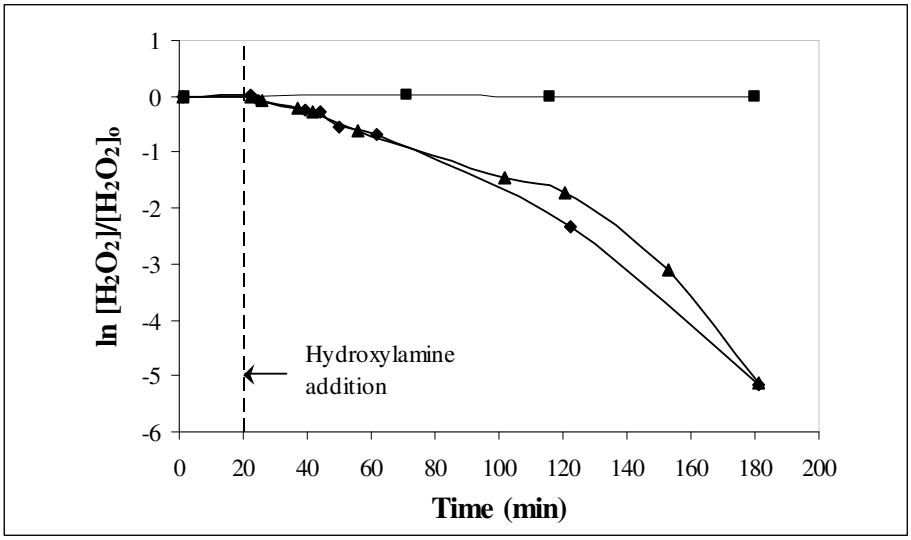

Figure 3.2.2-2(a)(b). PCE degradation and H_2O_2 loss in reactors containing Cu(II), H_2O_2 and PCE. Initial conditions: [Cu(II)]=30mM, [PCE]=$6x10^{-5}$ M, [H_2O_2]=60mM, [NH_2OH]=10mM (added after 20 min). Legend: Reactors with NH_2OH (♦,▲), without NH_2OH (■) or lacking both NH_2OH and H_2O_2 (□).

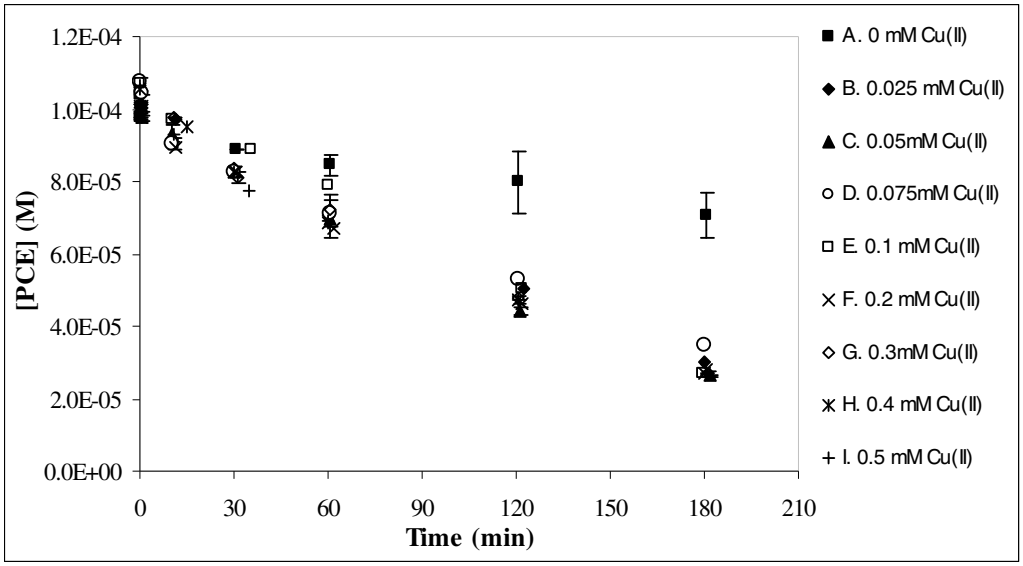

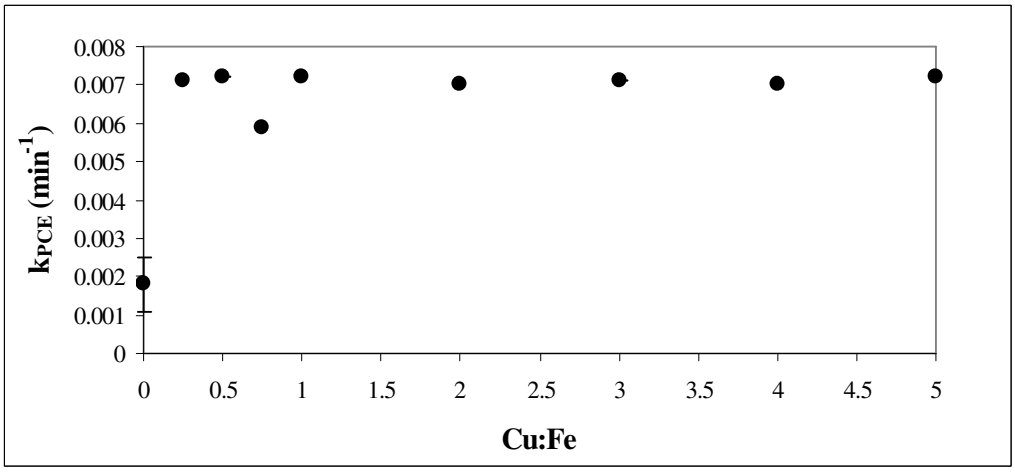

Figure 3.2.2-3(a)(b). Effect of Cu(II) addition on the pseudo-first-order rate constant for Fenton-driven PCE transformation. Initial conditions: (a) $[Fe(III)]_T$ = 0.1 mM, $[H_2O_2]_o$=0.10 M,$[PCE]_o$=10x10^{-5} M, [Cu(II)] from 0 to 0.5 mM, pH = 2.0, T = 30ºC. Ordinate values are the rate constants measured in the presence of copper at the molar Cu:Fe ratio indicated. Reactors were run in duplicate for [Cu(II)]=0,0.05, and 0.3mM. Symbol indicates the average value. Error bars were calculated for some data points (n=2).

3.2.2.1 Mechanism of Rate Enhancement by Copper

The acceleration of PCE degradation by copper addition at Cu/Fe ratios of 0.25 to 5 can be explained in the following way. The reaction of Cu(II) with H_2O_2 may be very slow or not possible. This is supported by the lack of PCE degradation in iron-free mixtures that initially contained Cu(II), H_2O_2, and PCE. When both Cu and Fe were present, the superoxide radicals produced by the Fe-Fenton system may reduce the Cu(II) to Cu(I). The Cu(I) so formed may react directly with H_2O_2 or reduce Fe(III) to yield Fe(II), regenerating Cu(II) (Figure 3.2.2.1-1). In the Fenton's system without copper amendment, iron reduction limits the rate of hydroxyl radical generation. Thus, acceleration of ferrous iron production by copper addition would increase the overall rate of hydroxyl radical generation (both directly and indirectly), and thus the pseudo-first-order rate constant for PCE disappearance. That is, the following sequence of reactions would yield additional free radicals and accelerate PCE oxidation:

$$Fe(III) + H_2O_2 \rightarrow Fe(II) + HO_2\bullet + H^+ \qquad [3.2.2.1\text{-}1]$$

$$Cu(II) + HO_2\bullet/O_2\bullet^- \rightarrow Cu(I) + O_2 + H^+ \qquad [3.2.2.1\text{-}2]$$

$$Cu(I) + Fe(III) \leftrightarrow Fe(II) + Cu(II) \qquad [3.2.2.1\text{-}3]$$

$$Fe(II) + H_2O_2 \rightarrow Fe(III) + \bullet OH + OH^- \qquad [3.2.2.1\text{-}4]$$

$$Cu(I) + H_2O_2 \rightarrow Cu(II) + \bullet OH + OH^- \qquad [3.2.2.1\text{-}5]$$

Superoxide radicals produced in reaction 3.2.2.1-1, may reduce Cu(II) or another metal ion yielding molecular oxygen. The cuprous ion may also terminate the chain reaction that propagates the PCE conversion reaction. That is,

$$Cu(I) + R\bullet \rightarrow Cu\ (II) + R^- \qquad [3.2.2.1\text{-}6]$$

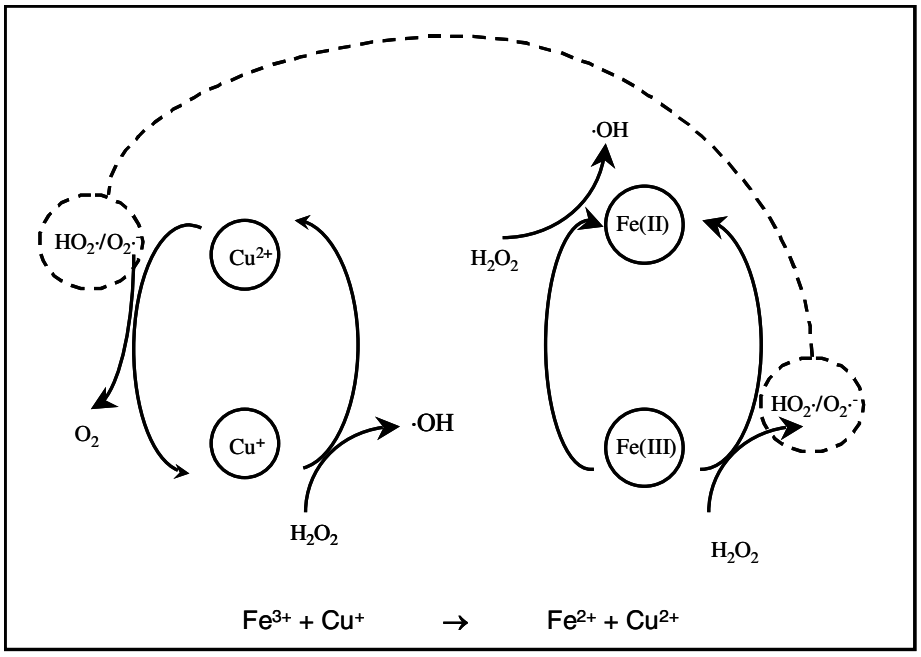

Figure 3.2.2.1-1. Schematic of the Mechanism of Rate Enhancement by Copper.

The ability of copper addition to accelerate PCE degradation is fairly modest (3.5x), at least at 32°C. Furthermore, copper-dependent effects on contaminant treatment kinetics may be greater at higher temperatures.

3.2.2.2 Temperature Effects

Dependence of the first-order rate constant for PCE disappearance on temperature was established for both copper-free and copper-amended reaction mixtures. It is apparent that the copper-dependent mechanism of PCE destruction is more sensitive to temperature than is the conventional (Cu-free) Fenton-driven mechanism. Arrhenius plots (Figure 3.2.2.2-1) corresponding to the Cu-free and Cu/Fe = 8:1 cases provided different activation energies and pre-exponential factors, indicating that the addition of copper to

the Fenton's reactants alters the mechanism of destruction, including the rate-limiting step. In the copper-free solution, at least, rate limitation is thought to arise from reduction of Fe(III)-peroxo complexes by H_2O_2. The greatest benefit of copper addition, in terms of accelerated PCE destruction was achieved in the highest temperature range investigated (40 – 54°C). At 54°C, the expected rate constant for PCE transformation was increased almost four-fold by copper addition at an 8:1 molar (Cu/Fe) ratio. At 30°C, rates with and without copper addition were essentially indistinguishable. Because Fenton's reaction is exothermic, reaction heat could enhance the benefits of copper addition to hydroxyl radical generation and PCE degradation rates. Iron was provided at nearly its solubility limit in these experiments (at pH 2.0 Fe(III) solubility is about $2x10^{-3}$ M). Therefore, acceleration of Fenton's reaction via further iron addition is infeasible. Thus, copper addition offers an attractive method for further enhancing reaction rates, particularly at higher temperatures.

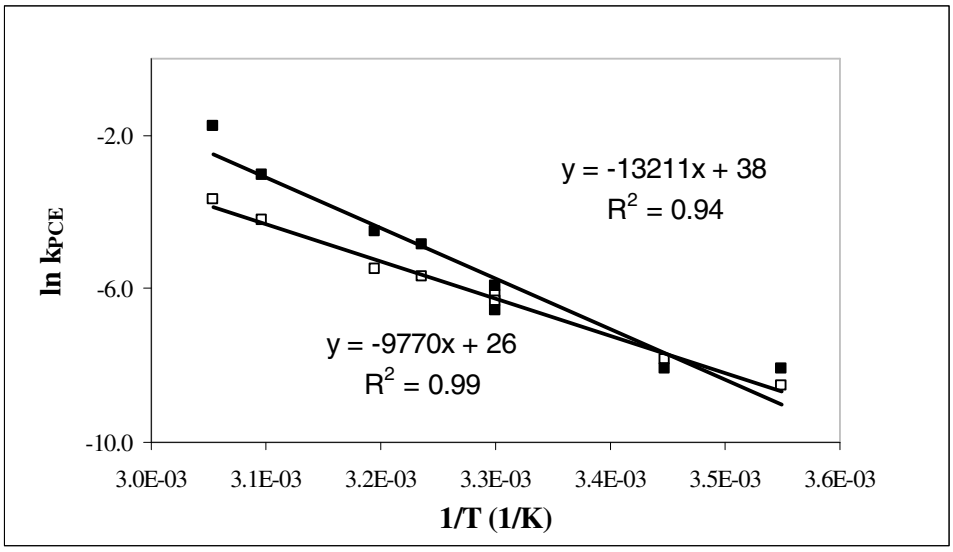

Figure 3.2.2.2-1. Arrhenius plots for copper-free and fixed Cu:Fe ratio (8:1) cases. Initial concentrations: $[Fe(III)]_T = 0.1$ mM, $[H_2O_2]_o = 0.10$ M, $[PCE]_o = 9.0\times10^{-5}$ M. Temperature range: 8.8-54.4°C. Symbols used: □ Fenton's system without copper and ■ Fenton's system with copper.

3.3 PCE Degradation Rate Enhancement - Summary and Conclusions

- Fenton-dependent tetrachloroethylene (PCE) degradation followed first order kinetics with a rate constant that was about proportional to total soluble iron. The reaction proceeded with essentially no lag following the addition of H_2O_2, indicating that near steady concentrations of iron species and hydroxyl radical were established quickly.
- Quinones are known electron shuttles that may facilitate iron reduction. 1,4-Hydroquinone (HQ), 1,4-benzoquinone (BQ) and 9,10-anthraquinone-2,6-disulfonic acid all initially increased PCE degradation in Fenton's system. The increase was proportional to the quinone concentration. However, as with hydroxylamine addition, the rate enhancement was not sustained, suggesting that

the quinones were gradually destroyed. The PCE degradation rate stabilized at a rate that was slower than that of the unamended Fenton's system suggesting that the by-products of quinone degradation may themselves retard the contaminant degradation rate.

- PCE degradation was negligible when Fe(III) was replaced with Cu(II) in the Fenton system. However, when both copper and iron were present at a Cu:Fe ratio of 0.25 to 5, the first order rate constant for PCE degradation increased by a factor of 3.5.
- PCE was degraded in the presence of copper only when hydroxylamine was used to reduce Cu(II) to Cu(I). The data suggest that Cu(I) can react with H_2O_2 to produce •OH. Other work (unpublished M.S. thesis Yan, 2006) has shown that when isopropanol is added to scavenge •OH, PCE is not degraded, suggesting that PCE transformation proceeds mainly via •OH radical attack.
- Analysis of potential chemical mechanisms accounting for copper effects suggests that Cu(II) is reduced to Cu(I) by $HO_2\bullet/O_2\bullet^-$ (produced in the iron-Fenton reaction) after which Cu(I) reduces Fe(III) to Fe(II). This sequence of reactions may provide a more rapid pathway for iron reduction than direct reaction with H_2O_2. Cu(I) may also react with H_2O_2 directly to produce •OH.
- The pseudo-first-order rate constant for PCE degradation increases more rapidly with increasing temperature in the copper:iron system than when iron alone is provided. Thus, the kinetic benefit of copper addition is greater in Fenton systems operated above ambient temperature.

4. HOMOGENEOUS MODEL FORMULATION

A mathematical model based on the kinetic model of De Laat and Gallard (1999) is presented in this section. The model describes the decomposition of hydrogen peroxide by iron in a homogeneous aqueous solution, taking into account the rapid formation and the slower decomposition of Fe(III)-hydroperoxo complexes ($Fe^{III}(HO_2)^{2+}$ and $Fe^{III}(OH)(HO_2)^{+}$). The objective of this modeling effort is to achieve a better understanding of the effect that the operational parameters in Fenton's reaction, such as pH and initial concentrations of H_2O_2 and iron, have on the utility of the system for degradation of organic toxins.

In Fenton's mechanism, successive reactions of hydrogen peroxide cycle iron between the plus two and plus three oxidation states, generating two radical species (•OH, and HO_2•/O_2•$^-$) in each cycle. The radicals produced are capable of oxidizing/reducing many organic targets per the following simplified mechanism:

$$Fe(III) + H_2O_2 \rightarrow Fe(II) + HO_2\bullet + H^+ \qquad [4.0\text{-}1]$$

$$Fe(II) + H_2O_2 \rightarrow Fe(III) + \bullet OH + OH^- \qquad [4.0\text{-}2]$$

$$\bullet OH + R \rightarrow OH^- + \bullet R \qquad [4.0\text{-}3]$$

4.1 Complexation with H_2O_2 and complex disproportionation – implication for pH effects on rate of reaction

Gallard *et al*. (1999) identified two ferric hydroperoxo complexes by spectrophotometric analysis. These two complexes are formed rapidly after mixing

Fe(III) and H_2O_2 in solution. The species are formulated as $[Fe^{III}]^{3+}(HO_2^-)$ (or $Fe^{III}(HO_2)^{2+}$; I_1) and $[Fe^{III}](OH)^{2+}$, (HO_2^-) (or $[Fe^{III}](OH)(HO_2)^+$; I_2), which are in acid base equilibrium ($K_{I1/I2}$ = 1.8 x10^{-4} M) (Table 4.1-1). Once generated, these species are assumed to decompose to Fe^{2+} and HO_2• (Table 4.1-1).

TABLE 4.1-1. Reaction Mechanism for Fe(III)-Catalyzed Decomposition of H_2O_2 (25 °C; *I* = 0.1 M)

No.	Reactions	constants
(1)	$Fe^{3+} + H_2O \leftrightarrow FeOH^{2+} + H^+$	K_1= 2.9 x 10^{-3} M
(2)	$Fe^{3+} + 2H_2O \leftrightarrow Fe(OH)_2^+ + 2H^+$	K_2= 7.62 x 10^{-7} M^2
(3)	$2Fe^{3+} + 2H_2O \leftrightarrow Fe_2(OH)_2^{4+} + 2H^+$	$K_{2,2}$ = 0.8 x 10^{-3}M
(4)	$Fe^{3+} + H_2O_2 \leftrightarrow Fe^{III}(HO_2)^{2+} + H^+$	KI_1 = 3.1 x 10^{-3}
(5)	$FeOH^{2+} + H_2O_2 \leftrightarrow Fe^{III}(OH)(HO_2)^+ + H^+$	KI_2 = 2.0 x 10^{-4}
(6a)	$Fe^{III}(HO_2)^{2+} \rightarrow Fe^{2+} + HO_2$•	$k_{6,I1}$ = 2.7 x 10^{-3} s^{-1}
(6b)	$Fe^{III}(OH)(HO_2)^+ \rightarrow Fe^{2+} + HO_2$• + OH^-	$k_{6.I2}$ = 2.7 x 10^{-3} s^{-1}
(7)	$Fe^{2+} + H_2O_2 \rightarrow Fe^{3+}$ + •OH + OH^-	k_7 = 63.0[a] M^{-1} s^{-1}
(8)	Fe^{2+} + •OH $\rightarrow Fe^{3+} + OH^-$	k_8 = 3.2 x 10^8 M^{-1} s^{-1}
(9)	•OH + $H_2O_2 \rightarrow HO_2$• + H_2O	k_9 = 3.3 x 10^7 M^{-1} s^{-1}
(10a)	$Fe^{2+} + HO_2$• $\rightarrow Fe^{III}(HO_2)^{2+}$	k_{10a} = 1.2 x 10^6 $M^{-1}s^{-1}$
(10b)	$Fe^{2+} + O_2^{\bullet-} + H^+ \rightarrow Fe^{III}(HO_2)^{2+}$	k_{10b} = 1.0 x 10^7 M^{-1} s^{-1}
(11a)	Fe(III) + HO_2• $\rightarrow Fe^{2+} + O_2 + H^+$	k_{11a} < 2 x 10^3 M^{-1} s^{-1}
(11b)	Fe(III) + $O_2^{\bullet-} \rightarrow Fe^{2+} + O_2$	k_{11b} = 5 x 10^7 M^{-1} s^{-1}
(12a)	HO_2• $\rightarrow O_2^{\bullet-} + H^+$	k_{12a} = 1.58 x 10^5 s^{-1}
(12b)	$O_2^{\bullet-} + H^+ \rightarrow HO_2$•	k_{12b} = 1 x 10^{10} M^{-1} s^{-1}
(13a)	HO_2•+ HO_2• $\rightarrow H_2O_2 + O_2$	k_{13a} = 8.3 x 10^5 M^{-1} s^{-1}
(13b)	HO_2• + $O_2^{\bullet-} + H_2O \rightarrow H_2O_2 + O_2 + OH^-$	k_{13b} = 9.7 x 10^7 M^{-1} s^{-1}
(14a)	•OH + HO_2• $\rightarrow H_2O + O_2$	k_{14a} = 0.71 x 10^{10} M^{-1} s^{-1}
(14b)	•OH + $O_2^{\bullet-} \rightarrow OH^-$+ O_2	k_{14b} = 1.01 x 10^{10} M^{-1} s^{-1}
(15)	•OH + •OH $\rightarrow H_2O_2$	k_{15} = 5.2 x 10^9 M^{-1} s^{-1}

NOTE: [a] Apparent second-order rate constant for the reaction of H_2O_2 with Fe(II) at pH < 3.5.
SOURCE: De Laat and Gallard, 1999. De Laat and Gallard (1999) fit k_6 to the experimental data (pH <3.5), where I_1 is the predominant Fe(III)-hydroperoxy complex.

The reaction rate constants and the equilibrium constants for the species involved in the Fenton's reaction and included in the model are listed in Table 4.1-1. Reactions (1) to (5) are sufficiently fast to be at equilibrium in this application.

In a constant volume batch system, the reactions listed in Table 4.1-1 lead to the following mass balances:

$$d[Fe^{2+}]/dt = k_6([I_1]+ [I_2]) - k_7[Fe^{2+}][H_2O_2] - k_8[Fe^{2+}][\bullet OH] - k_{10a}[Fe^{2+}][HO_2\bullet] - k_{10b}[Fe^{2+}][O_2\bullet^-] + k_{11a}[Fe(III)][HO_2\bullet] + k_{11b}[Fe(III)][O_2\bullet^-] \quad [4.1\text{-}1]$$

$$d[Fe(III)]_T/dt = -d[Fe^{2+}]/dt \quad [4.1\text{-}2]$$

$$d[H_2O_2]/dt = - k_7[Fe^{2+}][H_2O_2] - k_9[H_2O_2][\bullet OH] + k_{13a}[HO_2\bullet][HO_2\bullet] + k_{13b}[O_2\bullet\text{-}][HO_2\bullet] + k_{15}[\bullet OH]^2 \quad [4.1\text{-}3]$$

$$d[\bullet OH]/dt = k_7[Fe^{2+}][H_2O_2] - k_8[Fe^{2+}][\bullet OH] - k_9[H_2O_2][\bullet OH] - k_{14a}[\bullet OH][HO_2\bullet] - k_{14b}[\bullet OH][O_2\bullet^-] - 2k_{15}[\bullet OH]^2 \quad [4.1\text{-}4]$$

$$d[HO_2\bullet]/dt = k_6([I_1]+[I_2]) + k_9[H_2O_2][\bullet OH] - k_{10a}[Fe^{2+}][HO_2\bullet] - k_{11a}[Fe(III)][HO_2\bullet] - k_{12a}[HO_2\bullet] + k_{12b}[O_2\bullet^-][H^+] - 2k_{13a}[HO_2\bullet]^2 - k_{13b}[O_2\bullet^-][HO_2\bullet] - k_{14a}[\bullet OH][HO_2\bullet] \quad [4.1\text{-}5]$$

$$d[O_2\bullet^-]/dt = -k_{10b}[Fe^{2+}][O_2\bullet^-] - k_{11b}[Fe(III)][O_2\bullet^-] + k_{12a}[HO_2\bullet] - k_{12b}[O_2\bullet^-][H^+] - k_{13b}[O_2\bullet^-][HO_2\bullet] - k_{14b}[\bullet OH][O_2\bullet^-] \quad [4.1\text{-}6]$$

The total concentration of Fe(III) and the concentration of non-hydroxy Fe(III) species are given by:

$$[Fe(III)]_T = [Fe(III)] + [I_1] + [I_2] \quad [4.1\text{-}7]$$

$$[Fe(III)] = [Fe^{3+}] + [FeOH^{2+}] + [Fe(OH)_2^+] + 2[Fe_2(OH)_2^{4+}] \quad [4.1\text{-}8]$$

The system of nonlinear ordinary differential equations was solved numerically using the fourth-order Runge-Kutta method. Steady-state conditions were assumed for the rate of radical species ($d[\bullet OH]/dt = d[HO_2\bullet]/dt = d[O_2\bullet^-]/dt = 0$) and the resulting system of nonlinear equations was solved using Newton's method. The reaction parameters (pH, $[H_2O_2]_o$, $[Fe(III)]_o$), rate constants and equilibrium constants were specified as inputs to the program. The concentration - time profiles for H_2O_2, and Fe^{2+} were calculated by the

program, and the concentration of H_2O_2 predicted by the model was compared to experimental measurements and/or published data when available.

4.2 Model limitations

Precipitation reactions of Fe(III) have not been incorporated in the model, hence the model should not be applied in situations for which Fe(III) precipitation is expected or observed (typically pH> 3.0).

One major limitation of the model is the numerous parameters used, which cannot be determined independently.

Differences between the experimental conditions in our study and those employed in the investigation by De Laat and Gallard (1999) are worth mentioning. De Laat and Gallard conducted their kinetic study at 25.0°C and ionic strength = 0.1 M ($HClO_4/NaClO_4$), while our experiments were performed at 31±1°C (water bath), and the ionic strength varied from trial to trial but was typically about 0.02 M. In contrast to De Laat and Gallard's use of ferric perchlorate salt, ferric sulfate salt was used in all experiments and the pH was adjusted using sulfuric acid (H_2SO_4), to avoid adding background chloride in the system. In Fenton's reaction, destruction of chlorinated compounds results in accumulation of chloride ions in solution. Therefore, ferric sulfate was chosen over ferric chloride for iron addition, to avoid the complication of a high initial chloride ion concentration when attempting to sort out chloride effects. In addition, a rate constant for the reaction of the hydroxyl radical and sulfate was found in the

literature (3.5 x 10^5 $Lmol^{-1}s^{-1}$, Radiation Chemistry Data Center, 2003). No value was found for the hydroxyl radical and perchlorate reactions.

4.3 Inorganic Radical Formation

4.3.1 Chloride, perchlorate, sulfate and nitrate

De Laat *et al*. (2004) studied the effect of chloride, perchlorate, sulfate and nitrate ions on the rate of decomposition of H_2O_2 and transformations of organic compounds (atrazine, 4-nitrophenol, and acetic acid) by Fenton's reaction. They observed that the rates of reaction between iron (added as Fe(II)) and H_2O_2 were increased by specific anions. Relative effects were in the order of $SO_4^{2-}>ClO_4^-=NO_3^-=Cl^-$. When iron was provided as Fe(III), sulfate and chloride decreased both the decomposition rate of H_2O_2 and the rate of disappearance of specific organic targets. It was suggested that the latter observation was due to decreased formation of Fe(III) - hydroperoxy complexes, and that H_2O_2 does not complex with Fe(III)-sulfato complexes (De Laat and Giang Le, 2005). The pseudo-first-order kinetic constant (k_{obs}) for the initial rate of decomposition of H_2O_2 by Fe(III) decreased by 30%, and almost 20% of the iron was complexed as sulfato-Fe(III) at pH 2.0, I = 0.2 M, $[SO_4^{2-}]$ = 2 mM (lowest concentration studied in the range 0-200 mM). Almost complete inhibition of the rate was observed at $[SO_4^{2-}]$ = 67 mM, where 93% of iron was complexed with sulfate (De Laat and Giang Le, 2005). Nevertheless, under our experimental conditions, sulfate ($[SO_4^{2-}]$ = 1.5 mM) effects on H_2O_2 decomposition were not evident.

In the study by De Laat et al. (2004), inhibitory effects observed in the presence of chloride (100 mM) or sulfate (33.33 mM) were explained by a decrease in the

hydroxyl radical production rate due to the formation of non-reactive (with H_2O_2) Fe(III) complexes and the formation of inorganic radicals from •OH (SO_4•$^-$ and Cl_2•$^-$) that are less reactive than •OH. The same study suggested that kinetic models validated in $NaClO_4/HClO_4$ solutions should not be used to predict Fenton reaction rates in the presence of chloride and sulfate. Moreover, De Laat and Giang Le (2006) recently showed that in the presence of 50 mM chloride, 20% of the Fe(III) was complexed by the Cl^-, decreasing the H_2O_2 degradation rate by 23%.

Tables 4.3.1-1 through 4.3.1-3 provide reaction rates for the decomposition of hydrogen peroxide and the fraction of Fe(III) that is complexed with the different anions at the concentrations given.

Table 4. 3.1-1. Apparent first-order rate constant for the decomposition of H_2O_2 (k_{obs})

Anion	[Fe(III)] (μM)	[H_2O_2] (mM)	[Anion] (mM)	Complexes Fe(III) (%)	k_{obs} (min^{-1})
Perchlorate	200	10	100	0	$4.67x10^{-3}$
Nitrate	200	10	100	0	$4.66x10^{-3}$
Chloride	200	10	100	21.0	$3.95x10^{-3}$
Sulfate	200	10	33.33	83.7	$7.37x10^{-4}$

Source: De Laat et al., (2004)

Table 4.3.1-2. Measured Pseudo-First-Order Kinetic Constants (k_{obs}) for the Initial Rate of Decomposition of H_2O_2 –Sulfate effect

I(M)	$[SO_4^{2-}]_o$ mM	$[H^+]_o$ (mM)	$[Fe(III)]_o$ mM	$[H_2O_2]_o$ (mM)	pH	Complexes Fe(III) (%)	k_{obs} (10^{-5} s^{-1})	([•OH]/[SO_4•$^-$])
0.2	0	10	1.0	49.9	2.00	0	10.46	
0.2	2	10	1.0	50.0	2.01	19.6	8.04	4418
0.2	5	11	1.0	50.1	2.00	38.8	5.78	1688
0.2	10	11.5	1.0	49.7	2.01	57.3	4.02	855
0.2	20	13.5	1.0	49.4	2.01	74.6	2.41	419
0.2	40	19	1.0	49.3	2.00	87.0	1.25	193
0.2	66.67	25	1.0	48.9	2.01	92.8	0.79	114
0.6	200	40	1.0	48.5	2.02	97.7	0.53	51

Note: T = 25.0±0.5°C; ionic strength adjusted with $NaClO_4$.
Source: De Laat and Giang Le (2005).

Table 4.3.1-3. Measured Pseudo-First-Order Kinetic Constants (k_{obs}) for the Initial Rate of Decomposition of H_2O_2 –Chloride effect

I(M)	$[Cl^-]_T$ mM	$[Fe(III)]_o$ mM	$[ClO_4^-]_o$ (mM)	$[H_2O_2]_o$ (mM)	pH	Complexes Fe(III) (%)	k_{obs} (10^{-5} s^{-1})	($[Cl_2\bullet^-]/[\bullet OH]$)
0.2	0	1.0	200	49.9	2.00	0	10.46	0
0.2	50	1.0	150	49.5	2.00	17.2	8.07	$6x10^2$
0.2	100	1.0	100	49.7	2.00	30.6	6.80	$1.6x10^2$
0.2	200	1.0	0	50.2	2.02	49.6	5.12	$3.8x10^3$
0.2	400	1.0	0	50.5	2.02	49.6	5.16	$3.8x10^3$
0.4	500	1.0	0	48.2	2.00	65.5	3.81	$8.4x10^3$
0.5	800	1.0	0	47.5	2.00	71.2	3.56	$1.1x10^4$
0.8	1000	1.0	0	48.6	1.92	84.5	2.67	$1.8x10^4$

Note: $[[HClO_4]_o$ = 10 mM in all experiments.
Source: De Laat and Giang Le (2006).

4.3.2 Carbonate ($CO_3^{\cdot -}$) and carboxyl ($CO_2^{\cdot -}$) radicals

Carbonate system effects may be important in reactions involving oxygen containing free radicals. Michelson and Maral (1983) reported an increase in the oxidation of luminal by hydrogen peroxide in the presence of bicarbonate and carbonate anions. The following mechanism was proposed:

$$H^+ + O_2^{\cdot -} + HCO_3^- \rightarrow CO_3^{\cdot -} + H_2O_2 \qquad [4.3.2\text{-}1]$$

$$2H^+ + 2O_2^{\cdot -} \rightarrow H_2O_2 + O_2 \qquad [4.3.2\text{-}2]$$

$$H_2O_2 + CO_3^{2-} \rightarrow HO^{\cdot} + HO^- + CO_3^{\cdot -} \qquad [4.3.2\text{-}3]$$

The increase in luminal destruction was attributed to reaction with the carbonate radical. The carbonate radical is much less reactive than the hydroxyl radical, but enjoys a relatively long lifetime (Michelson and Maral, 1983).

Both the superoxide and hydroxyl radicals (produced in the Fenton's reaction) are able to react with carbonate ions (CO_3^{2-}) to produce carbonate radicals ($CO_3^{\cdot -}$).

$$CO_3^{2-} + \cdot OH \rightarrow CO_3^{\cdot -} + HO^- \qquad [4.3.2\text{-}4]$$

In addition, reduction of carbonate by superoxide radical can produce formate radicals:

$$H^+ + CO_3^{2-} + O_2^{\cdot -} \rightarrow CO_2^{\cdot -} + O_2 + HO^- \qquad [4.3.2\text{-}5]$$

However, the formate radical so formed further reacts to reform carbonate radical via:

$$H^+ + CO_3^{2-} + CO_2^{\cdot -} \rightarrow CO_3^{\cdot -} + HCOO^- \qquad [4.3.2\text{-}6]$$

Thus, each pathway yields carbonate radicals from superoxide radicals.

The formate radical anion ($CO_2^{\cdot -}$) is widely used in free-radical studies due to its ease of formation in aqueous solutions by ionizing radiation, and its excellent reductive properties [$E(CO_2/CO_2^{\cdot -})$=-1.9V] (Flyunt et al., 2001) (Table 4.3.2-1). The product of the bimolecular decay of $CO_2^{\cdot -}$ depends strongly on the pH of the solution with an inflection point at pH 3.8. In acidic solution, CO_2 is the main product, while in neutral to basic solution oxalate is dominant. To explain the dependence of product formation on pH, Flyunt et al. (2001) proposed that $CO_2^{\cdot -}$ radicals react mainly (>90%) by head-to-tail recombination to form an intermediate. In this mechanism, rearrangement of the intermediate competes with the proton-assisted disproportionation reactions.

Table 4.3.2-1. Carboxyl Radical Anion, $CO_2^{\cdot -}$, Properties

$E(CO_2/CO_2^{\cdot -})$	-1.9V
$pKa(\cdot CO_2H)$[1]	2.3
Bimolecular decay rate constant[2]	$2k \approx 1.4 \times 10^9$ $dm^3mol^{-1}s^{-1}$
Products[3]	CO_2 and oxalate anion

Note: [1]determined by pulse radiolysis with conductometric detection, [2]independent of pH in the range 3-8 at constant ionic strength, [3]depend on pH.
Source: Flyunt et al., 2001.

The carboxyl radical has also been reported to enhance HCOOH oxidation kinetics by assisting in the redox cycling of iron (Duesterberg et al., 2005).

$$CO_2^{\cdot -} + Fe(III) \rightarrow CO_2 + Fe(II) \qquad [4.3.2\text{-}7]$$

In the absence of oxygen, Fe(II) concentrations are higher due to the absence of autoxidation, which leads to higher steady-state hydroxyl radical concentrations in Fenton-driven systems. However, in the presence of oxygen (air-saturated solutions) rate enhancement is diminished by competition for the organic intermediates. With O_2 present, the carboxyl radical reacts at diffusion-limited rates to yield CO_2 and superoxide radicals

$$CO_2^{\cdot -} + O_2 + H^+ \rightarrow CO_2 + HO_2^{\cdot}/O_2^{\cdot -} \qquad [4.3.2\text{-}8]$$

Oxygen is the primary carboxyl radical scavenger. The superoxide radicals produced can then reduce Fe(III) or oxidize Fe(II) in the Fenton system. In the presence of oxygen, organic radicals are converted into species that can both oxidize and reduce Fe. Under anoxic conditions, only reducing species are available.

The large difference in species profiles between air-saturated and deaerated experiments demonstrates that oxygen reactions should be included in the kinetic models to accurately simulate system behavior. However, under this project's experimental conditions, oxygen is always present in the aqueous solutions (see oxygen generation section). Thus, the effect of the carboxyl radical is not likely to be significant in our system.

4.3.3 Radical formation kinetics and reactivity

Hydroxyl radical scavenging by bicarbonate (HCO_3^-) or carbonate (CO_3^{2-}) should not have been an issue in project's trials due to the low pH. At a pH <3, both ions are present at low concentrations.

Hydroxyl radical reaction rates with perchlorate are not available in the literature. If a perchlorate radical is formed by reaction, it does not affect the rate of hydrogen peroxide decomposition by either Fe(II) or Fe(III), as discussed above. Even though, nitrate radicals can be formed by reaction of hydroxyl radicals with nitric acid ($k_{OH,HNO3} = 5.3x10^7\ M^{-1}\ s^{-1}$, www.rcdc.nd.edu), their formation does not affect the rate of reaction in the Fenton's system.

Hydroxyl radical reaction rates with sulfate, hydrogen peroxide, chloride and PCE under conditions expected here are compared in Table 4.3.3-1. The data indicate that hydroxyl radicals are consumed mainly by reacting with hydrogen peroxide, PCE, and chloride (produced from PCE dechlorination) and to a much lesser extent, sulfate. Hence, the computer modeling efforts neglected sulfate effects on •OH.

Table 4.3.3-1. Rate Constants for Potential Hydroxyl Radical Sinks

	$^*k_{OH}$, $M^{-1}\ s^{-1}$	Concentration, M	Rate, s^{-1}
SO_4^{2-}	$3.5x10^5$	$15x10^{-5}$	52.5
H_2O_2	$3.3x10^7$	0.1	$3.3\ x10^6$
Cl^-	$3.0x10^9$	$200x10^{-6}$	$6.0x10^5$
PCE	$2.0x10^9$	$50x10^{-6}$	$1.0\ x10^5$

Note: $[Fe(III)]_T$ = 0.1mM, $[SO_4^{2-}]=(3/2)[Fe(III)]_T$ since the source of sulfate in our experiments is the $Fe_2(SO_4)_3$, $[PCE]_o$ = 50μM, $[Cl^-]_o$=0 but $[Cl^-]_f = 4x[PCE]_o$ when mineralization is complete.
Source: *www.rcdc.nd.edu.

Moreover, typical groundwater concentrations of chloride and sulfate in Tucson, AZ where the field studies were conducted are 0.45 mM and 0.50 mM, respectively. At these concentrations, the effect of the anions on H_2O_2 consumption is insignificant, but buildup of chloride from the dechlorination of compounds like PCE/TCE may eventually interfere with •OH generation and degradation kinetics. Nitrate and perchlorate do not seem to affect the rate of H_2O_2 reactions in Fenton systems (De Laat et al., 2004). Typical groundwater concentrations of nitrate and perchlorate in Tucson, AZ are low - less than 1 mg/L and < 0.01 mg/L, respectively.

4.4 Model Applications

4.4.1 Simulation of H_2O_2 decomposition

The model used here was validated by applying it to published data from De Laat and Gallard (1999) for H_2O_2 decomposition for varying H_2O_2 initial concentrations at a fixed iron concentration (Figure 4.4.1-1). The model provides a good fit except for longer times (>18 hours). The rate limiting step in Fenton-dependent destruction of organic compounds is typically the disproportionation of the ferric hydroperoxy species ($k_{6,I1}$ and $k_{6,I2}$ of Table 4.4.1-1). In the De Laat and Gallard (1999) formulation, these rate constants were assumed to be equal, and their value was obtained by fitting their experimental data. However, experimental trials in that study were conducted at much higher ionic strengths and lower hydrogen peroxide concentrations than those used in the present work.

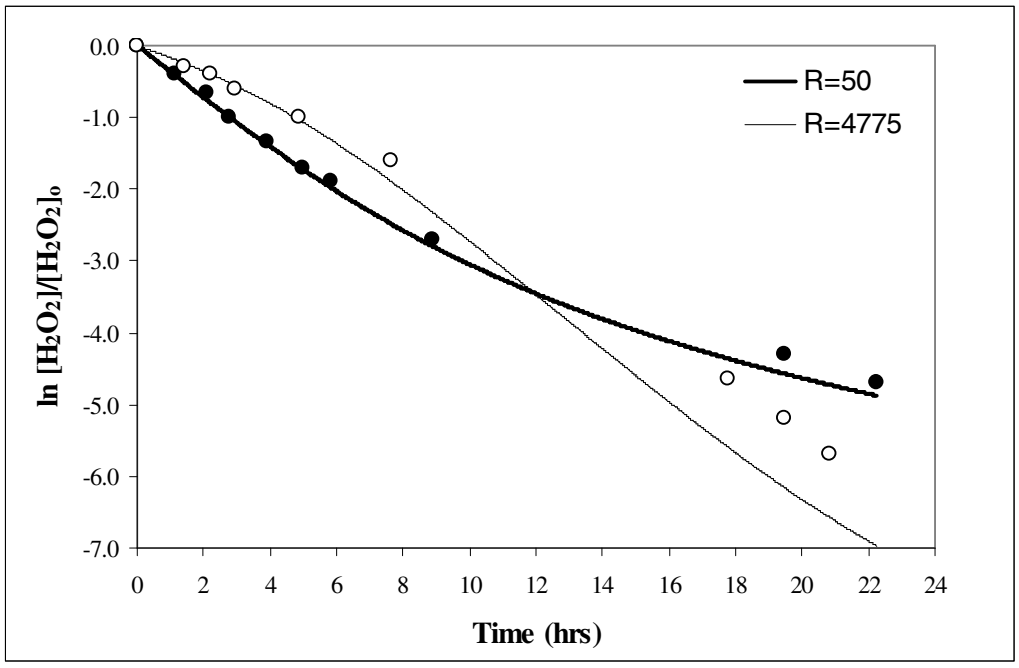

Figure 4.4.1-1. Simulation of H_2O_2 decomposition at initial concentrations of 0.01 and 0.955 M at constant Fe(III) concentration. Initial conditions: pH = 3.0 (25°C, I=0.1M; $R=[H_2O_2]_o/[Fe(III)]_o$, $[Fe(III)]_o=2x10^{-4}$ M. Data from De Laat and Gallard, 1999. Solid lines: model fits.

4.4.2 Effect of pH on the observed rate constant for decomposition of H_2O_2 by Fe(III)

The effect of pH on Fenton kinetics has been studied extensively (Burbano *et al*., 2005; Kremer, 2003; De Laat and Gallard, 1999). The apparent first-order rate constant (k_{obs}) for the decomposition of H_2O_2 by catalytic iron increases with pH in the range 1-3.2, but decreases above pH 3.2. This decrease can be attributed to the precipitation of Fe(III), as confirmed by measurements of dissolved Fe(III) concentrations (De Laat and Gallard, 1999).

In an effort to validate our mathematical model, the effect of pH on the observed first-order rate constant (k_{obs}) for the decomposition of H_2O_2 in Fenton's mixtures was simulated (Figure 4.4.2-1) and compared to data from De Laat and Gallard (1999).

This study's model produced similar results prior to pH 3, after which Fe(III) precipitation began. The model values for k_{obs} were obtained at t = 0. It is important to mention that decomposition of H_2O_2 did not follow first-order kinetics.

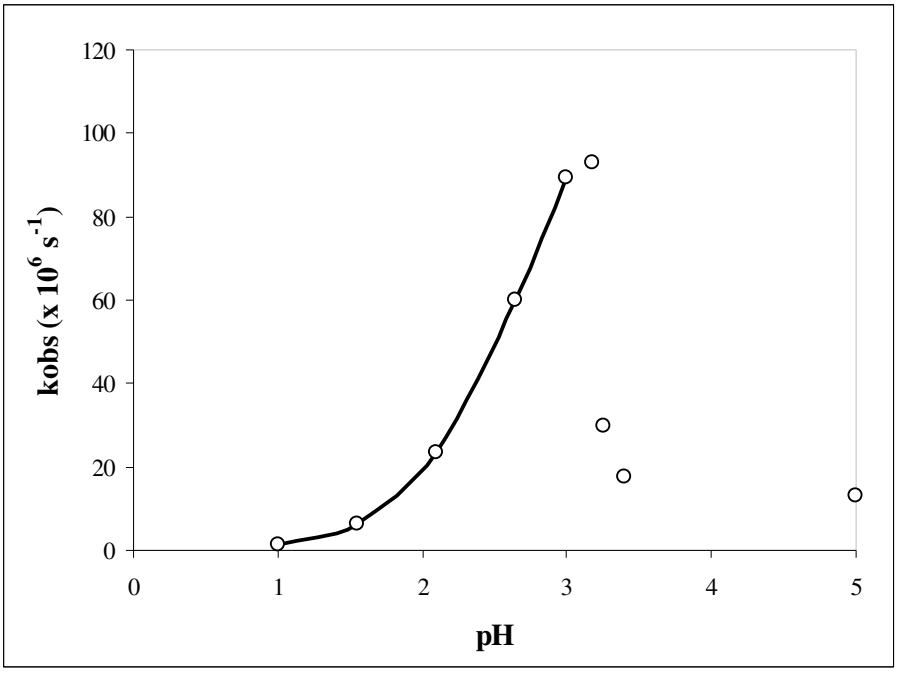

Figure 4.4.2-1. Computer simulation showing the effect of pH on the simulated first order rate constant for the decomposition of H_2O_2 by Fe(III) (solid line). Initial conditions: $[Fe(III)]_o$=200μM, $[H_2O_2]_o$=10mM. Data points (observations) were obtained from De Laat and Gallard (1999).

4.4.3 Degradation of non-halogenated organics in homogeneous systems

Table 4.4.3-1 shows hydroxyl radical reaction rate constants for various species. These constants were incorporated into the mathematical model to analyze the transformation rates of the target compounds. Duesterberg *et al*. (2005) studied the effect of oxygen and by-product formation on the oxidation rate of HCOOH in a Fenton's system with initial Fe(II) concentrations of 100-200 μM and H_2O_2

concentrations from 0.2 - 2.2 mM. It was reported that the intermediate, carboxyl radical, enhances oxidation efficiency by assisting in the redox cycling of iron. However, in the presence of molecular oxygen the improvement was attenuated.

In our experiments, we made no effort to remove oxygen as it was generated. The effect of the carboxyl radical was neglected at initial formic acid concentrations that were low relative to the dissolved oxygen concentration (DO_{sat} = 2.7x10^{-4} M at 25°C) (Duesterberg, et al. 2005). That is, under the experimental conditions employed in the simulation, the intermediate generated by reaction 1 (Table 4.4.3-1) is assumed to be oxidized immediately to CO_2. Therefore, a simplified version of the oxidation pathway of formic acid (Table 4.4.3-1) was included in our mathematical model to simulate formic acid degradation in Fenton's reaction (Figure 4.4.3-1). The mathematical model simulates satisfactorily the oxidation of HCOOH (Figure 4.4.3-1) as reported by Duesterberg et al (2005) in an Fe(II)/H_2O_2 system.

Table 4.4.3-1. Additional second order reaction rate constants for organic targets with •OH

No.	Reactions	constants
(1)	$\bullet OH + HCOOH \rightarrow CO_2 + HO_2\bullet/O_2\bullet^-$	k_{17} = 6.5 x10^8 M^{-1}s^{-1} [a]
(2)	$PCE + \bullet OH \rightarrow \bullet CCl_2CCl_2OH \rightarrow (CO_2 + HCl)$	k_{21} = 2.0 x 10^9 M^{-1}s^{-1} [b]
(3)	$Cl^- + \bullet OH \rightarrow ClOH^-$	k_{22} = 3.0 x 10^9 M^{-1}s^{-1} [b]
		k_{22} = 4.3 x 10^9 M^{-1}s^{-1} [c]

SOURCE: [a]Duesterberg et al., 2005; [b]www.rcdc.nd.edu; [c] Buxton et al., 1988.

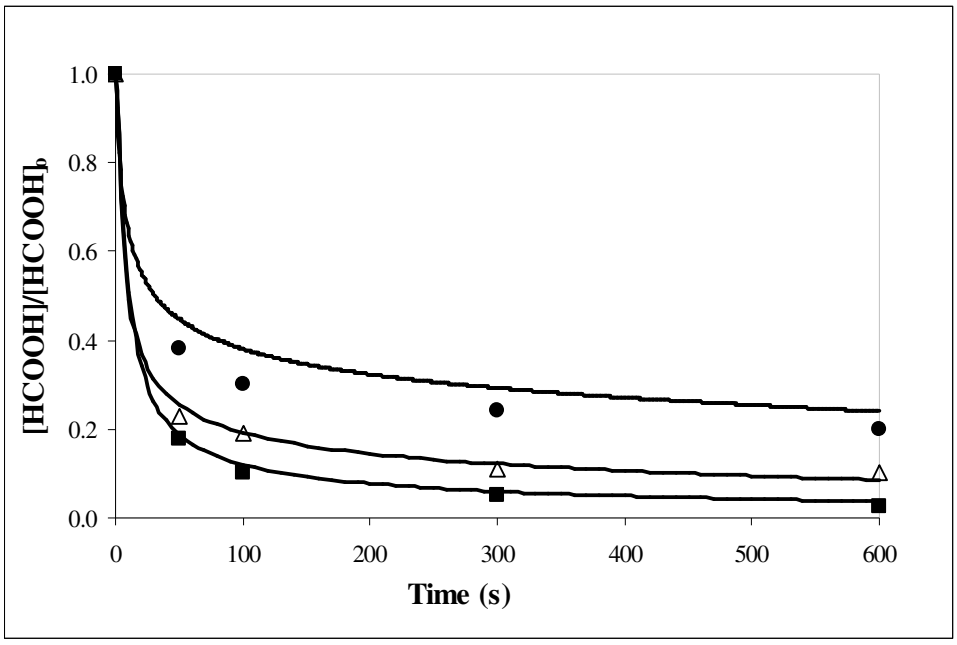

Figure 4.4.3-1. Computer simulation (solid lines) for the simplified oxidation of formic acid (HCOOH) in a H_2O_2/Fe(II) system (pH = 3). Experimental data (symbols) were obtained from Duesterberg et al., 2005. $[HCOOH]_o$=200 nM, $[H_2O_2]_o$=1.1 mM (■) or 2.2 mM (Δ,●),$[Fe(II)]_o$=200μM (■,Δ) or 100μM (●).

4.4.4 H_2O_2 and PCE degradation under our experimental conditions

Equilibrium and kinetic constants in Table 4.1-1 were obtained for ionic strength of 0.1 M and temperature 25 °C. Given the different experimental conditions employed here (generally, I = 0.02 M, T = 30 °C), direct use of the constants may not be possible without prior adjustment for ionic strength and temperature. Table 4.4.4-1 illustrates the expected dependence of the Fe(III) equilibrium constants on the ionic strength of the solution. Because the equilibrium constants for the Fe(III) species dominating in the sub-neutral pH range where the project trials were conducted are affected by factors of up to five, it is necessary that ionic strength corrections be incorporated in the modeling work.

Table 4.4.4-1. Equilibrium constants as a function of Ionic Strength

		ionic strength (M)					
Reaction		0	0.1	0.2	0.5	0.6	1
$Fe^{3+} + H_2O \leftrightarrow FeOH^{2+} + H^+$	$\log K_1$	-2.19	-2.63	-2.72	-2.79	-2.79	-2.72
$Fe^{3+} + 2H_2O \leftrightarrow [Fe(OH)_2]^+ + 2H^+$	$\log K_2$	-5.67	-6.33	-6.47	-6.57	-6.57	-6.47
$2Fe^{3+} + 2H_2O \leftrightarrow [Fe_2(OH)_2]^{4+}$	$\log K_{2,2}$	-2.95	-2.95	-2.95	-2.95	-2.95	-2.95

Source: De Laat and Giang Le, 2005.

The Davies equation was used to predict the activity coefficients in aqueous solution, which were used to adjust each constant for ionic strength variations. Detailed calculations are provided in appendix A.1.

The effect of temperature on reaction rate constants is analogous to its effect on equilibrium constants (Morel and Hering, 1993). In general, rate constants increase with increasing temperature. This dependence corresponds to the well-known Arrhenius equation:

$$k = A\exp(-E_a / RT) \qquad [4.4.4\text{-}1]$$

where E_a is the activation energy of the reaction and A is the preexponential factor.

From the Arrhenius plot (Figure 3.2.2.2-2),

$$\ln k(\min^{-1}) = -9770\left(\frac{1}{T(K)}\right) + 26 \qquad [4.4.4\text{-}2]$$

We can adjust the overall observed rate constant for PCE degradation and the rate-limiting rate constant (iron reduction) from a temperature of 25°C to our experimental conditions (T = 30°C). Table 4.4.4-2 shows the temperature corrections for the rate-limiting reactions in the model. However, temperature corrections were not used in the simulations shown in this chapter.

Table 4.4.4-2. Kinetic constants as a function of Temperature

Reaction	Constants	I (M)	Temperature (°C) 25*	30
$I_a \rightarrow Fe^{2+} + HO_2\bullet$	k_{13} (s^{-1})	0.1	$2.3x10^{-3}$	$3.95x10^{-3}$
$I_b \rightarrow Fe^{2+} + HO_2\bullet + OH^-$	k_{14} (s^{-1})	0.1	$2.3x10^{-3}$	$3.95x10^{-3}$
$I_a \rightarrow Fe^{2+} + HO_2\bullet$	k_{13}' (s^{-1})	$1.57x10^{-3}$	$1.36x10^{-3}$	$2.34x10^{-3}$
$I_b \rightarrow Fe^{2+} + HO_2\bullet + OH^-$	k_{14}' (s^{-1})	$1.57x10^{-3}$	$2.02x10^{-3}$	$3.47x10^{-3}$

SOURCE: *De Laat and Giang, 2005

4.4.4.1 Iron species distribution using MINEQL

The distribution of the iron species under the experimental conditions used here were determined using the program MINEQL. The first plot (Figure 4.4.4.1-1) shows the distribution of the species in water. The Fe^{3+} is the dominant species at low pH. Iron-hydroperoxy species are formed when H_2O_2 is added to the iron solution. Their formation is a function of both pH and H_2O_2 concentration (Figure 4.4.4.1-2). The distribution of the iron species does not changes significantly under our H_2O_2 experimental concentrations. It is expected, however, to observe higher I_1 (dominant species) concentrations at higher H_2O_2 concentrations. Addition of sulfate (added as $Fe_2(SO_4)_3$) affects the distribution of the iron species by complexing with iron to form $FeSO_4^+$ (among others). At pH 2, most of the iron remains in the free form (Fe^{3+} = 55.4%), 26% as $FeOH^{2+}$, 14.1% as $FeSO_4^+$, and 3.5% as I_1 (Figure 4.4.4.1-3). Because $FeSO_4^+$ is among the dominant species it is important to take into account the sulfate effect in our simulations. The sulfate species are distributed as 53.1% as SO_4^{2-}, 37.5% as HSO_4^-, 9.4% as $FeSO_4^+$. Sulfate anions may scavenge hydroxyl radicals and form sulfate radicals. These radicals may react with Fe(II) species in a non-productive way. Additional reactions in the presence of sulfate are detailed in Appendix A.2.

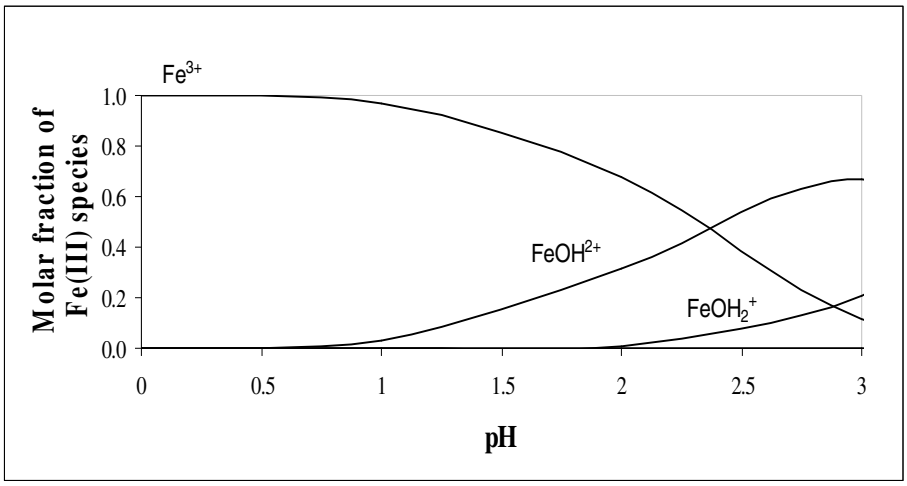

Figure 4.4.4.1-1. MINEQL Fe(III) species distribution in acidic aqueous solution. Initial conditions: [Fe(III)]=0.1mM, 25°C.

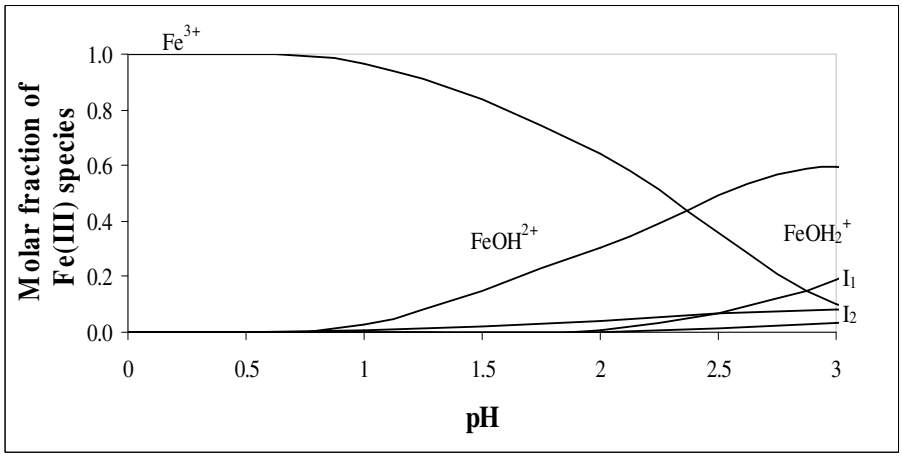

Figure 4.4.4.1-2. MINEQL Fe(III) species distribution in acidic aqueous solution in the presence of H_2O_2. Initial conditions: [Fe(III)]=0.1mM, [H_2O_2]=0.1M, 25°C**.**

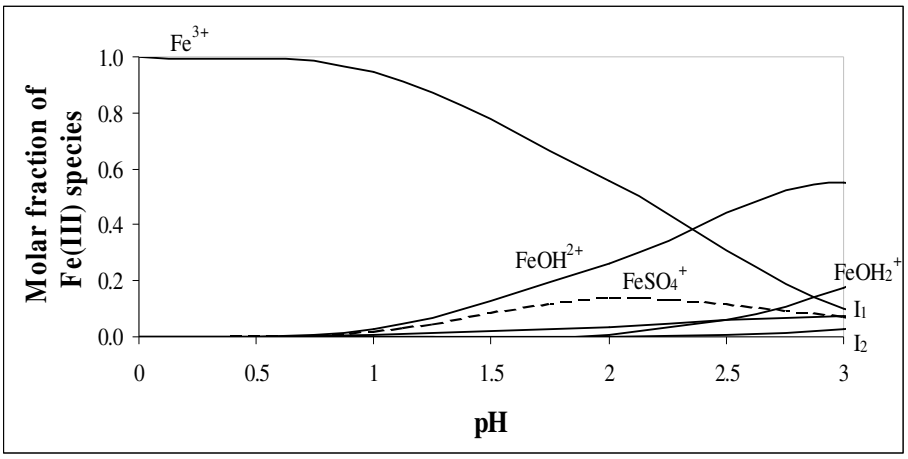

Figure 4.4.4.1-3. MINEQL Fe(III) species distribution in acidic aqueous solution in the presence of H_2O_2 and sulfate. Initial conditions: [Fe(III)]=0.1mM, $[H_2O_2]$=0.1M, $[SO_4^{2-}]$=0.15mM (from $Fe_2(SO_4)$ salt), 25°C. At pH 2: Fe^{3+} is 55.4%, $FeOH^{2+}$ is 26%, $FeSO_4^{+}$ is 14.1 and I_1 is 3.5%.

4.4.4.2 PCE destruction kinetics considering Cl^- effects

Degradation of PCE and other chlorinated solvents yields chloride ions that can accumulate in solution. Published second-order rate constants for the chloride ion reaction with the hydroxyl radical (reaction 3, 4.3.3-1) indicate chloride should be a significant, unavoidable radical scavenger in Fenton's destruction of chlorinated organics. Reported values for the rate constant for reaction of Cl^- with •OH are near that of PCE (Table 2.4.3-1 and 4.3.3-1). If mineralization is complete and the rate of production of chloride ion is four times the rate of PCE destruction, then the accumulation of chloride in the regenerant solution should be considered in terms of its effect on Fenton-dependent reactions.

In our model, the chloride ion is considered a conservative species. It reacts with the hydroxyl radical and generates a radical that does not participate in the organic degradation pathway, and then is regenerated by radical-radical reaction, resulting in

reestablishment of the chloride ion. Figure 4.4.4.2-1 shows the effect of different second-order reaction rate constants for the reaction of hydroxyl radical with the chloride ion. The literature value ($k = 3.0 \times 10^9$ $M^{-1}s^{-1}$) employed in this simulations was obtained in a system with $[Cl^-] = 1.2$ M (Grigor'ev *et al.*, 1987), which exceeds the range of concentrations studied here. The chloride rate constant was reported to decrease as $[Cl^-]$ increased in the range 3.5-12.2 M (Grigor'ev *et al.*, 1987). The lack of a reasonable model fit suggests that the literature value for the reaction constant may not be accurate at the much lower chloride concentrations of our experiments. Using k_{22} (rate constant for reaction of •OH and Cl^-, Table 4.3.3-1) as a fitting parameter, the model was applied to our experimental data to find reasonable empirical values for k_{22}. The data fall in between the simulation trials with k_{fit} of $0 - 3 \times 10^9$ $M^{-1}s^{-1}$. A k_{fit} value of 1.0×10^9 $M^{-1}s^{-1}$ is near optimal, as shown in Figure 4.4.4.2-1.

To further investigate chloride ion effects, PCE degradation experiments were conducted in which the initial chloride ion concentrations was varied from 0 – 0.058 M. Figure 4.4.4.2-2 shows the effect of chloride on the decomposition rate of PCE in Fenton's reaction. PCE loss decreases with increasing Cl^- concentration in the range 0 – 0.058 M Cl^-. At $[Cl^-]$=0.058 M, the observed first-order rate constant for PCE transformation was about one-fourth that of the chloride-free solution. The results show that the accumulation of chloride ion in the Fenton's solution can markedly decrease the rate of organic degradation.

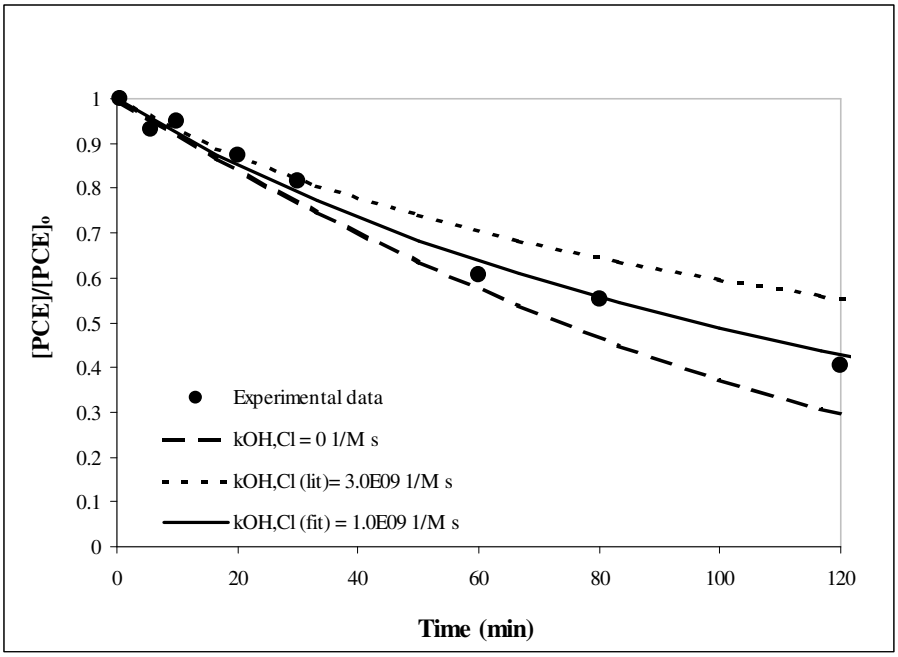

Figure 4.4.4.2-1. PCE degradation and model fits using various second-order •OH reaction rate constants ($k_{Cl,OH}$) for the reaction with Cl^- ion. The Cl^- is produced from PCE dechlorination and no Cl^- was added initially to the solution. Initial conditions: $[Fe(III)]_o$=0.1 mM, $[H_2O_2]_o$= 0.11 M, $[PCE]_o$=6.52E-5 M , pH = 2.0, T= 31±1°C. A literature value ($k_{Cl,OH} = 3.0 \times 10^9\ M^{-1}s^{-1}$), one k_{fit} and one neglecting the reaction of •OH with Cl^- were used for the simulation trials.

The oxidation of chloroalkenes such as PCE by •OH is expected to yield primarily mineralized products (CO_2 and HCl). No chlorinated intermediates were detectable via GC/ECD during the course of these experiments. There was no attempt to measure CO_2 evolution, however. Under these conditions, the accumulation of Cl^- due to target compound mineralization may eventually inhibit •OH-dependent pathways, as radical consumption by Cl^- begins to rival H_2O_2 as a sink for hydroxyl radicals**.** The accumulation of chloride in the regenerant due to the destruction of the target is a key aspect of the application of this process for the regeneration of chlorinated solvents adsorbed to the GAC. It is important to evaluate how much chloride would be added to a regenerating solution during one carbon recovery event and at what stage chloride

accumulation will matter. A simplistic, yet illustrative, approach is taken in Appendix A.3 to quantify the chloride accumulation from PCE destruction at the field-scale.

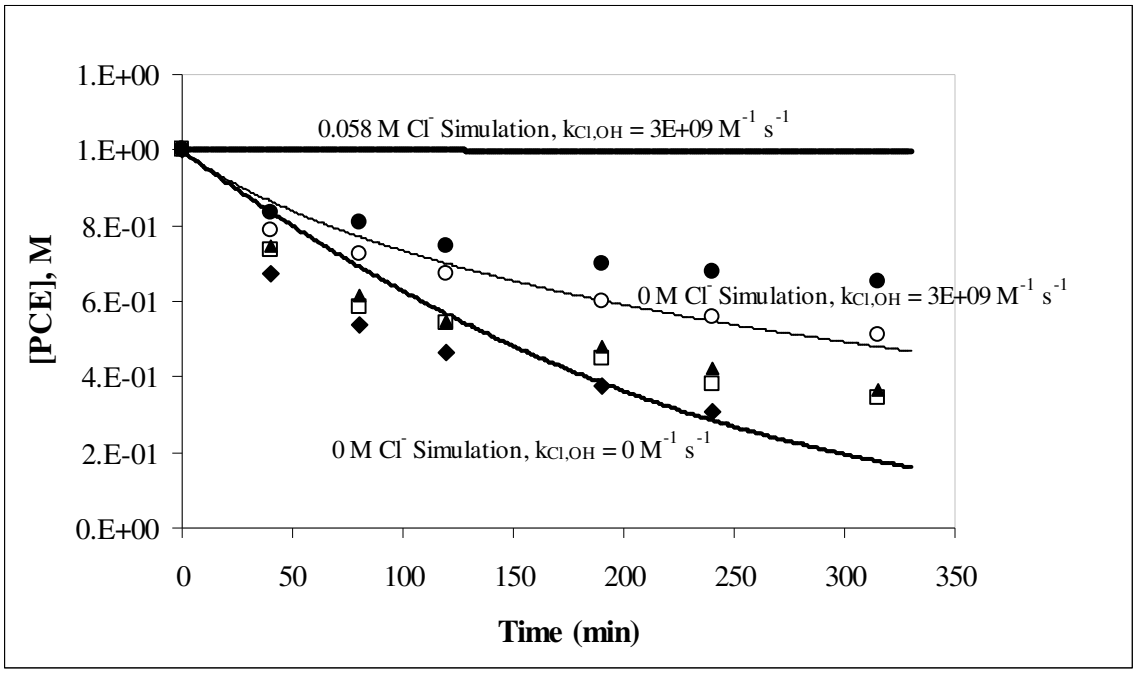

Figure 4.4.4.2-2. Effect of chloride ion concentration on the PCE degradation rate in Fenton's reaction. Initial conditions: $[Fe(III)]_o$ =0.09 mM, $[H_2O_2]_o$=0.11 M, $[PCE]_o$= 87 μM, pH = 2.0, T = 31±1°C. Chloride concentrations: 0 M (♦), 0.00198 M (□), 0.02 M (▲), 0.034M (○), and 0.058 M(●). Model simulations are shown by solid lines. Some lines were omitted for simplicity. Note: constants were corrected for the initial ionic strength only.

The reaction rate of chloride with the hydroxyl radical alone cannot fully explain the Cl^- effect observed (Figure 4.4.4.2-2). The literature rate constant ($k_{Cl,OH}$ = 3.0 x 10^9 M^{-1} s^{-1}) used in the mathematical model may not be appropriate for our experimental conditions, as discussed earlier in this section. Data and fit of the mathematical model for PCE degradation (accounting for reaction of Cl^- with •OH) were presented previously (Figure 4.4.4.2-2). The data fall between the simulation trials using k_{fit} of 0 – 3x 10^9 M^{-1} s^{-1}. A value to 1x 10^9 M^{-1} s^{-1} provided the best fit.

De Laat and Giang Le (2006) studied the effect of the chloride ion in Fenton's reaction. Its effect on the rate of H_2O_2 and organic degradation by Fenton's reaction is complex. Chloride complexes with iron in solution, changing the iron species distribution and can also scavenge hydroxyl radical to form halogen radical species (see appendix A.4 for reactions). Iron(III)-chlorocomplexes ($FeCl_2^+$ and $FeCl_2^+$) are the predominant Fe(III) species at [Cl^-] above 200 mM. The rate of decomposition of hydrogen peroxide decreases 49% at 200 mM Cl^-, and almost 84% at 1 M Cl^- (De Laat and Giang Le, 2006). Under field conditions for PCE-loaded GAC regeneration (appendix A.3), 190 mM Cl^- is produced per regeneration, which could have a significant impact on the rate of decomposition of H_2O_2 (Table 4.4.4.2-1). Based on this analysis, use of regenerant solution for multiple regenerations events would not be recommended due to the rate-suppressing effects of chloride ion accumulations.

Table 4.4.4.2-1. Calculated effect of chloride and perchlorate ion concentrations on rate of hydrogen peroxide degradation in Fenton's reaction

I, M	$[Cl^-]$, mM	$[ClO_4]_o$, mM	pH_o	$[H_2O_2]_o$, mM	α (%)	α ($I_a + I_b$) (%)	k_{obs} (10^{-5})
0.2	0	200	2.00	49.9	0	1.29	10.46
0.2	200	0	2.02	50.2	49.6	0.65	5.12
0.4	400	0	2.00	48.2	65.5	0.43	3.81
1	1000	0	1.76	46.1	90.7	0.09	1.64

Note: $[HClO_4]_o$=10mM except 15mM for 1000mM Cl^-, $[Fe(III)]_o$=1mM. α represents the molar fraction of Fe(III) present as iron(III)-chlorocomplexes, α ($I_a + I_b$) represents the fraction of Fe(III)-hydroperoxy species, and k_{obs} the rate of H_2O_2 decomposition.
Source: De Laat, J. and Giang Le, T. (2006)

4.4.4.3 Simulation of Fenton's reaction for PCE degradation as a function of pH

Numerous studies have shown that the Fenton rates of degradation of H_2O_2 and organic compounds are optimum near pH 3 (Gallard and DeLaat, 2000; Arnold *et al*.,

1995; Sedlak and Andren, 1991). In this section, experimental data for the degradation of PCE in the pH range 0.9-3.0 are reported and compared to simulations using the mathematical model described previously.

The PCE transformation rate increases with increasing pH (0.9-3.0), with a maximum near pH 3 (Figure 4.4.4.3-1). Most of the rate acceleration was evident in the pH range 2.1-3.0. PCE degradation experiments at pH>3.0 are not presented because precipitation (as indicated by solution turbidity) was observed. The effect of the precipitated Fe(III)-species on the PCE degradation rate is not completely understood. Precipitated Fe(III)-species are not likely to form complexes with hydrogen peroxide, which changes the rate of decomposition of H_2O_2 and that of any organic target in solution. The concentration of the Fe(III)-hydroperoxy species is greater at pH 3 than 2, which explains why Fenton's reaction is faster at pH 3.

Time dependent PCE concentrations are compared to model predictions in Figure 4.4.4.3-1. The simulations are not in good agreement with the experimental data, but model and experiment agree on the general effect of increasing pH. That is, increasing pH is expected to accelerate PCE degradation. At every pH except pH = 0.9, however, the model over-predicts the PCE transformation rate. Furthermore, the model predicts greater sensitivity to pH values from 0.9 to 2.1 than was observed.

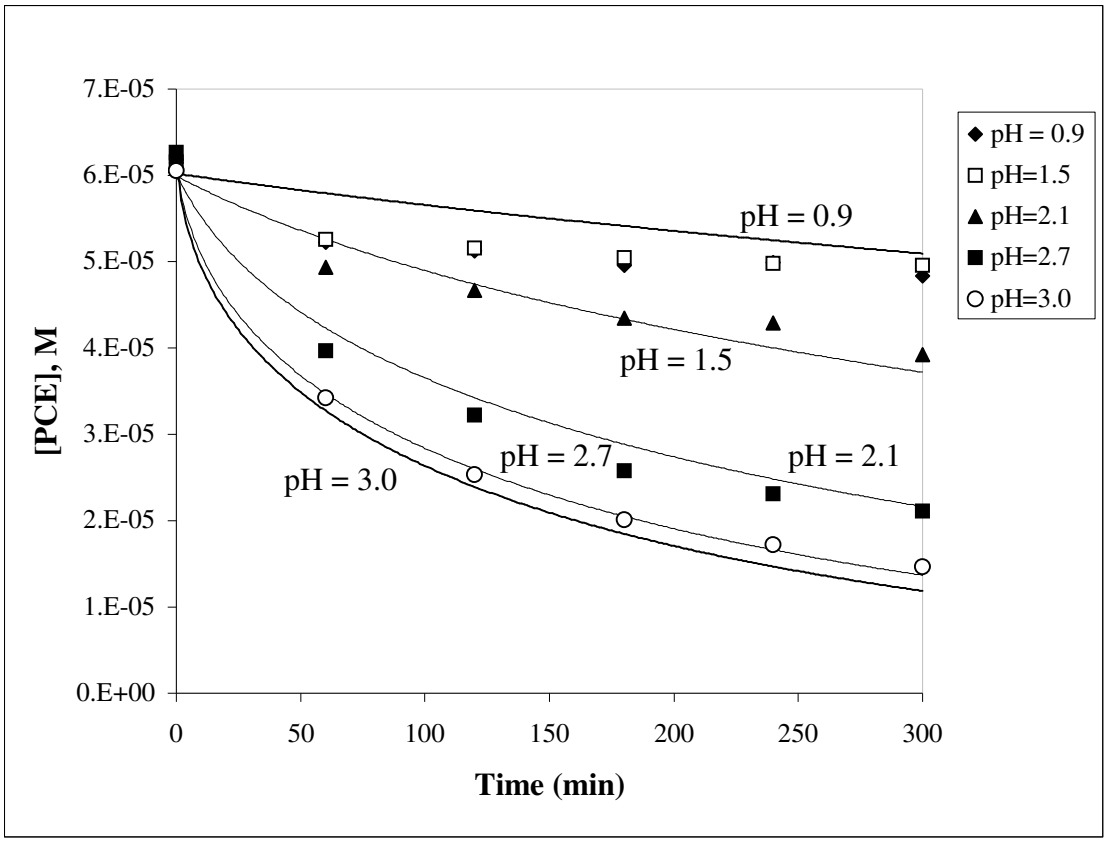

Figure 4.4.4.3-1. Effect of pH on the PCE degradation rate in Fenton's reaction. Initial conditions: $[Fe(III)]_o$ =0.103 mM, $[H_2O_2]_o$=0.11 M, $[PCE]_o$= 62 μM, T = 31±1°C, pH = 0.9 (♦), 1.5 (□), 2.1 (▲), 2.7 (■), and 3.0 (○). A literature value ($k_{Cl,OH}$ = 1.0 x $10^{10}M^{-1}s^{-1}$) was utilized in all simulations trials.

4.4.4.4 Role of superoxide radical ($O_2\bullet^-$) in Fenton's reaction

A number of studies suggest that a subset of the environmental contaminants of interest, including carbon tetrachloride (CT) and N-nitrosodimethylamine (NDMA), are transformed by a non-hydroxyl radical mechanism that probably involves direct attack by the superoxide radical anion (Roberts and Sawyer, 1981; Stark and Rabani, 1999; Watts et al., 1999; Teel and Watts, 2002; Smith *et al*., 2004; Kommineni *et al*., 2003).

Although the superoxide radical is a relatively weak reductant (Table 4.4.4.4-1), $O_2\bullet^-$ is an effective nucleophile in aprotic solvents (Roberts and Sawyer, 1981). As such, it

may react readily with heavily halogenated targets such as PCE and carbon tetrachloride. The reductive transformation of CT in dimethyl sulfoxide by $O_2\bullet^-$ follows second order kinetics with a rate constant, k = 3800 M^{-1} s^{-1} (Teel and Watts, 2002). However, the role of perhydroxyl radical, $HO_2\bullet$, in CT reduction was held to be negligible. Since the pKa for $HO_2\bullet$ in water is 4.8, the utility of superoxide radical as a reductant in the destruction of CT and similar (heavily halogenated) targets may be largely confined to waters with pH>4.

Table 4.4.4.4-1. Standard redox potentials

Equilibrium	E^o (V)
$Li^+_{(aq)}/Li_{(s)}$	-3.03
$K^+_{(aq)}/K_{(s)}$	-2.92
$Ca^{2+}_{(aq)}/Ca_{(s)}$	-2.87
$Na^+_{(aq)}/Na_{(s)}$	-2.71
$Mg^{2+}_{(aq)}/Mg_{(s)}$	-2.37
$Al^{3+}_{(aq)}/Al_{(s)}$	-1.66
$Zn^{2+}_{(aq)}/Zn_{(s)}$	-0.76
$Fe^{2+}_{(aq)}/Fe_{(s)}$	-0.44
$Pb^{2+}_{(aq)}/Pb_{(s)}$	-0.13
$H^+_{(aq)}/½H_{2(g)}$	0
$O_{2(aq)}/O_2\bullet^-_{(g)}$	**0.137[a]**
-pulse radiolysis (duroquinone-superoxide)	**0.13[a]**
- irradiated solutions	**0.33[b]**
-DMF	**0.86[b]**
-DMSO	**0.78[b]**
$Cu^{2+}_{(aq)}/Cu_{(s)}$	0.34
$Ag^+_{(aq)}/Ag_{(s)}$	0.8
$Au^{3+}_{(aq)}/Au_{(s)}$	1.5

NOTE: The standard reduction potential is that of the hydrogen electrode under standard conditions (1 M or 1 atm and pH 0.0). At pH 7.0, the potential of the hydrogen electrode is -. 42 V.
Solvents: dimethyl sulfoxide (DMSO), dimethylformamide (DMF).
[a]The standard reduction potential for the couple $O_{2(aq)}/O_2\bullet^-_{(g)}$ = 0.137 V was calculated from reversible electrochemical cell measurements without a liquid junction.
SOURCE: URL http://www.chemguide.co.uk/physical/redoxeqia/ecs.html#top (Dec 2005), except $O_2\bullet^-$ ([a]Petlicki and van de Ven, 1998; [b]Smith et al., 2004).

4.4.4.4.1 Solvent effects on $O_2\bullet^-$ reactivity in aqueous solutions

Carbon tetrachloride degradation in solutions containing KO_2 was reported to be insignificant compared to the loss in control reactors (deionized water). Only 25% of CT was lost over 2 hrs under the experimental conditions (1 mM CT, 2 M KO_2, 33 mM purified NaOH, 1 mM DTPA, pH = 14, T= 4±1°C) (Smith *et al*., 2004). The kinetics of this reaction, however, is substantially improved via the addition of specific organic co-solvents (Smith *et al*., 2004). In alkaline solutions (pH = 14) with H_2O_2 (as HO_2^-), cosolvent enhancement of CT transformation by $O_2\bullet^-$ was reported in the following order: acetone > 2-propanol > ethanol > H_2O_2 (as HO_2^-) > methanol> ethylene glycol. In Fenton's reaction, the kinetics of CT degradation increased as a function of acetone concentration in the range 0.01 M < [Acetone] < 1 M (Smith *et al.*, 2004). At sufficiently high concentrations (> 0.1 M), HO_2^- increased the observed rate of CT transformation. It was concluded that the superoxide radical, and not HO_2^-, initiated CT transformation in this reaction mixture, and that HO_2^- increased the reactivity of $O_2\bullet^-$ with CT through a co-solvent effect (Smith *et al*., 2004). Others (Peyton *et al*., 1995) have noted enhancement of degradation kinetics due to ethanol addition during H_2O_2/UV treatment of water containing CT.

The products of CT reaction with $O_2\bullet^-$ included primarily carbon dioxide and phosgene (Smith *et al*., 2004). Both products are consistent with a reductive mechanism initiated via nucleophilic attack by $O_2\bullet^-$ on CT.

A number of independent investigators have noted that the reaction of CT with •OH is slow ($<2x10^6$ M^{-1} s^{-1} Haag and Yao, 1992; $<6x10^5$ M^{-1} s^{-1} Buxton *et al*., 1988). These

observations support the existence of a reductive pathway involving superoxide radicals in Fenton-based systems. Moreover, inverse relationships between rates of hydrogenolysis of chlorinated targets and carbon-chlorine bond energies and/or the energy of formation of chloromethyl radicals from their chlorinated parents have been repeatedly shown for a number of relevant reductive systems (Liu *et al*., 2000). Carbon tetrachloride and other heavily halogenated targets are particularly well suited to transformation via hydrogenolysis due to their low carbon-chlorine bond energies (Table 4.4.4.4.1-1).

The existence of a reductive transformation pathway for CT in Fenton's solutions was supported by observation of CT reactivity in the presence of •OH-scavenging reactants at concentrations that should have quenched •OH reaction with CT (Smith *et al*., 2004). A reductive mechanism for CT degradation was also suggested by the results of experiments in which excess $CHCl_3$ was added to react with superoxide radicals (Teel and Watts, 2002). Reduction pathways have been proposed for other advanced oxidation processes (Stark and Rabani, 1999; Glaze *et al*., 1993).

Table 4.4.4.4.1-1. Carbon-chlorine bond dissociation energies for chlorinated compounds

Species	Abbreviation	Experimental enthalpies (C-Cl) (kcal/mol)	Theoretically calculated D(C-Cl) (kcal/mol)
CCl_4	CT	72.0±2.1	72.65
$CHCl_3$	CF	77.8±1.4	77.54
CH_2Cl_2	DCM	82.1±1.3	81.85
CH_3Cl	CM	83.5±0.9	NA
$CCl_2=CCl_2$	PCE	91.0	94.52
$CCl_2=CHCl$	TCE	93.3	93.56
$CCl_2=CH_2$	1,1-DCE	93.8	93.67
Trans-CHCl=CHCl	trans-DCE	88.7	97.33
cis-CHCl=CHCl	cis-DCE	88.2	98.98
$CHCl=CH_2$	VC	107.6±2.3	NA
C_2Cl_6	HCA	71.2±3.3	68.83
C_2HCl_5	PCA	68.4±3.6	68.95
$CHCl_2CHCl_2$	1,1,2,2-TeCA	NA	74.65
CCl_3CH_2Cl	1,1,1,2-TeCA	NA	70.19
$CH_2ClCHCl_2$	1,1,2-TCA	NA	76.04
CH_3CCl_3	1,1,1-TCA	NA	73.6
CH_2ClCH_2Cl	1,2-DCA	82.8±2.8	82.23
CH_3CHCl_2	1,1-DCA	79.2±2.7	79.12
C_2H_5Cl	CA	84.4±0.8	84.13

NOTE: Experimental enthalpies for C-Cl bond dissociation were derived from enthalpies of formation. Theoretical calculations of D(C-Cl) values were performed at G2MP2 level using Gaussian 94.
SOURCE: Liu et al., 2000.

4.4.4.4.2 Fenton-driven transformation of PCE

Advanced oxidation processes are known to promote both oxidative and reductive contaminant transformations. In TiO_2-mediated photocatalysis, for example, PCE degradation occurs via both oxidative and reductive pathways (Glaze *et al.*, 1993). It was suggested that the reductive pathway involved electrons that were elevated to the

conduction band by photons and produced di-chlorinated byproducts. The oxidative pathway involved semiconductor holes and produced both mineralized products and tri-chlorinated intermediates. Peyton *et al*. (1995) observed products from reductive transformations of chlorinated target compounds in UV/ozone reactors, and Watts *et al*. (1999) indicated that in Fenton systems, PCE is degraded exclusively by hydroxyl radicals only when reducing species are consumed by a suitable radical scavenger. In soil systems, PCE desorption was enhanced via co-solvent addition (Watts *et al*., 1999), suggesting that similar methods could be used to circumvent transport/desorption limitations to PCE recovery in heterogeneous systems such as the GAC adsorption/destruction system described elsewhere in this report.

Our own investigation and work by others showed that PCE destruction by Fenton's reagents in homogeneous, aqueous solutions is fast (Figure 4.3.4.6.3-1). Here PCE reached the method detection limit after about 100 minutes. Again, halogenated intermediates derived from PCE conversion were not detected via GC/ECD analysis of reactor contents at any time during the experiments. The published second-order rate constant for PCE reaction with hydroxyl radical is 2.0×10^{9} M^{-1} s^{-1} (www.rcdc.nd.edu). This is near the diffusion limitation. Addition of 1.0 M IP stabilized the PCE concentration in the same two-hour experiments (Figure 4.4.4.4.2-1). Results suggest that under the conditions used here (low pH), reaction with hydroxyl radical accounts for observable PCE degradation. In this system, under these conditions, it seems that a reductive pathway for initiation of PCE destruction can be neglected. Reduction reactions

may still play a role, however, in subsequent transformations involving reaction intermediates.

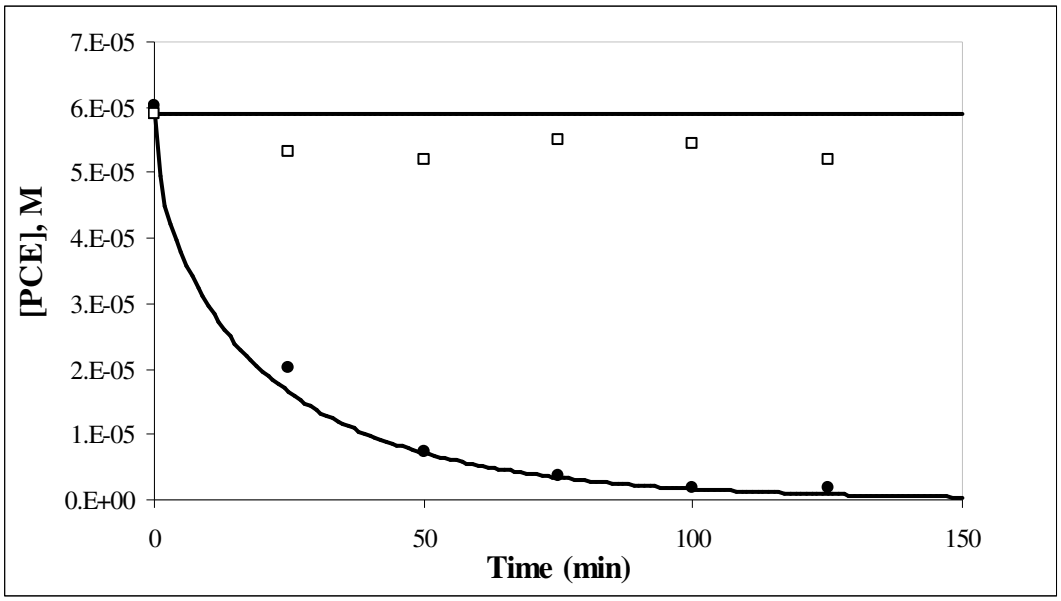

Figure 4.4.4.4.2-1. Effect of IP as •OH radical scavenger on PCE transformation rate in Fenton's system. Initial conditions: $[Fe(III)]_T$ = 0.389 mM, $[H_2O_2]_o$ =0.3 M, pH = 2.8, $[PCE]_o$ = 61 μM, $[IP]_o$= 1 M, T = 31± 1 °C. Data points represent the experimental data with (□) and wihtout (●) IP, and the continuous lines the simulation using the mathematical model described previously in this report. Source: Yan, 2006.

Consistent inhibition of PCE transformation was observed in a series of experiments with Fenton's reagents. The experiments were designed to investigate the inhibitory effect of IP on reactions involving •OH. The second-order rate constant for the reaction between IP and •OH is $1.9.0x10^9$ M^{-1} s^{-1} (http://www.rcdc.nd.edu/) making the isopropanol a strong candidate for inhibition of Fenton-driven oxidations. Results indicate that PCE oxidation by •OH was essentially eliminated by IP addition.

Elimination of hydroxyl radical-dependent reaction pathways by IP addition and competition for Fenton-derived hydroxyl radicals was expected. The initial concentration of IP (1 M) was more than 16,000 times that of PCE (61 μM) (Figure 4.4.4.4.2-1). Since

reported second-order rate constants for reaction of IP and PCE are similar (Table 4.3.3-1), the very high concentration of IP employed should have virtually eliminated the direct reaction of •OH with PCE in these experiments. A comparison of reaction rates for PCE, H_2O_2 and IP with hydroxyl radical follows:

$$\frac{d[PCE]}{dt} = k_{PCE,\cdot OH}[PCE][\cdot OH] \qquad k_{PCE,\cdot OH} = 2.0x10^{9} M^{-1}s^{-1} \qquad [4.4.4.4.2\text{-}1]$$

$$\frac{d[H_2O_2]}{dt} = k_{H_2O_2,\cdot OH}[H_2O_2][\cdot OH] \qquad k_{H_2O_2,\cdot OH} = 3.3x10^{7} M^{-1}s^{-1} \qquad [4.4.4.4.2\text{-}2]$$

$$\frac{d[IP]}{dt} = k_{IP,\cdot OH}[IP][\cdot OH] \qquad k_{IP,\cdot OH} = 1.9x10^{9} M^{-1}s^{-1} \qquad [4.4.4.4.2\text{-}3]$$

If $[\bullet OH]_{ss}=1.0x10^{-12}$ M and $[PCE]_o$ = 61 μM, $[H_2O_2]_o$ =0.3 M, $[IP]_o$ = 1 M, then it is clear that the IP rate exceeds by nearly four orders of magnitude that of PCE.

$$\frac{d[PCE]}{dt} = 2.0x10^{9}[61x10^{-6}][1.0x10^{-12}] = 1.22x10^{-7} Ms^{-1} \qquad [4.4.4.4.2\text{-}4]$$

$$\frac{d[H_2O_2]}{dt} = 3.3x10^{7}[0.3][1.0x10^{-12}] = 9.9x10^{-6} Ms^{-1} \qquad [4.4.4.4.2\text{-}5]$$

$$\frac{d[IP]}{dt} = 1.9x10^{9}[1][1.0x10^{-12}] = 1.9x10^{-3} Ms^{-1} \qquad [4.4.4.4.2\text{-}6]$$

Since IP, PCE and H_2O_2 all compete for the same hydroxyl radical pool and the IP is in excess, it is expected that the direct PCE reaction with •OH will be essentially eliminated through the addition of IP.

4.4.4.5 Copper enhanced PCE degradation

The effect of copper on the enhancement of the PCE degradation rate was modeled by incorporating significant reactions. Table 4.4.4.5-1 shows copper reactions that may be important in our system. In the current modeling effort, most reactions were considered except for (i) copper oxidation by oxygen, and (ii) copper complexation reactions with •OH.

Table 4.4.4.5-1. Copper chemistry

Reagents	Products	Kinetic Constants (M^{-n+1} s^{-1})
$Fe^{3+} + Cu^{+}$	$Fe^{2+} + Cu^{2+}$	$5.5x10^{6}$
$Cu^{+} + \bullet OH$	$Cu^{2+} + OH^{-}$	$3.0x10^{9}$
$Cu^{+} + O_2$	$Cu^{2+} + O_2\bullet^{-}$	$4.6x10^{5}$
$Cu^{+} + H_2O_2$	$Cu^{2+} + \bullet OH + OH^{-}$	$7.0x10^{3}$
$Cu^{+} + HO_2\bullet + H^{+}$	$Cu^{2+} + H_2O_2$	$3.5x10^{9}$
$Cu^{+} + O_2\bullet^{-} + 2H^{+}$	$Cu^{2+} + H_2O_2$	$9.4x10^{9}$
$Cu^{2+} + HO_2\bullet$	$Cu^{+} + O_2 + H^{+}$	$1.0x10^{8}$
$Cu^{2+} + O_2\bullet^{-}$	$Cu^{+} + O_2$	$8.0x10^{9}$
$Cu^{2+} + \bullet OH$	$Cu(\bullet OH)^{2+}$	$3.5x10^{8}$
$Cu(\bullet OH)^{2+}$	$Cu^{2+} + \bullet OH$	$3.0x10^{4}$

Source: Deguillaume et al., 2005

Addition of copper reactions to the system of equations used to model the degradation of H_2O_2 and PCE (without sulfate effect) and the use of the hydroxyl radical second order rate constant for chloride as a fitting parameter provides a poor fit of the data (Figure 4.4.4.5-1). A second order constant for the reaction of the hydroxyl radical and the chloride ion has been used to fit the experimental data for PCE degradation. Here, the fitted constant with a value of $1.5x10^{10}$ M^{-1} s^{-1} shows no enhancement on PCE degradation by addition of copper to the iron/H_2O_2 solution.

These results also suggest that extension of the model by addition of the sulfate complexation reactions and the effect of chloride ion as a radical scavenger may be necessary in order to simulate our experimental data.

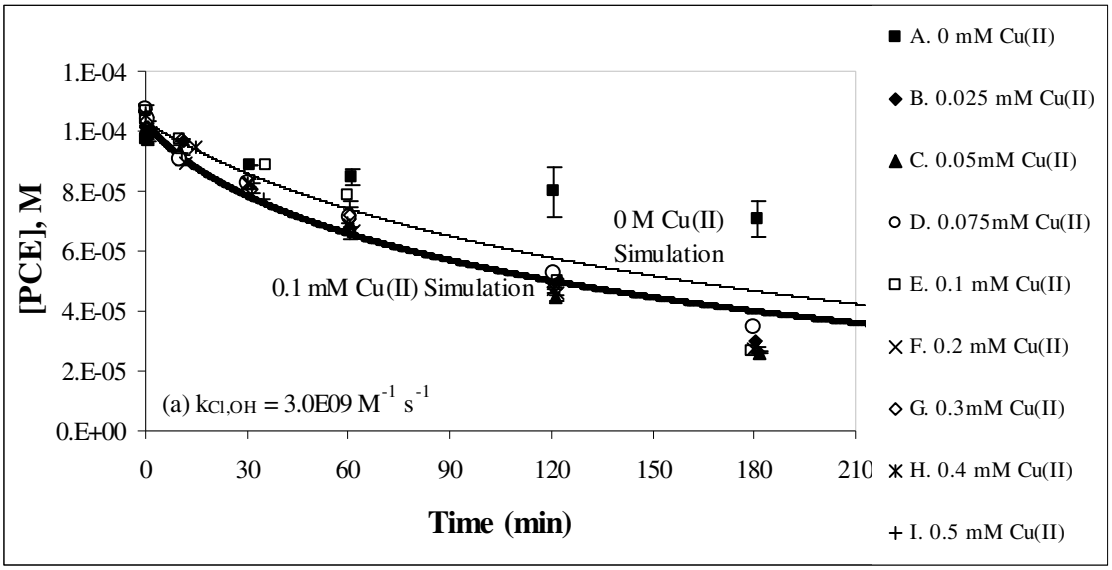

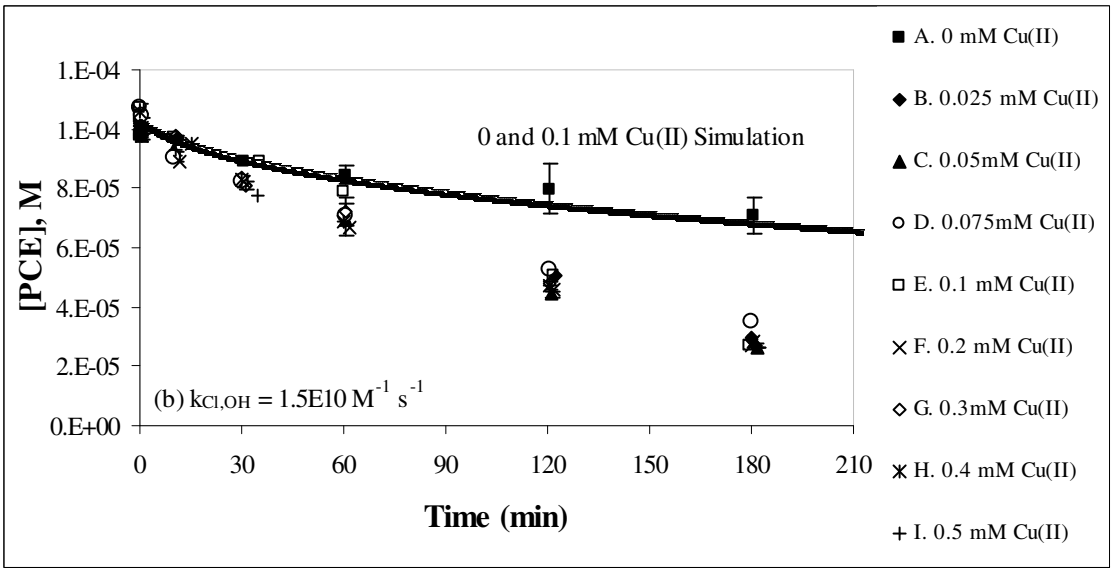

Figure 4.4.4.5-1(a)(b). Simulation of the copper effect on PCE degradation rate enhancement. (a) literature value: $k_{Cl/OH}=3.0x10^{9}$ M^{-1} s^{-1} (b) fit: $k_{Cl/OH}=1.5x10^{10}$ M^{-1} s^{-1}.

4.5 Homogeneous Model Formulation – Summary and Conclusions

- A homogeneous phase kinetic model was formulated based on earlier work by De Laat and Gallard (1999). The rate constant for disproportionation of the Fe(III)-hydroperoxy complex (rate limiting step for radical production kinetics) was fitted to H_2O_2 utilization data. The model was capable of reproducing the trends exhibited by the data.
- The homogeneous model was used to simulate published data for H_2O_2 (De Laat and Gallard, 1999) and non-halogenated organic degradation (Duesterberg et al., 2005). The simulation provided a satisfactory fit using the rate constants at ionic strength 0.1 M and 25°C. However, when the same set of constants was used to simulate the data obtained in this work, the fit was not adequate. This suggests that complications such as the effect of ions in solution (e.g. sulfate, chloride), ionic strength and temperature need to be considered.
- As chlorinated VOCs are degraded in Fenton systems, chloride anions will build-up in the regenerant solution. The magnitude of the rate constants for the reaction of hydroxyl radical with chloride ion indicates that chloride accumulation through repeated carbon bed regenerations will retard VOC degradation rates. However, model simulations using the literature rate constant for the $\bullet OH/Cl^-$ reaction overestimated chloride ion effects in experimental trials. A revised $\bullet OH/Cl^-$ rate constant was fitted on the basis of these data. Our second-order rate constant was lower than the previously reported value by a factor of 3.

- The rate of PCE degradation by Fenton's reaction increases with increasing pH in the range 1≤ pH ≤3. Above pH 3, iron solubility limits free iron concentration availability, lowering the rate of PCE degradation. Observed PCE degradation rates at 0.9≤ pH ≤3 (data from Yan, 2006) were compared to the results of mathematical simulations. There was considerable difference between experiment and simulation, although general effects of pH were in agreement. At every pH (except pH = 0.9), the model over-predicted the PCE transformation rate.
- PCE degradation was inhibited by the presence of isopropanol in solution. Isopropanol was used as a •OH radical scavenger as its reactivity with the radical is high and it was added in large amounts. The model predicted that no PCE would be degraded in this scenario.
- PCE decomposition rate via Fenton's reaction is enhanced when copper is added to an iron/H_2O_2 solution at acidic pH. The second order rate constant for the reaction of chloride with hydroxyl radical with a value of $1.5x10^{10}$ M^{-1} s^{-1} was used to fit the PCE data at 0 M Cu(II). Even though this value provided a good fit for the data, the model predicted no enhancement on the PCE degradation rate in the presence of copper.

5. BENCH-SCALE, HETEROGENEOUS EXPERIMENTS

The experiments described in this section were designed to examine the sources of rate limitation when halogenated contaminants were initially adsorbed to activated carbon. Possibilities included rates of reaction between hydroxyl radicals and either the adsorbed or (bulk) aqueous-phase contaminant, the rate of contaminant desorption, the rate of diffusive transport of contaminants from the carbon interior, or some combination of these.

5.1 Adsorption Isotherms

Freundlich isotherm parameters for GAC (URV-MOD 1) adsorption of all compounds tested are summarized in Table 2.4.3-1 (repeated below). The data for adsorption of methylene chloride, a representative contaminant, are provided as Figure 5.1-1.

Table 2.4.3-1 (Repeated from Earlier Section). Chemical Properties of the Organic Compounds Studied

Name	*Formula*	*Log K_{ow}*[a]	*$k_{M,OH}$ (M^{-1} s^{-1})*[b]	*Diffusivity (cm^2/s)*[c]	*Freundlich Parameters*[d] *K (mg/g) (L/mg)$^{1/n}$*	*1/n*
Methylene Chloride (MC)	CH_2Cl_2	1.15	9.00E+07	1.21E-05	0.07	1.06
1,2-DCA	$C_2H_4Cl_2$	1.47	7.90E+08	1.01E-05	0.04	1.33
1,1,1-TCA	$C_2H_3Cl_3$	2.48	1.00E+08	9.24E-06	0.65	0.87
Chloroform (CF)	$CHCl_3$	1.93	5.00E+07	1.04E-05	1.48	0.77
Carbon Tetrachloride (CT)	CCl_4	2.73	2.00E+06	9.27E-06	12.30	0.59
TCE	C_2HCl_3	2.42	2.90E+09	9.45E-06	5.82	0.70
PCE	C_2Cl_4	2.88	2.00E+09	8.54E-06	45.66	0.56

NOTE: $k_{M,OH}$ is the second-order rate constant for the reaction of hydroxyl radical with the target organic compound.

SOURCE: [a]Swarzenbach et al., 1993; [b]www.rcdc.nd.edu, except carbon tetrachloride (Haag and Yao, 1992); [c]calculated from Wilke-Chang equation (Logan, 1999); [d]From isotherm data obtained in this lab at 32ºC.

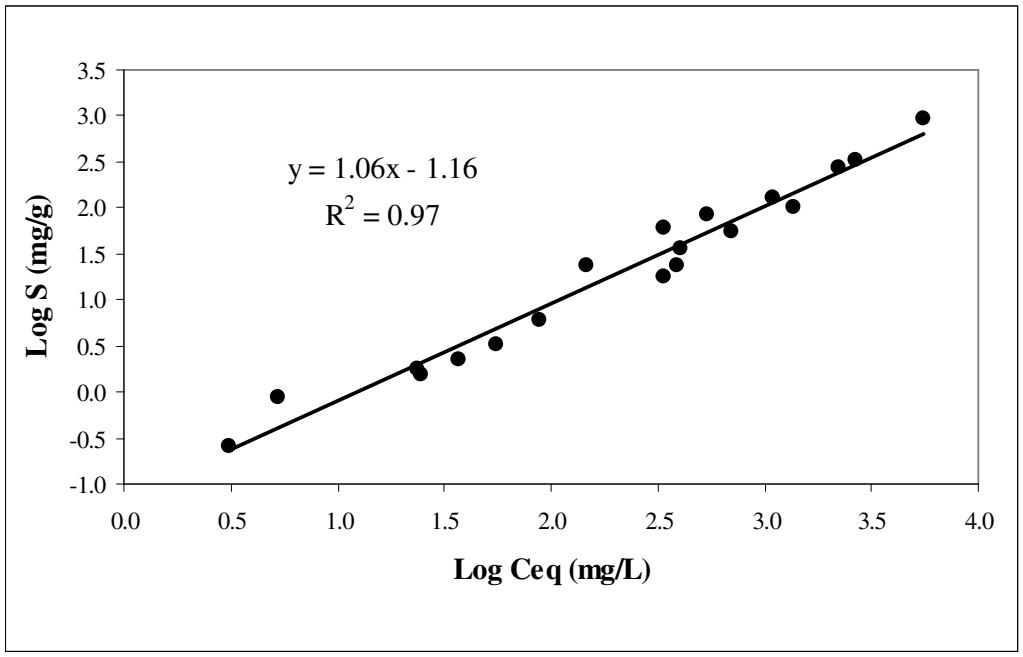

Figure 5.1-1. Isotherm data for methylene chloride on URV-MOD 1 (32°C).

5.2 Bench-scale Column Experiments

5.2.1 Recovery using Fenton's reagents

Contaminants with a range of compound hydrophobicities and reactivities with •OH (Table 1-1) were selected for Fenton-driven regeneration experiments in which spent GAC was regenerated in columns. Preliminary carbon recovery experiments were run at 24 ± 2°C for seven chlorinated VOCs: (methylene chloride (MC), 1,2-dichloroethane (DCA), chloroform (CF), 1,1,1-trichloroethane (TCA), carbon tetrachloride (CT), TCE and PCE). The same experiments were repeated at 32º C. Carbon recovery data for MC, CF and TCE at 32ºC are summarized in Figure 5.2.1-1. Recovery kinetics followed the order MC>CF>TCE. The data are shown on a semi-log plot in Figure 5.2.1-2. After an initial period of rapid recovery that lasted 1-3 hours, further reductions in the sorbed concentration conformed to first-order kinetics. TCE removal from GAC was only 50%

complete after 14 hours. This was unexpected since the second-order rate constant ($k_{\bullet OH,R}$, Table 2.4.3-1) for the reaction of hydroxyl radical with TCE (2.9E+09 $M^{-1}s^{-1}$) is near the molecular-collision diffusion limit (10^8-10^{11} M^{-1} s^{-1}) (www.rcdc.nd.edu) and is higher than the rate constants for reaction of •OH with MC and CF. Lack of dependence of recovery kinetics on reaction rate with •OH suggests that the kinetics of Fenton-driven recovery of GAC is controlled by mass transport, as opposed to the rates of hydroxyl radical generation or radical reaction with contaminant targets.

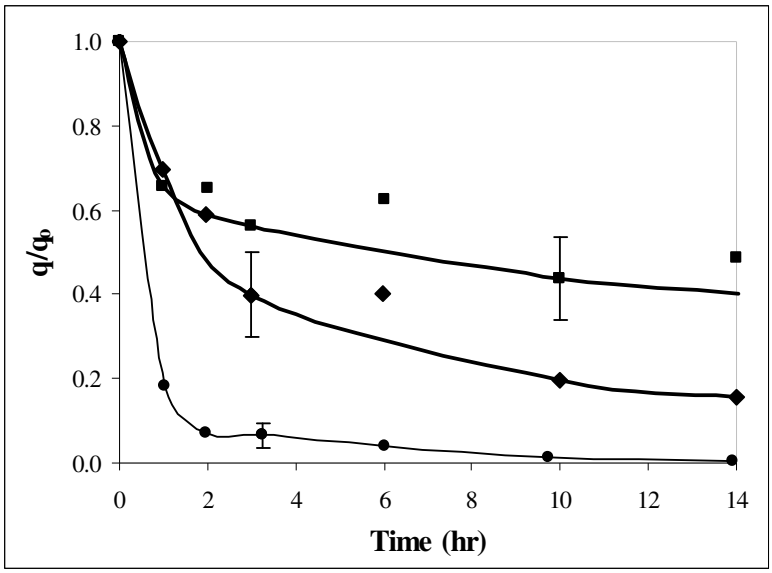

Figure 5.2.1-1. Fractional removal of adsorbate from GAC for MC (●), CF (♦) and TCE (■). Fractional q/q_o represents the mass of contaminant remaining in the carbon. The regenerant solution contained 10 mM iron, pH = 2.0, and 0.15 M H_2O_2 average concentration throughout the experiment. Temperature was controlled in the reservoir at 32°C. The lines are a smoothed fit to the data. Average error bars are indicated for each curve. n=2 for each data point (average between top and bottom samples).

The shapes of the recovery curves (Figure 5.2.1-1) are consistent with an intraparticle diffusion limitation: at short times, target concentrations in most of the GAC pores were nearly uniform, until concentration profiles developed along particle radii. With time the

concentration gradient penetrated further into the particle increasing the apparent diffusion length and leading to slower, nearly first-order contaminant removal kinetics. The apparent first-order rate constants derived from the latter portion of each experiment are summarized in Table 5.2.1-1.

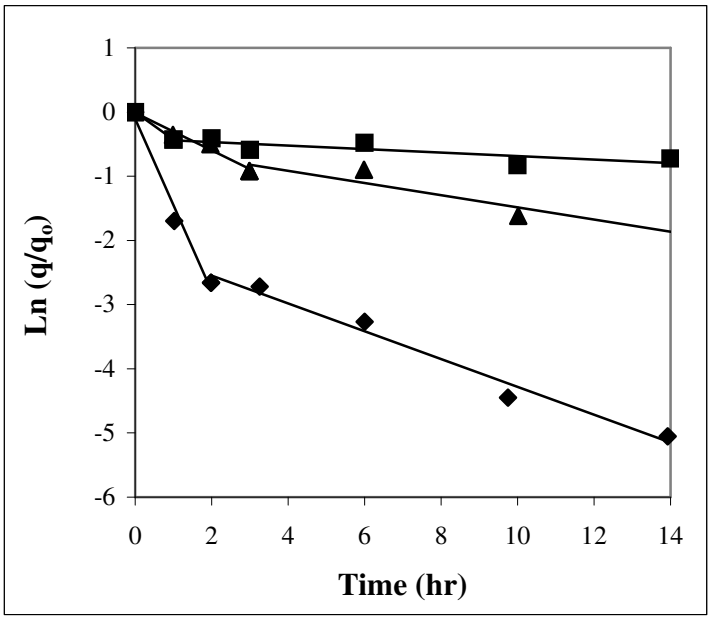

Figure 5.2.1-2. Semi-log plot of the data in Figure 5.2.1-1 for MC (♦), CF (▲) and TCE (■). The slopes of lines from about t= 2 h to the end of the experiment were used to calculate the observed rates (k_{obs}) in Table 5.2.1-1.

Experimental results (Figure 5.2.1-2 and related discussion) suggest that mass transfer rates limit the slow recovery stage in GAC regeneration under the conditions employed in this work. If intraparticle diffusion controls the overall recovery rate, the concentration of the target compound in the bulk liquid should be low due to rapid consumption via Fenton's reaction in the bulk liquid phase. In that case, it can be shown that the flux of contaminant from the particle surface (J) follows a relation like

$$J = k_m \overline{C_p} \qquad [5.2.1\text{-}1]$$

where k_m is a hybrid, conditional coefficient and $\overline{C_p}$ is the average concentration of the target compound in the liquid that fills the pores of the particles. If adsorption and desorption rates are fast, the local aqueous- and solid-phase concentrations of the adsorbate are in equilibrium so that:

$$C_p = \left(\frac{q}{K}\right)^n \qquad [5.2.1\text{-}2]$$

When the Freundlich isotherm is linear (n=1), equation 5.2.1-2 can be expressed in terms of average concentrations so that:

$$\overline{C_p} = \frac{\bar{q}}{K} \qquad [5.2.1\text{-}3]$$

without error. For the analysis that follows, it was assumed that average concentrations could be inserted in the non-linear isotherm (equation 5.2.1-2) without generating excessive error, so that

$$\overline{C_p} = \left(\frac{\bar{q}}{K}\right)^n \qquad [5.2.1\text{-}4]$$

Table 5.2.1-1. Summary Table for Rates Observed (k_{obs}) at 24°C and 32°C at the Bench and Field Scales

	k_{obs} (hr^{-1})			
Compound	*Bench-scale*[a] *T=24 °C*	*Bench-scale*[b] *T= 32 °C*	*Bench-scale Desorption*[c] T= 32°C	*Field-scale*[d]
MC	0.17	0.25	0.19	0.12
1,2-DCA	0.10	0.24	N/A	N/A
1,1,1-TCA	0.075	0.058	N/A	N/A
CF	0.066	0.11	0.11	0.059
CT	0.052, 0.060	N/A	N/A	N/A
TCE	0.045	0.027, 0.060	0.043	0.015 0.033 0.068
PCE	0.037, 0.062	0.042	N/A	0.011

NOTE: [a]Bench-scale regeneration column experiments at 24°C (Figure 5.2.1-2), and [b] T= 32°C (Figure 5.2.1-1). [c]Bench-scale desorption experiments (clean water, no Fenton reagents as eluant – Figure 5.2.1-3). [d]Field-scale regeneration column experiments.

We recognize, however that the magnitude of error introduced by this approximation increases with the degree of non-linearity in respective isotherms.

A mass balance on the adsorbate in the carbon particles, assuming that aqueous-phase mass can be neglected, then yields:

$$M \frac{d\bar{q}}{dt} = -JA_s \qquad [5.2.1\text{-}5]$$

where M and A_s are the total carbon mass and total active surface area of GAC, respectively, and $\bar{q}$ is the average concentration of the adsorbate on the carbon surface. The preceding equation can be solved with the initial condition

$$\bar{q} = \bar{q}_o \text{, at t = 0} \qquad [5.2.1\text{-}6]$$

Substituting equations (5.2.1-1) and (5.2.1-4), equation (5.2.1-5) becomes

$$M\frac{d\bar{q}}{dt} = -A_s k_m \left(\frac{\bar{q}}{K}\right)^n \qquad [5.2.1\text{-}7]$$

This equation implies that the initial rate of decrease of the average target concentration in the solid, $\frac{d\bar{q}}{dt}\Big/(q_o)^n$ at t = 0, should be directly proportional to $(1/K^n)$ for all target compounds, assuming that k_m does not vary appreciably among the various targets. A rigorous analysis would show that k_m is equal to the observed pseudo-first order rate constant for target removal (k_{obs}).

The preceding analysis motivated us to plot the observed pseudo-first order rate constant for target removal (k_{obs}) vs. $1/K^n$ for all target compounds (Figure 5.2.1-3). The k_{obs} were calculated from the initial linear drop for each contaminant (Figure 5.2.1-2). The fact that most compounds follow the expected trend (positive correlation between $1/K^n$ and rate of adsorbate loss) is consistent with the hypothesis that intraparticle mass transfer controls the overall carbon recovery process.

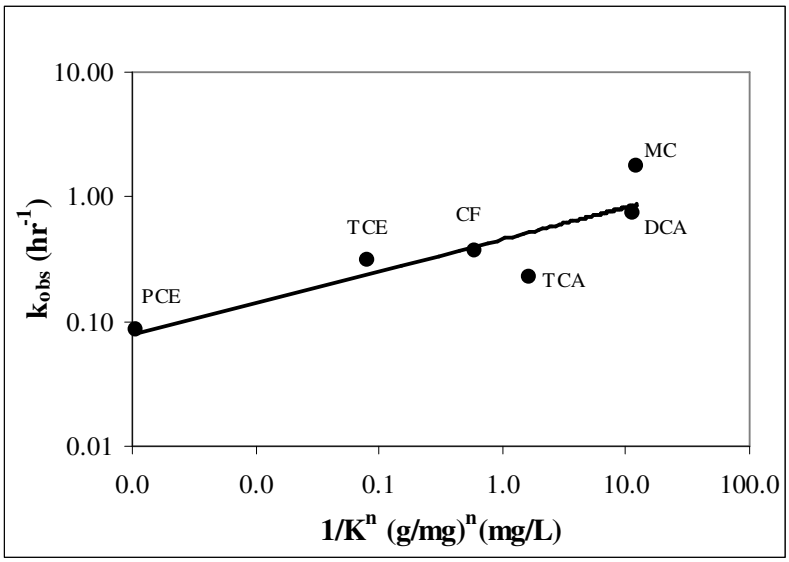

Figure 5.2.1-3. Correlation between first-order observed rate constant (k_{obs}) and compound-specific $(1/K)^n$. Experimental conditions: 10 mM iron, 0.1-0.15 M H_2O_2, pH = 2.0. Experiments were conducted at 32°C. The line is a linear fit of the log- transformed data. The initial observed rates (k_{obs}) were calculated from the initial slopes (up to 1 h) for each column regeneration experiment.

5.2.2 Clean water and Fenton-driven recovery experiments

Comparison of clean water (no Fenton's reagents present) and Fenton-driven recovery experiments (Figure 5.2.2-1) indicate that carbon recovery trajectories for the Fenton-driven and no-reaction (clean-water elution) cases matched for MC and TCE (Figure 5.2.2-1). For those contaminants, it seems evident that contaminant reaction did not limit recovery kinetics. For CF, however, degradation in the presence of Fenton's reagents was slower than in the clean water circulation experiments. This occurred because the bulk aqueous-phase concentration was maintained near zero in the latter experiments by continuously feeding clean influent to the column reactor. Since the reaction of •OH with CF is relatively slow (Table 2.4.3-1), it is likely that CF

accumulated to some extent in the bulk liquid when Fenton's reaction was relied upon to eliminate CF from the recirculated fluid. This diminished the driving force for CF transport from the GAC and protracted the recovery period. This interpretation is supported by liquid-phase CF measurements during GAC recovery using Fenton's reagents (Figure 5.2.2-2). It is apparent that recovery kinetics were limited, at least in part, by the rate of reaction of bulk liquid phase CF.

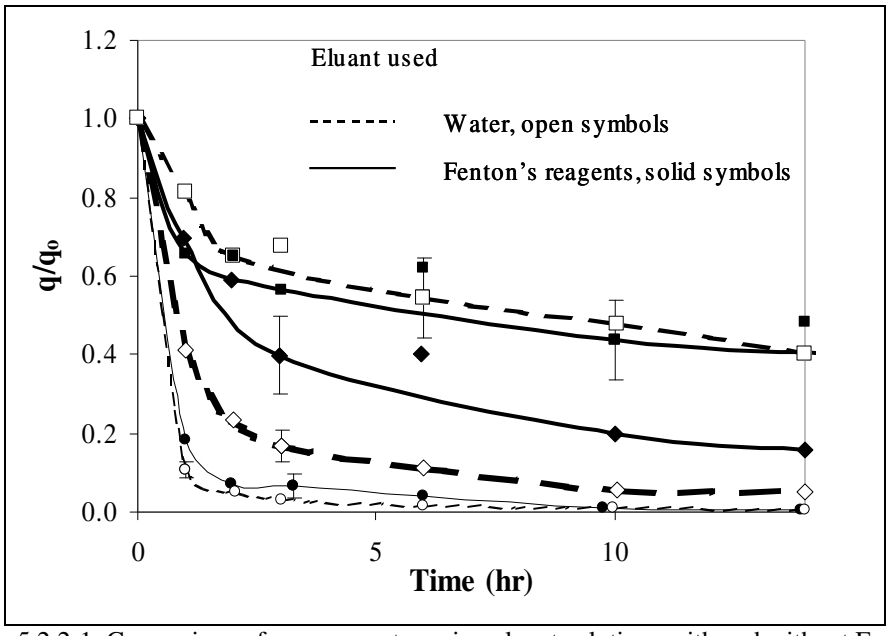

Figure 5.2.2-1. Comparison of recovery rates using eluant solutions with and without Fenton's reagents. When eluant consisted of water, bulk aqueous phase contaminants were near zero. Target compounds were MC (●/○), CF (♦/◊), and TCE (■/□). Regenerant solutions contained 10 mM iron, 0.15 M average H_2O_2, pH = 2.0, T = 32°C. Concentrations are normalized by the initial contaminant concentration on the carbon (q/q_o). Data points represent the average value between carbon extractions of GAC samples from the top and bottom of the GAC bed. An average error bar is indicated for one data point for each curve.

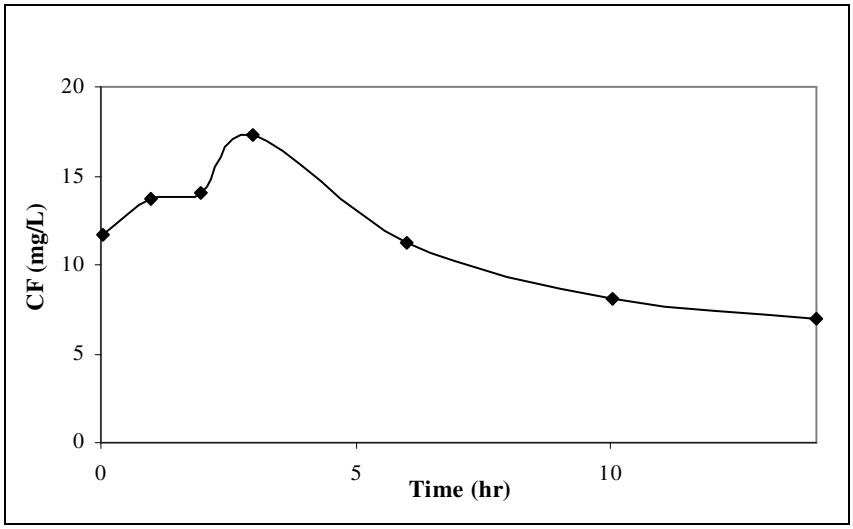

Figure 5.2.2-2. Liquid phase reservoir concentrations for CF-loaded GAC recovery. Times of data points correspond to those in Figure 5.2.2-1.

5.2.3 Role of iron phase (precipitated vs. dissolved)

The following section evaluates the effectiveness of loading iron onto the surface of GAC prior to the Fenton treatment. Localizing the reaction on the carbon surface was hypothesized to be a means to increase contaminant destruction efficiency and minimize reagent use. That is, it was hypothesized that radical production in the immediate vicinity of adsorbed contaminants would allow a higher proportion of radicals to react with the target compounds as opposed to H_2O_2 and other competitors. In addition, the eluant reservoir size was reduced to decrease non-productive (outside the column) H_2O_2 consumption.

To test this hypothesis, native and iron-amended GAC were used in parallel column regeneration trials. Both types of GAC (15 g each) were loaded with TCE and regenerated. Results were compared with previous column experiments with iron in solution. After 14 hours, TCE recovery was essentially the same in all three situations

(Figure 5.2.3-1). Table 5.2.3-1 summarizes the results, as well as column iron content, and volume of H_2O_2 used in each trial. Precipitating the iron on the surface of the GAC lowers the use of H_2O_2, which is the primary cost associated with the GAC regeneration process (see later section on process cost estimation). Iron addition to the carbon surface, however, provided little advantage in terms of the rate of carbon recovery.

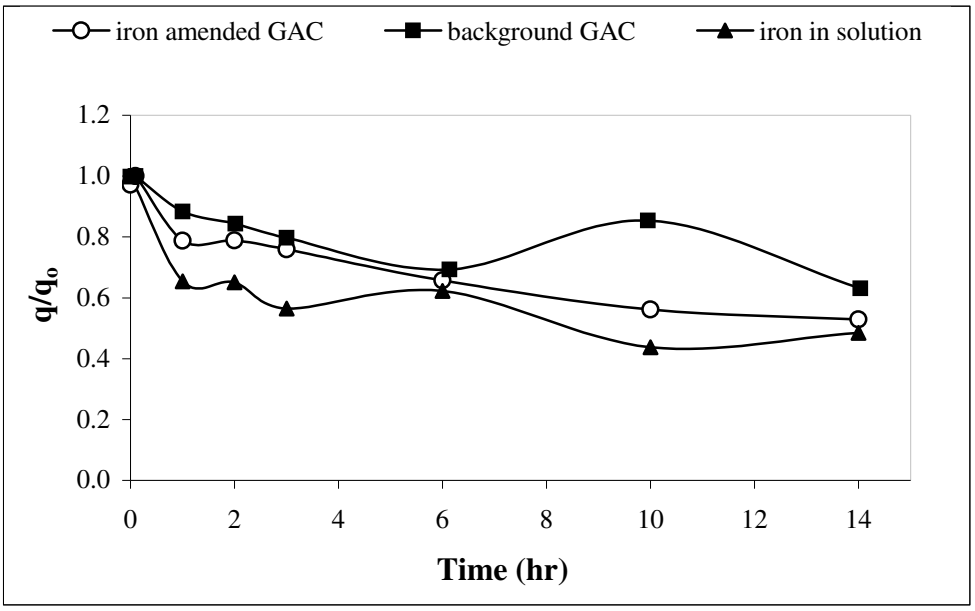

Figure 5.2.3-1. TCE recovery with background GAC, iron amended GAC and iron in solution.

Bench-scale PCE regeneration column experiments (Table 5.2.3-2) were conducted using a lower iron loading (approximately 4 mg Fe/g GAC) than in the TCE trials (Table 5.2.3-1). In this set of experiments, the effect of pH on PCE recovery was established. Iron-amended GAC was loaded with PCE and regenerated at pH 2 and 3 (Figure 5.2.3-2). As in the TCE trials, PCE destruction efficiencies with iron-amended GAC and with iron

in solution (pH 2) were very similar, however H_2O_2 use was reduced by almost a factor of three (Table 5.2.3-2) by iron-amendment on the carbon. Results also suggest that pH is not an important process parameter in the range $2.0 \leq pH \leq 3.0$.

Table 5.2.3-1. Characteristics of GAC and Results after 14 hours of Iron-Amended, Regeneration Trials

GAC type	Iron Content	C/Co (TCE)	H_2O_2 (mL)
Background GAC, pH 4.67	2 mgFe/gGAC (1.4mM)	37%	9
Iron-amended GAC, pH 2	7.4mgFe/gGAC (5 mM)	47%	25.8
Iron in Solution, pH 2	10 mM	50%	160-224

Results indicate that iron and H_2O_2 additions for the degradation of chlorinated solvents can be reduced significantly below the levels used in earlier experiments without significant deterioration of carbon recovery rate. Unfortunately, enhancement of degradation rates for compounds that are diffusion or desorption limited has not yet been achieved. Alternative methods, such as use of alternative solvents and GAC with a greater proportion of surface area in macropores, should be explored to overcome the kinetic limitations arising from mass transport.

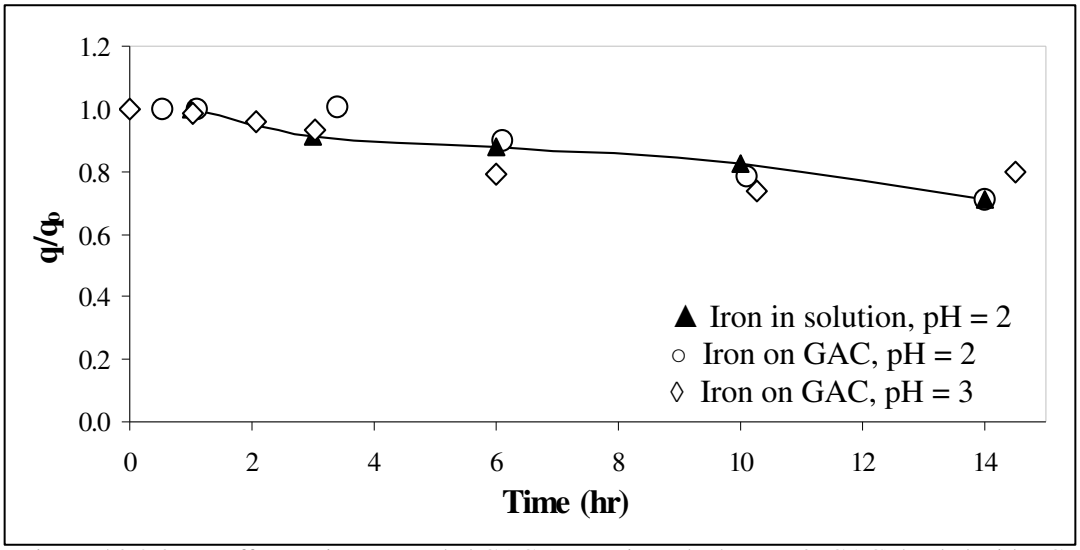

Figure 5.2.3-2. pH effect on iron-amended GAC (approximately 4 mg Fe/g GAC) loaded with PCE in column regeneration trials.

Table 5.2.3-2. Observed Degradation Rate Constant and Average Hydrogen Peroxide Use for PCE-Laden GAC Regeneration With and Without Iron-Amended to the Carbon

pH/Iron	k_{obs} (hr^{-1})	H_2O_2 added (mls/hr)
2/Iron in solution	0.024	16
2/Iron-amended GAC	0.025	5.6
3/Iron-amended GAC	0.034	5.6

NOTE: The theoretical iron content on the iron-amended GAC used in these trials is 4.3 mg Fe/g GAC (based on comparison of similar iron-amended GAC). However, the iron content on the GAC was not accurately measured.

5.3 Heterogeneous Batch Kinetic Experiments

5.3.1 pH dependence on H_2O_2 degradation in the presence of GAC

The pH dependence on hydrogen peroxide degradation was evaluated in water, and in the presence of background (clean) GAC and iron-amended GAC in the pH range 3 to 7. All trials were conducted in a water bath at 32°C and stirred with an overhead mixer. Figure 5.3.1-1(a) and (b) show the hydrogen peroxide degradation in water at pH 3, 5, and 7. The data shows that this reaction is very slow and no significant H_2O_2 degradation was observed at any pH. Figure 5.3.1-2(a) and (b) show the degradation of H_2O_2 in the presence of background GAC at pH 5. About 80% H_2O_2 degradation was observed after 20 min. In contrast, when iron amended GAC was used, H_2O_2 disappearance occurred in less than half of the time (Figures 5.3.1-3 through 5.3.1-6). Figures 5.3.1-3 – 5.3.1-6 show H_2O_2 consumption in the presence of iron-amended GAC at different pH between 3 and 7. A comparison of the rates of H_2O_2 decomposition in this system (Figure 5.3.1-7) suggests no pH dependence. The data also indicates that H_2O_2 degradation occurs at a much faster rate in the presence of iron-amended GAC than with background GAC. Similar results were observed in column experiments when comparing the H_2O_2 consumption in the presence of both GACs (data not shown).

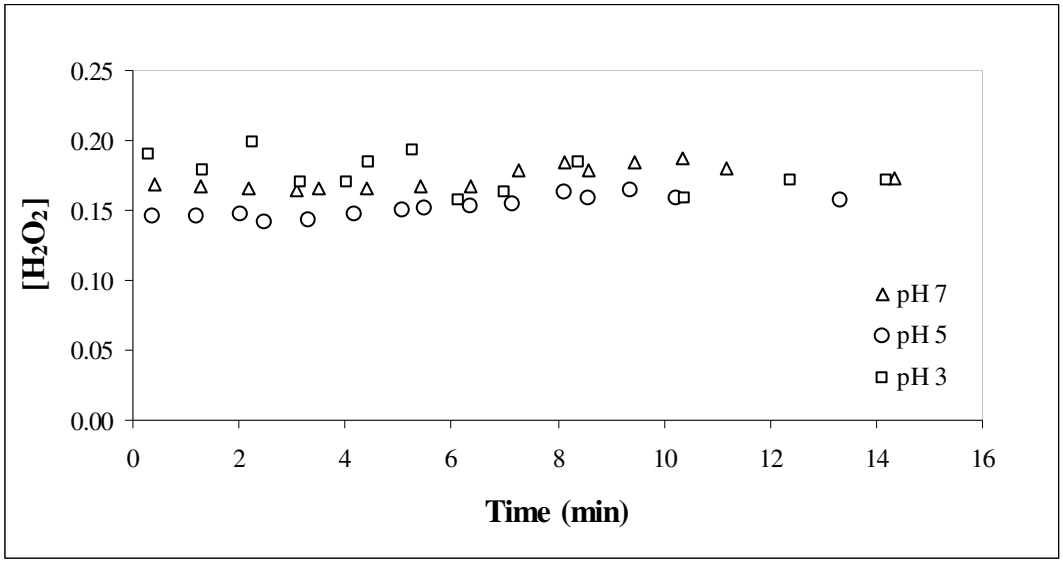

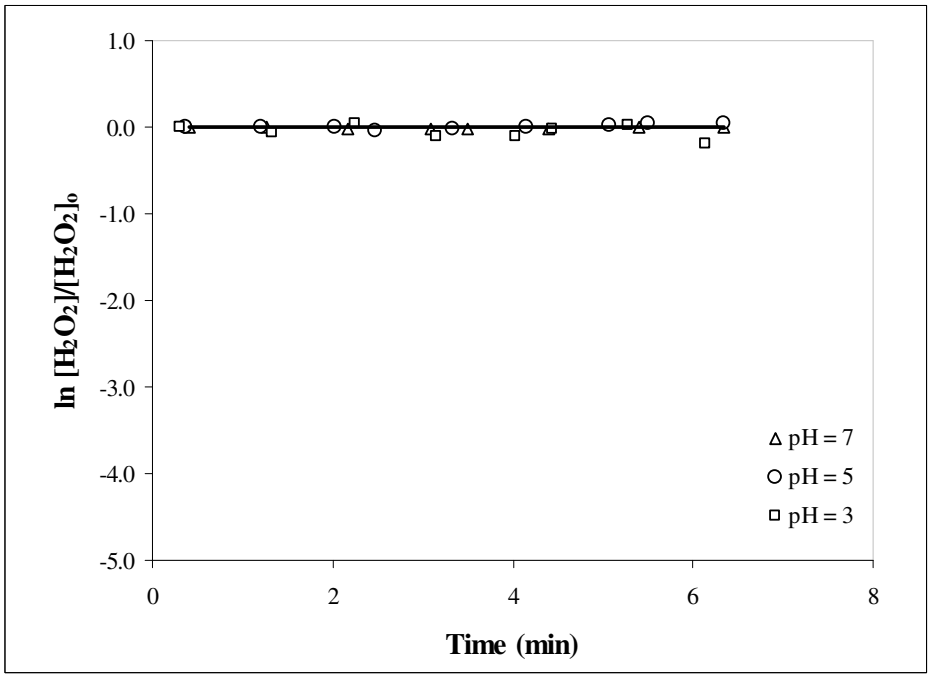

Figure 5.3.1-1(a)(b). Hydrogen peroxide degradation in water at pH 3,5,and 7. Initial conditions: 100 mLs water, 0.18M H_2O_2, and T = 32°C.

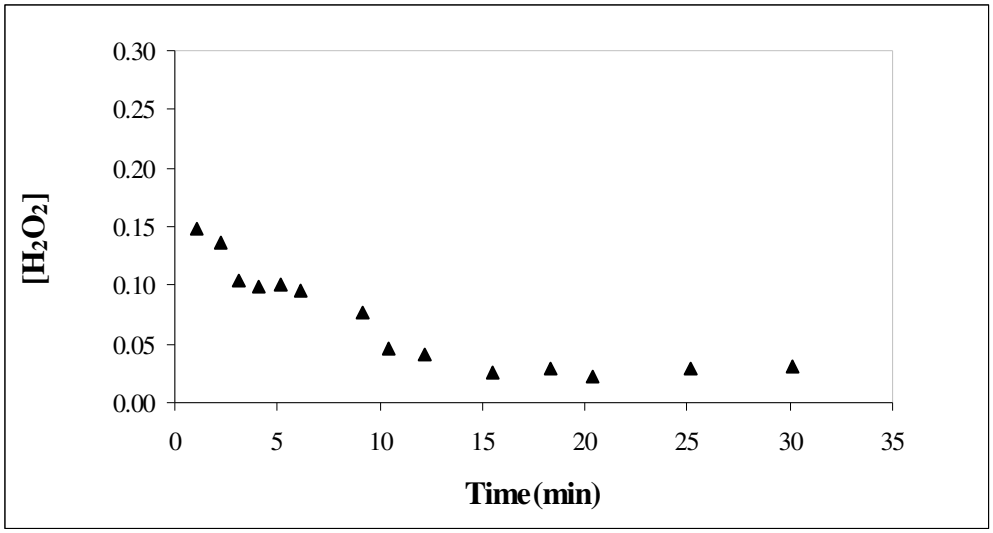

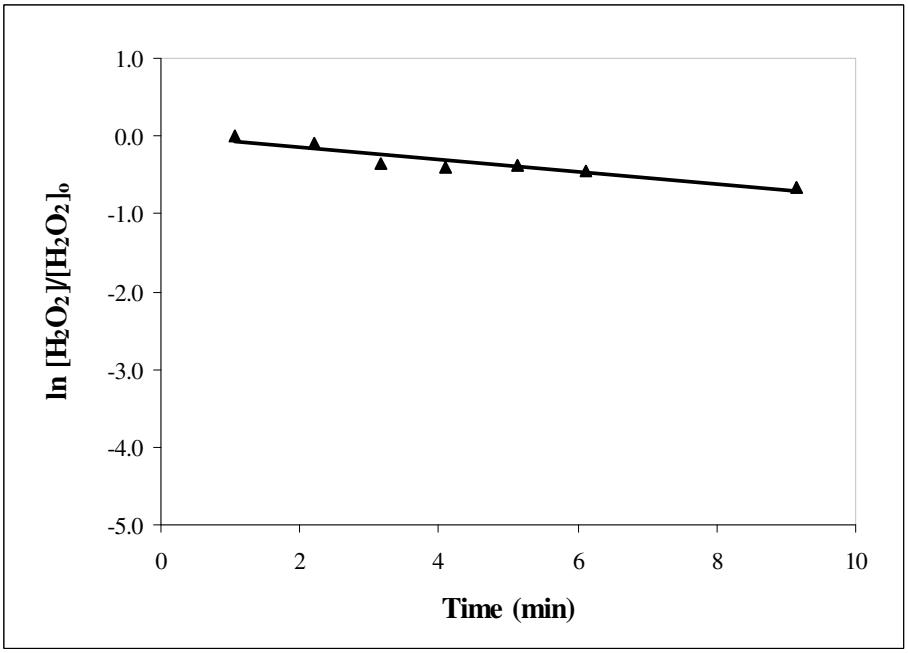

Figure 5.3.1-2(a)(b). H_2O_2 degradation in the presence of background GAC at pH 5. Initial conditions: 12 g GAC, 100 mLs water, and 0.18M H_2O_2, T = 32°C.

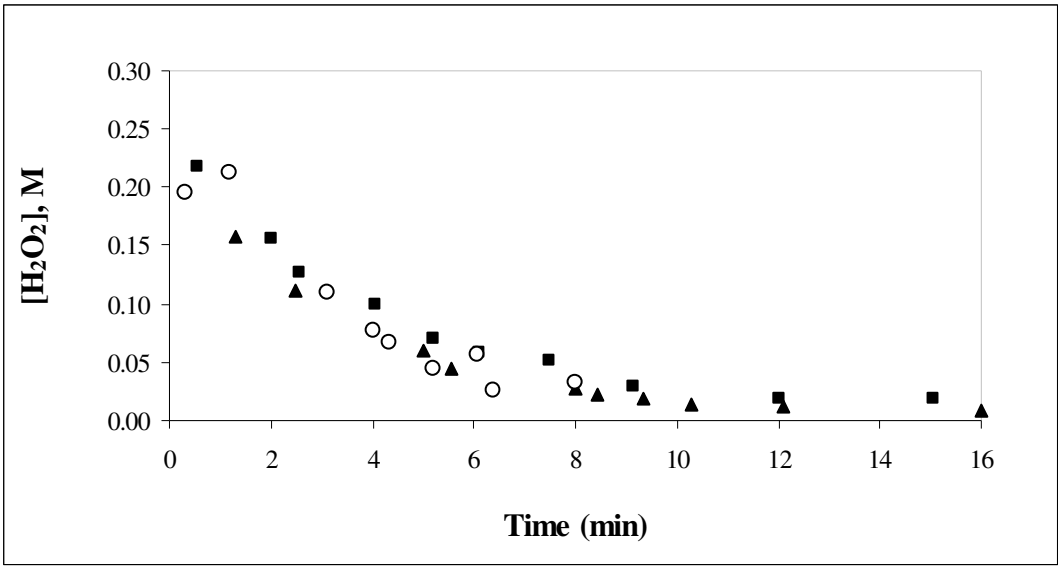

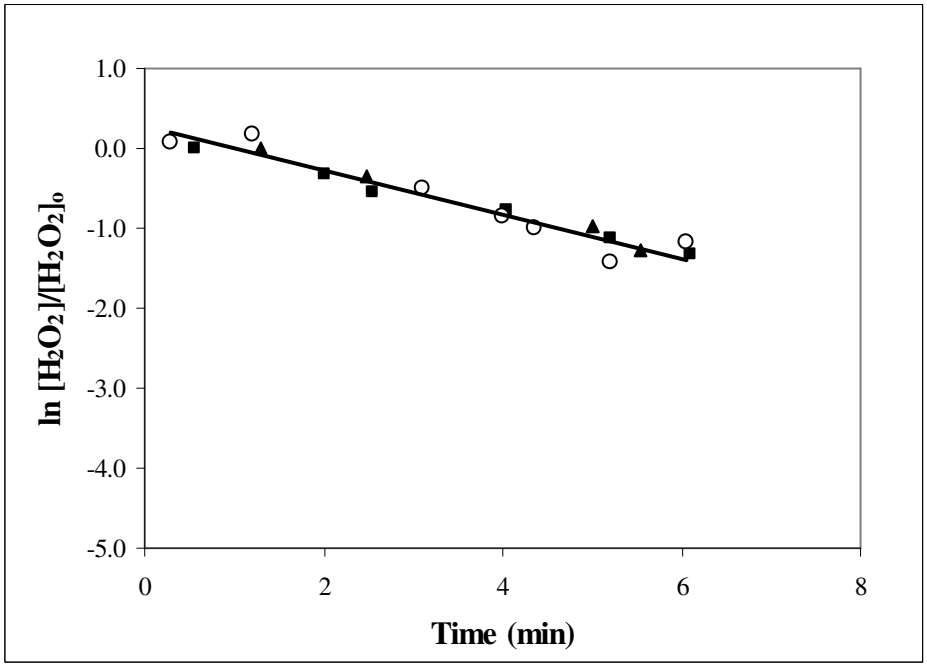

Figure 5.3.1-3(a)(b). H_2O_2 degradation in the presence of iron-amended GAC (7 mg Fe/g GAC) at pH 3. Initial conditions: 12 g GAC, 100 mLs water, and 0.18M H_2O_2, T = 32°C. k_{obs} = 0.27 min^{-1}. Different symbols indicate multiple trials under the same conditions.

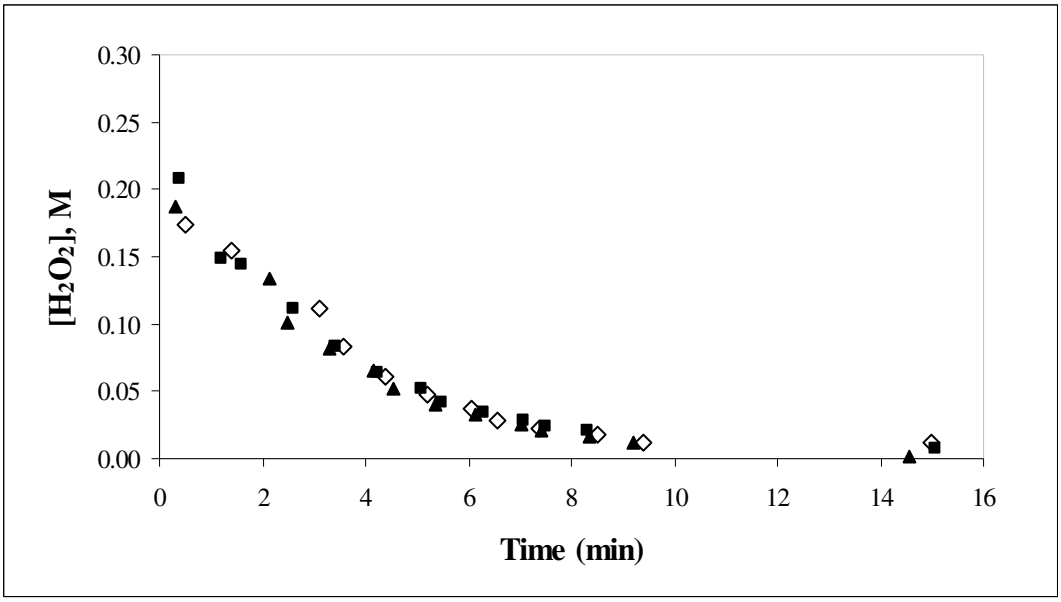

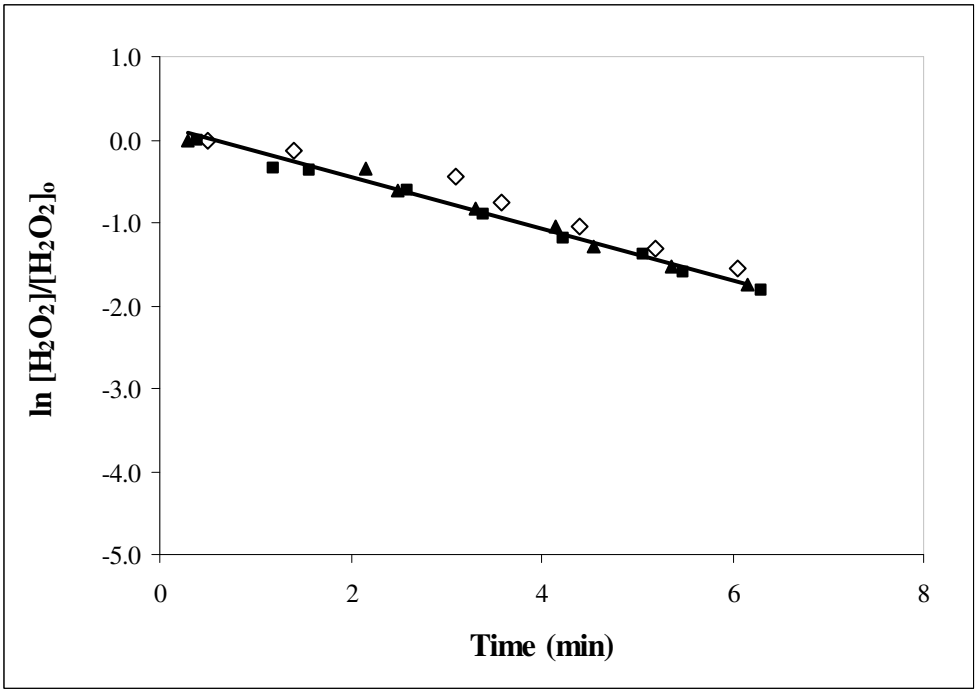

Figure 5.3.1-4(a)(b). H_2O_2 degradation in the presence of iron-amended GAC (7 mg Fe/g GAC) at pH 4. Initial conditions: 12 g GAC, 100 mLs water, 0.18M H_2O_2, and T = 32°C. k_{obs} = 0.30 min^{-1}. Different symbols indicate multiple trials under the same conditions.

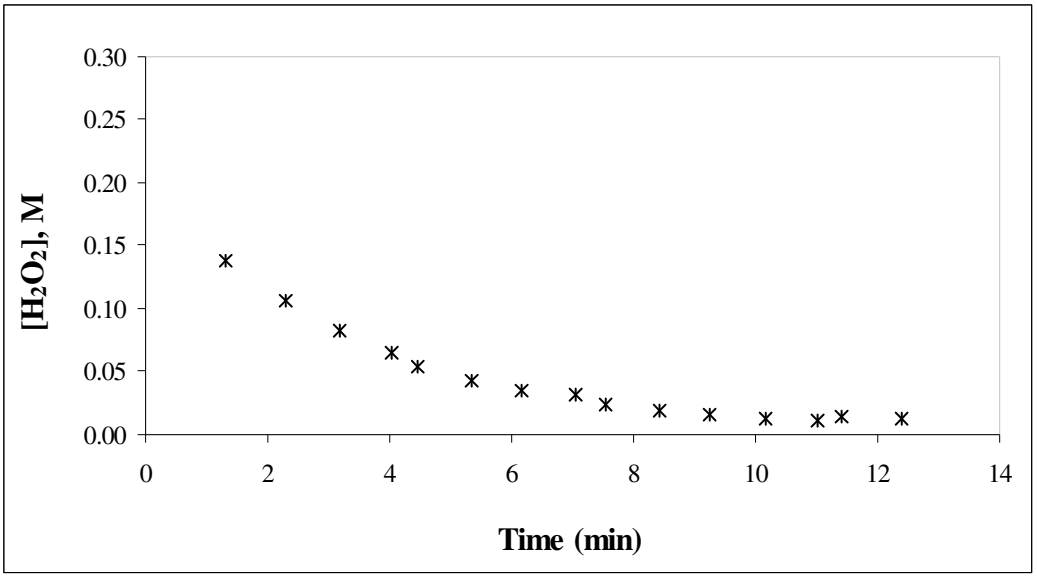

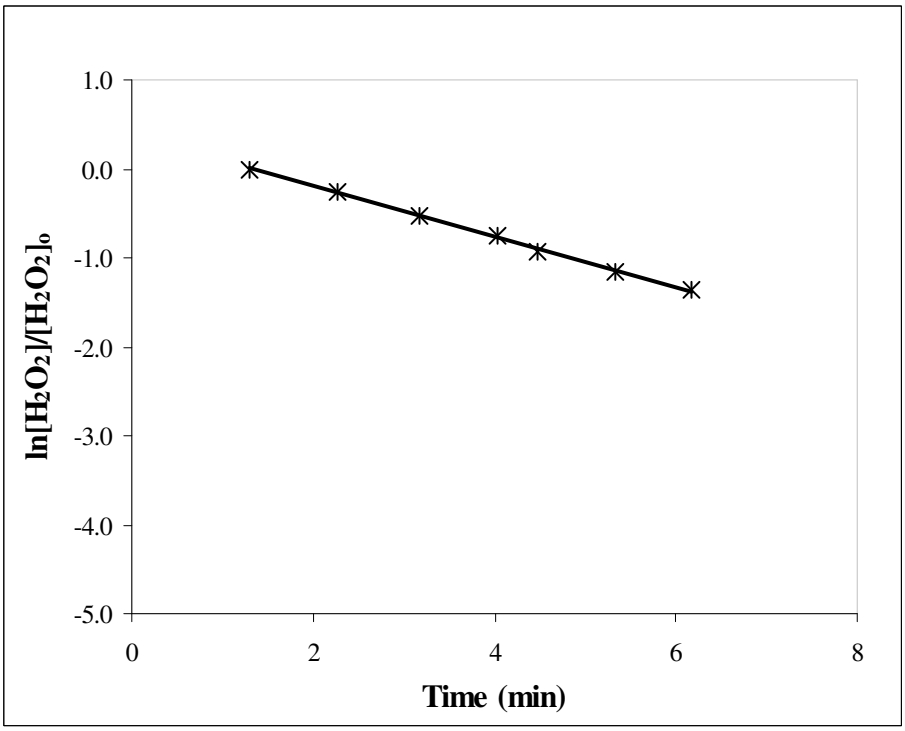

Figure 5.3.1.5(a)(b). H_2O_2 degradation in the presence of iron-amended GAC (7 mg Fe/g GAC) at pH 5. Initial conditions: 12 g GAC, 100 mLs water, and 0.18M H_2O_2, T = 32°C. k_{obs} = 0.28 min^{-1}.

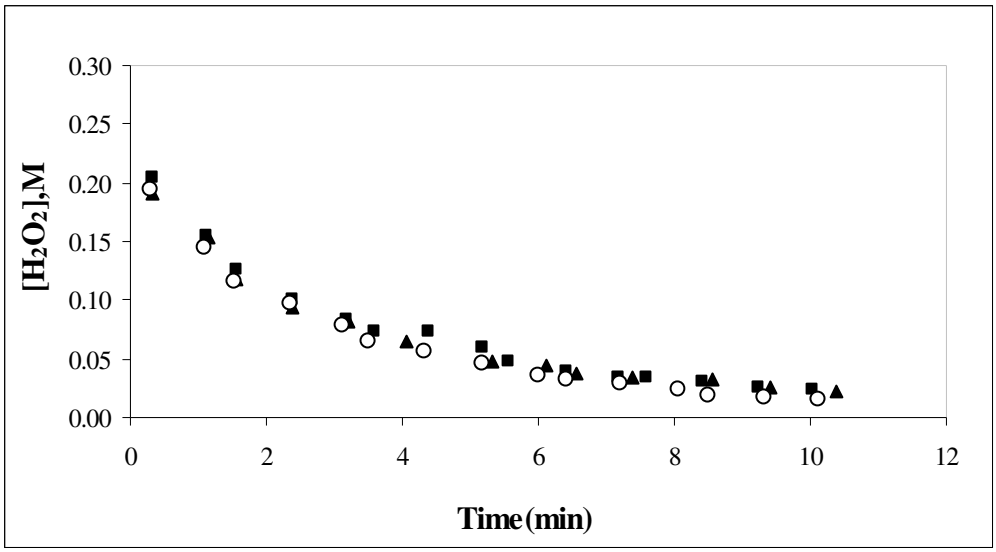

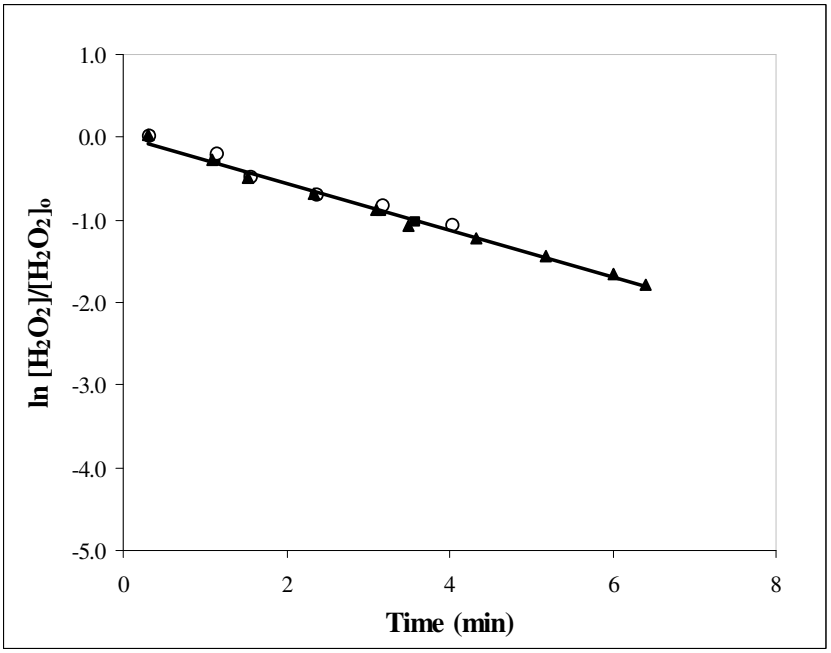

Figure 5.3.1-6(a)(b). H_2O_2 degradation in the presence of iron-amended GAC (7 mg Fe/g GAC) at pH 7. Initial conditions: 12 g GAC, 100 mLs water, 0.18M H_2O_2, and T = 32°C. k_{obs} = 0.30 min^{-1}. Different symbols indicate multiple trials under the same conditions.

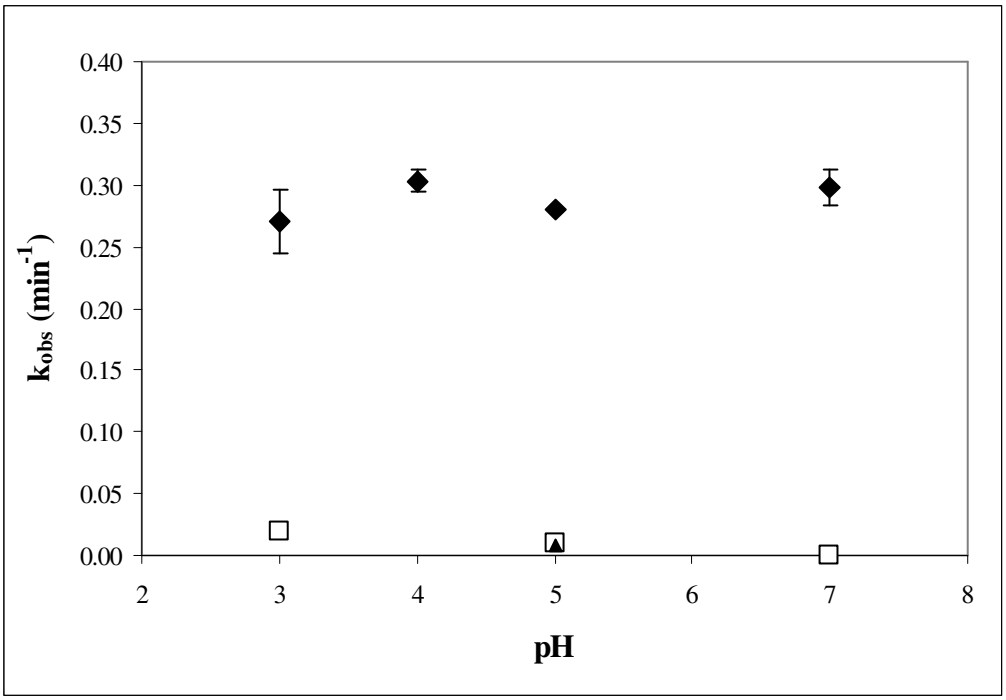

Figure 5.3.1-7. Comparison for H_2O_2 degradation rates observed in the presence of water, background, and iron-amended GAC in the pH range 3-7. Initial conditions: 12 g GAC, 100 mLs water, and 0.18M H_2O_2, T = 32°C. Legend: iron-amended GAC (♦), background GAC (▲), and H_2O_2 in water (□).

5.3.2 pH dependence of H_2O_2 and TCE degradation with iron-amended GAC

Kinetics of hydrogen peroxide degradation were studied at pH 3 and 7 for three types of GAC. In these trials 2 g of background (clean), iron-amended and SolmeteX (iron-amended) GAC were utilized. The iron content on these carbons was approximately 2, 7, and 57 mgFe/gGAC, respectively. Liquid samples were analyzed for both hydrogen peroxide and TCE in solution. At the end of each trial, the GAC was extracted using ethyl acetate and analyzed for TCE. From 60-90% of the H_2O_2 was degraded within 5 hours at pH 7 with iron-amended (Figure 5.3.2-1), SolmeteX (Figure 5.3.2-2) and background GAC (Figure 5.3.2-3). After 5 hours, H_2O_2 was added to the reactor to bring the solution concentration back to the initial conditions. Background carbon consumed the least H_2O_2.

Iron-amended and SolmeteX (iron-amended) GAC behave similarly with respect to H_2O_2 consumption.

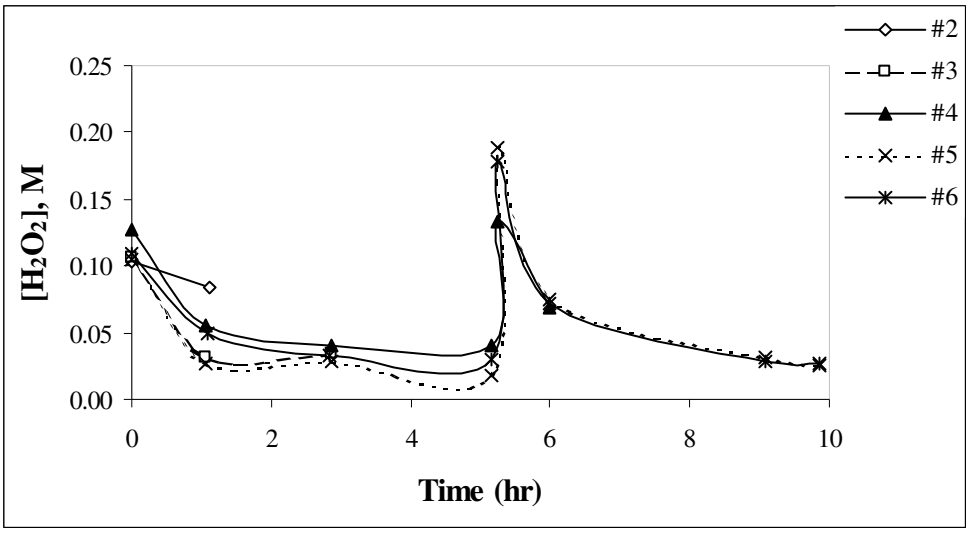

Figure 5.3.2-1. H_2O_2 degradation in the presence of iron-amended GAC loaded with TCE. Initial conditions: $[Fe]_{avg}$ = 7mg/g GAC, 2 g GAC, $[H_2O_2]_o$ = 0.12 M, pH = 7. Each data point represents a sacrificial reactor. Reactor #1 was sacrificed at time 0 hr and reactor #6 at time 24 hr.

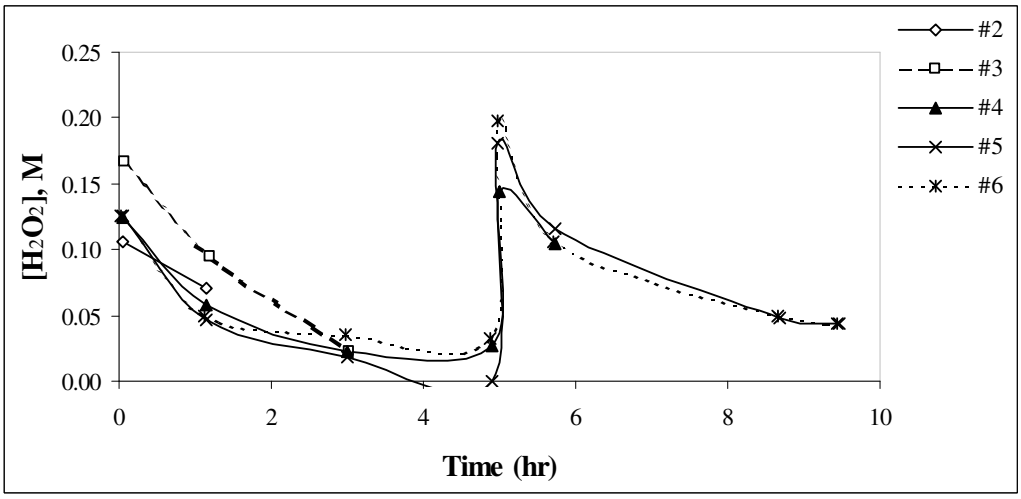

Figure 5.3.2-2. H_2O_2 degradation in the presence of SolmeteX (iron-amended) GAC loaded with TCE. Initial conditions: $[Fe]_{avg}$ = 57mg/g GAC, 2 g GAC, $[H_2O_2]_o$ = 0.12 M, pH = 7. Each data point represents a sacrificial reactor. Reactor #1 was sacrificed at time 0 hr and reactor #6 at time 24 hr.

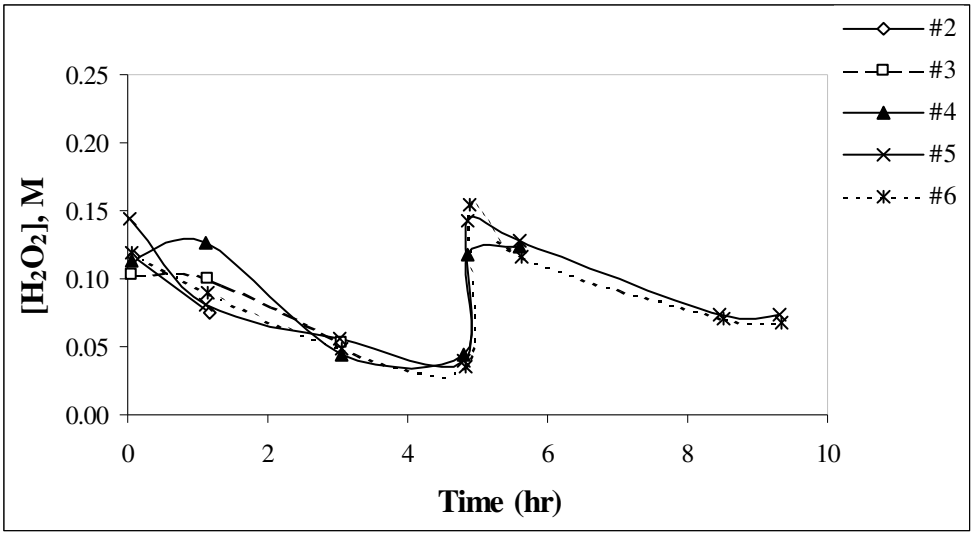

Figure 5.3.2-3. H_2O_2 degradation in the presence of background (clean) GAC loaded with TCE. Initial conditions: $[Fe]_{avg}$ = 2mg/g GAC, 2 g GAC, $[H_2O_2]_o$ = 0.12 M, pH = 7. Each data point represents a sacrificial reactor. Reactor #1 was sacrificed at time 0 hr and reactor #6 at time 24 hr.

When the reactors were sacrificed at different times, the pH was also measured. The results show that hydrogen peroxide was consumed and that this reaction produced protons as indicated by the decreasing pH (Figure 5.3.2-4). A significant pH drop was observed in Fenton reaction at near neutral and neutral pHs (Burbano *et al*., 2005). The extracted GAC samples showed only minimal TCE degradation at pH 7 (Figure 5.3.2-5).

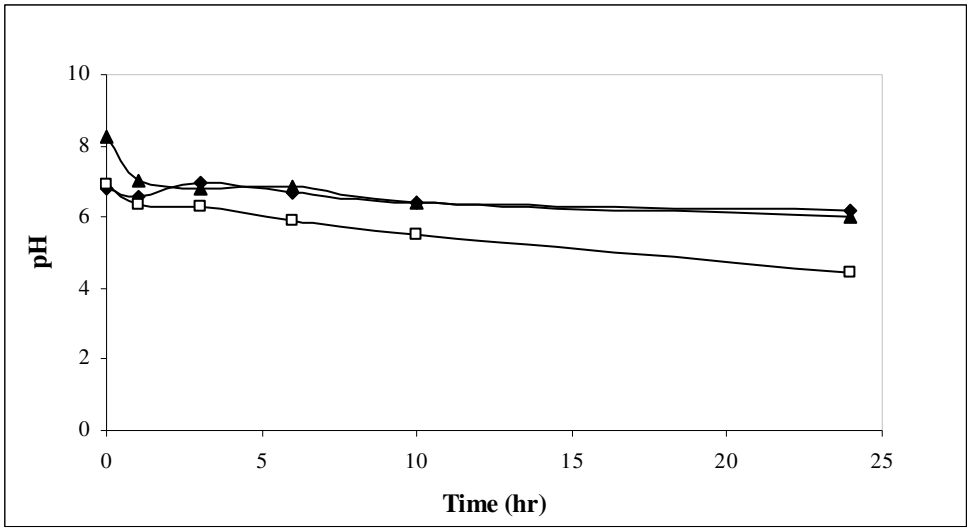

Figure 5.3.2-4. pH variations in each of the reactors sacrificed. Legend: iron-amended GAC(♦), SolmeteX (iron-amended) GAC (□) and background (clean) GAC (▲).

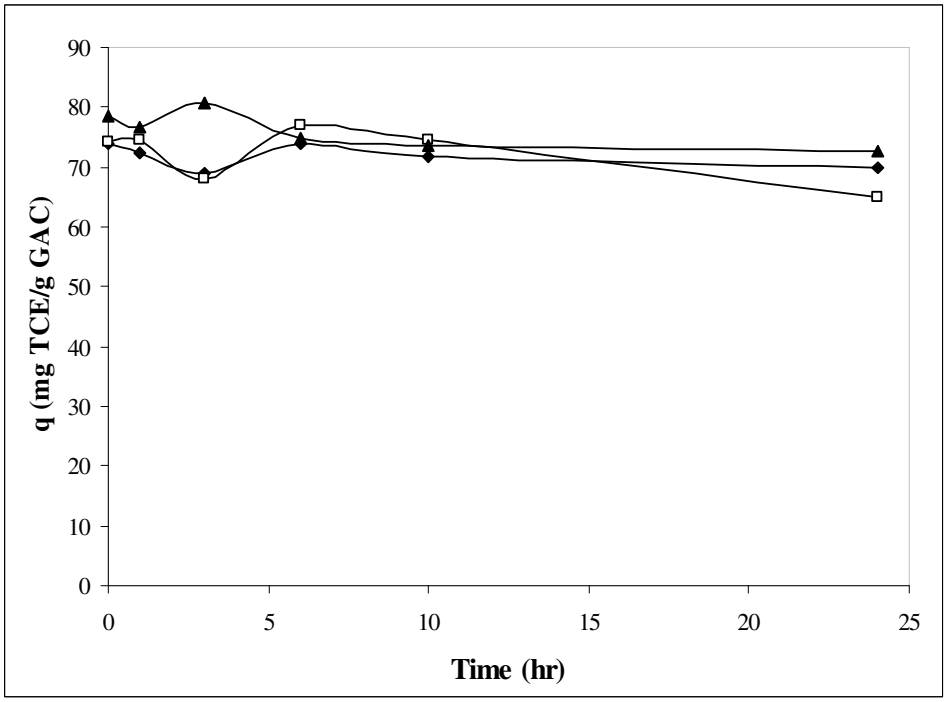

Figure 5.3.2-5. TCE-loaded carbon regeneration in heterogeneous batch experiments. Background (clean) GAC (▲), iron-amended GAC (♦) and SolmeteX (iron-amended) GAC (□) were tested and their corresponding iron content was 2, 7, 57 mg/g GAC, respectively. Initial conditions: 2 g GAC, $[H_2O_2]_o$ = 0.12 M, pH = 7.

A similar study was conducted at pH 3. In these trials, 5 g of each GAC (background, iron-amended and SolmeteX) was used to study the kinetics of hydrogen peroxide degradation. The GAC was first hydrated, pH adjusted and then loaded with a TCE-water saturated solution. After the equilibrium period (approximately 5 days), 1 mL (50%) H_2O_2 was added to each reactor (with 140 mLs of liquid volume) to start the reaction. Again, liquid samples were analyzed for H_2O_2 and TCE. Once the reactor was sacrificed, the pH was measured and the GAC was extracted for analysis of TCE. Hydrogen peroxide was nearly completely consumed after 2 hours and then H_2O_2 was re-added to bring the concentration back to the initial conditions. Again, for both iron-amended (Figure 5.3.2-6) and SolmeteX GAC (Figure 5.3.2-7) the H_2O_2 consumed was comparable, while the background GAC (Figure 5.3.2-8) consumed the least. The pH measurements show that both iron-amended GAC and SolmeteX GAC drop the pH from 2.80 to nearly 2.4, while the background GAC pH dropped from 3.00 to 2.81 (Figure 5.3.2-9).

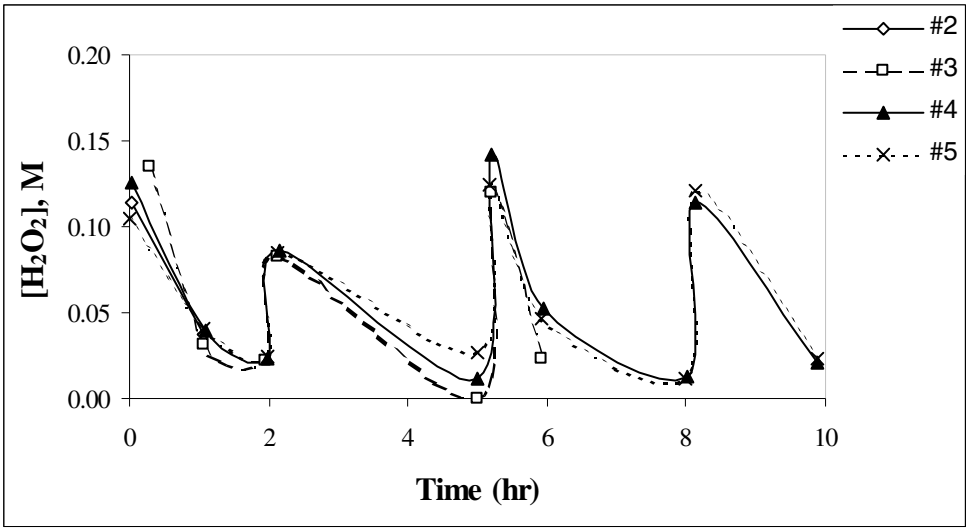

Figure 5.3.2-6. H_2O_2 degradation in the presence of iron-amended GAC loaded with TCE. Initial conditions: $[Fe]_{avg}$ = 7mg/g GAC, 5 g GAC, $[H_2O_2]_o$ = 0.11 M, pH = 3. Each line represents the H2O2 concentration in a separate reactor sacrificed at different times during the ten-hour trial. Reactor #1 was sacrificed at time 0 hr and reactor #6 at time 24 hr.

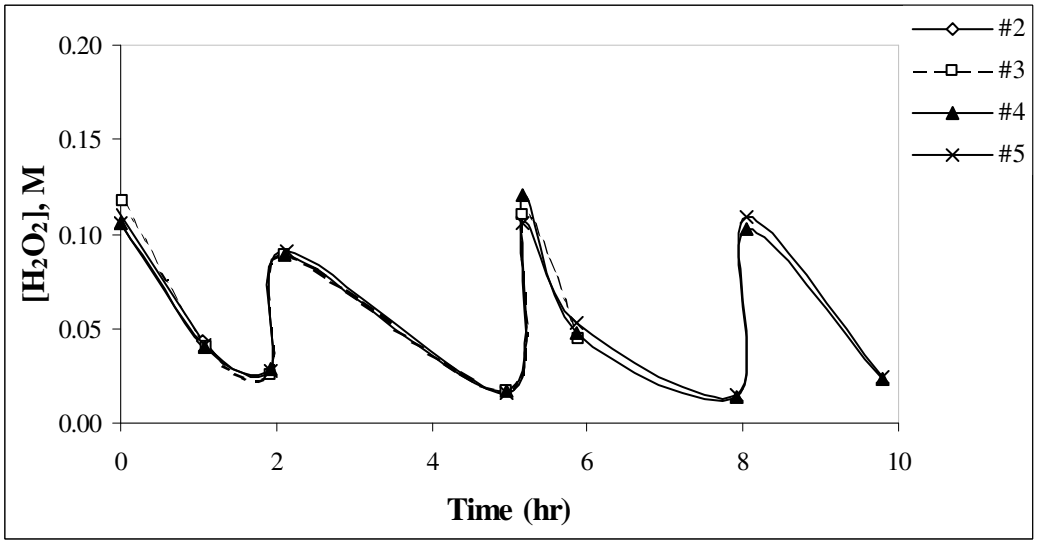

Figure 5.3.2-7. H_2O_2 degradation in the presence of SolmeteX GAC loaded with TCE. Initial conditions: $[Fe]_{avg}$ = 57mg/g GAC, 5 g GAC, $[H_2O_2]_o$ = 0.11 M, pH = 3. Each line represents the H2O2 concentration in a separate reactor sacrificed at different times during the ten-hour trial. Reactor #1 was sacrificed at time 0 hr and reactor #6 at time 24 hr.

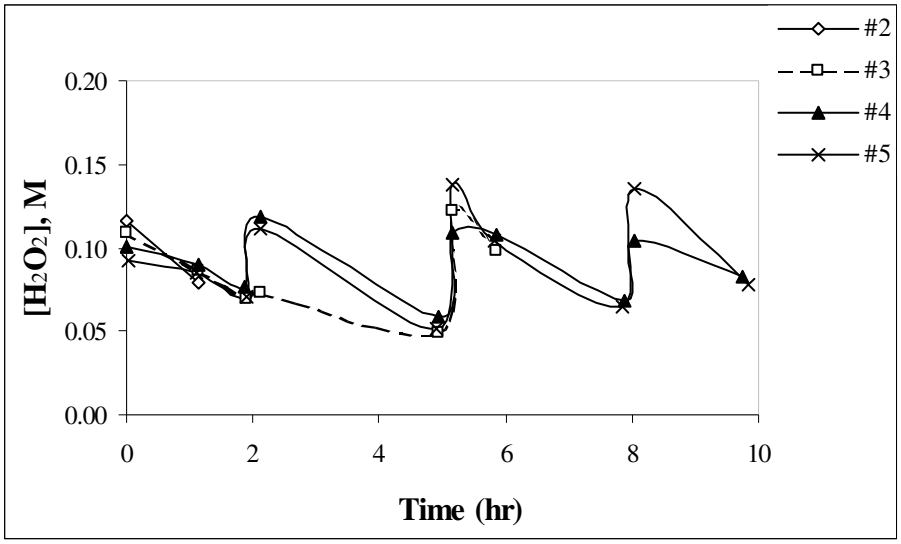

Figure 5.3.2-8. H_2O_2 degradation in the presence of background (clean) GAC loaded with TCE. Initial conditions: $[Fe]_{avg}$ = 2mg/g GAC, 5 g GAC, $[H_2O_2]_o$ = 0.11 M, pH = 3. Each line represents the H2O2 concentration in a separate reactor sacrificed at different times during the ten-hour trial. Reactor #1 was sacrificed at time 0 hr and reactor #6 at time 24 hr.

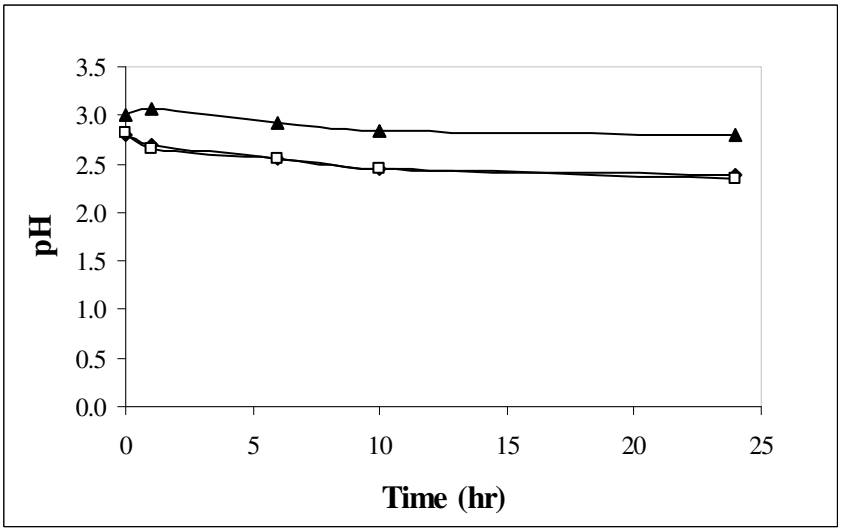

Figure 5.3.2-9. pH variations in each of the reactors sacrificed. Legend: iron-amended GAC (♦), SolmeteX (iron-amended) GAC (□) and background (clean) GAC (▲).

TCE degradation seems to have occurred to some extent on the GAC at pH 3. The data shows (Figure 5.3.2-10) that 35% of the TCE adsorbed to the SolmeteX GAC was

degraded in 24 hours, 15% degradation was observed on the iron-amended GAC and 5% on the background GAC. The studies described were specifically designed to assess whether iron amendment on the GAC surface would enhance GAC regeneration rates and potentially improved the Fenton-driven rates in circum neutral pH conditions in which iron is sparingly soluble. Although pH dependence was observed, the results were of insufficient duration and total change in VOC concentration to allow clear conclusions to be reached.

A comparison of the observed first-order rate constant for H_2O_2 degradation as a function of the total iron in the system at each pH suggests that H_2O_2 decomposition is a function of both total iron and pH (Figure 5.3.2-11). However, this is not a monotonic dependence and an optimum amended iron mass is suggested. The total iron in the system was calculated by multiplying the average (measured) iron content for each GAC (in mg Fe/g GAC) by the grams of GAC used in each trial. Experimental results at both pHs indicate that the H_2O_2 decomposition rate will increase with iron content and then plateaus or decreases at greater iron masses at each pH. The H_2O_2 degradation rate is higher at lower pH for the same iron mass.

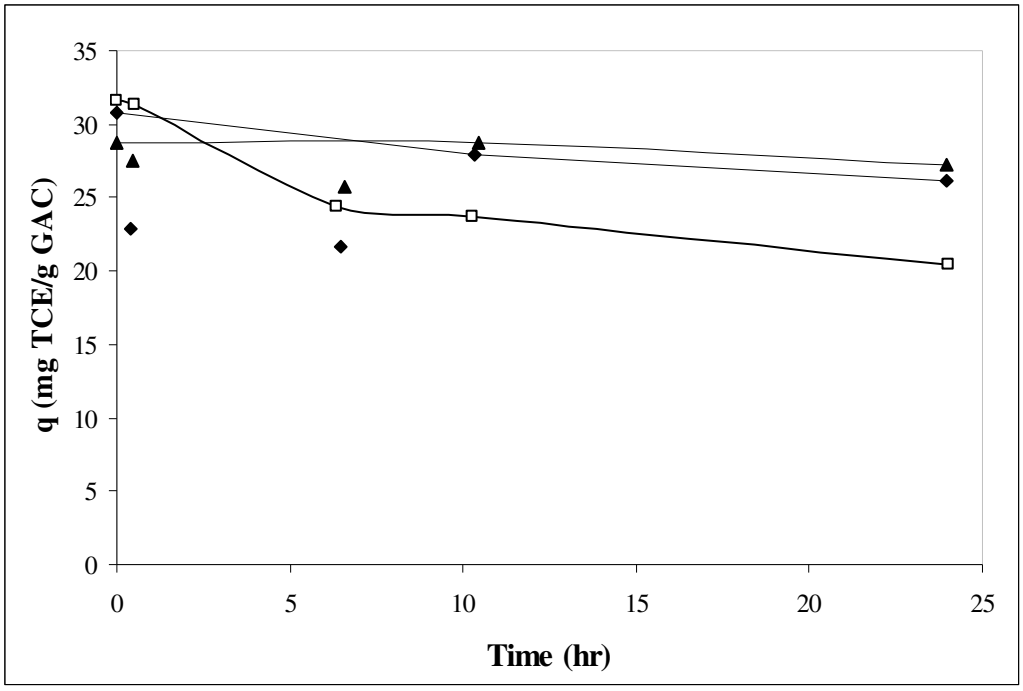

Figure 5.3.2-10. Carbon regeneration for TCE in heterogeneous batch experiments. The GAC utilized were background (clean) GAC (▲), iron-amended GAC (♦) and SolmeteX (iron-amended) GAC (□) and their corresponding iron content is 2,7,57 mg/g GAC, respectively. Initial conditions: 5 g GAC, $[H_2O_2]_o$ = 0.11 M, pH = 3.

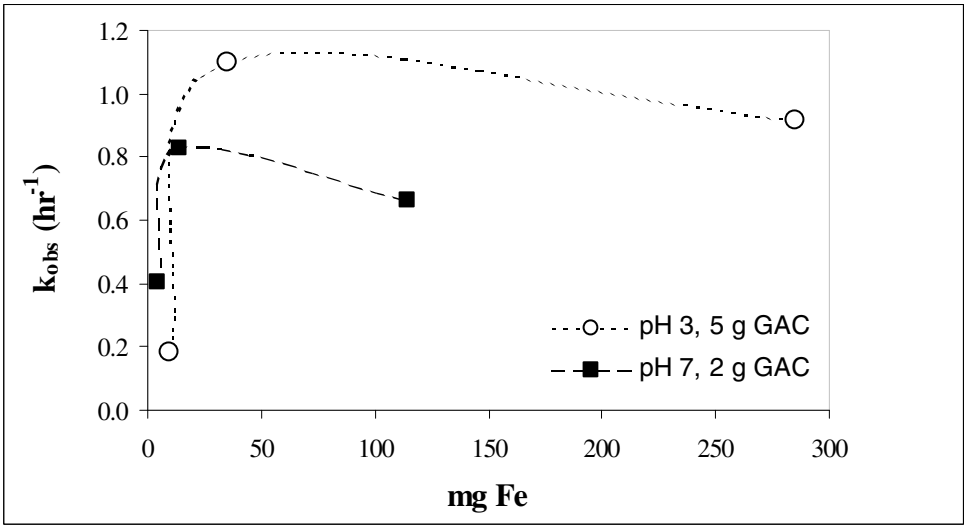

Figure 5.3.2-11. First-order rate constants for H_2O_2 degradation in the presence of TCE-loaded GAC at pH 3 and 7. The GACs utilized were background (clean) GAC, iron-amended GAC and SolmeteX GAC with a corresponding iron content of approximately 2,7, and 57 mg/g GAC, respectively. Initial conditions: 2 g GAC (pH 7) and 5 g GAC (pH 3), $[H_2O_2]_o$ = 0.11-0.12 M.

5.4 Heterogeneous, Bench-Scale Experiments - Summary

- Degradation of GAC adsorbed chlorinated VOCs in heterogeneous Fenton's systems indicated that carbon recovery rates were bi-phasic. A fast initial degradation phase was followed (after 1-3 hours) by a slower second phase. The fraction of contaminant degraded in the initial rapid phase increased as the aqueous-phase solubility and $(1/K)^n$ value of the contaminants increased. Results suggest that intraparticle diffusion of the contaminant limits the recovery rate during the slow phase treatment, for at least the more insoluble subset of the compounds tested.
- When GAC was loaded with CF and recovery was accomplished by rapidly flushing the carbon with clean water, the rate of CF recovery was inversely related to the size of carbon particles. This suggests that pore and/or surface diffusion, and thus particle size, affect the overall removal rate of chloroform from Calgon URV-MOD 1 carbon in Fenton-driven systems.
- Based on the experimental results, it was concluded that mass transport mechanisms can limit the effectiveness of Fenton's reaction for carbon recovery, at least for slightly soluble compounds that are reactive with Fenton's reagents in homogeneous systems. Therefore, optimal design for this type of treatment would maximize contaminant flux from the sorbent, while minimizing the use of H_2O_2, the primary contributor to process cost (see economics analysis in the following chapter).

- Trials were conducted using Calgon URV-MOD 1 carbon on which iron had been precipitated onto the pore and outer surfaces. No iron was added to the bulk regenerant (Fenton's solution). It was hypothesized that this would localize the Fenton-driven radical generation near the GAC surface, in the vicinity of target compounds, and potentially minimize the rate limitations due to pore and surface diffusion and/or compound desorption from the carbon surface. Improvement in the rate of carbon recovery due to the iron amendment was negligible, however. However, iron amendment to the carbon surface did decrease by about 3-fold the rate of H_2O_2 usage (for the same extent of TCE destruction), which is the primary driver in operating cost of the system.
- The pH dependence on H_2O_2 degradation was evaluated using three types of GAC in the presence and absence of an organic target. The GACs utilized in these trials were background (clean), iron-amended and SolmeteX GAC with approximately 2, 7 and 57 mgFe/g GAC, respectively. The pH dependence was studied at pH 3 and 7. H_2O_2 degradation was a function of total iron content and pH. The total iron content in some of the experiments was sufficient to saturate the system with respect to iron such that the H_2O_2 degradation will increase with iron until certain extent and then plateau. The data seems to indicate that addition of total iron, even at concentrations above solubility, will increase the rate of H_2O_2 degradation, but not directly proportional to the iron concentration. Results suggest that the rate of decomposition of both H_2O_2 and TCE seems to be greater at pH 3.

6. FIELD-SCALE REGENERATION TRIALS

6.1 Equipment Testing - Methylene Chloride and Chloroform Recovery Tests

Initial field regeneration trials were carried out using a larger column (I.D. =5 cm, L=30 cm, V=600 mL, residence time = 2 s) containing 100 g URV-MOD 1 GAC that was pre-loaded with MC or CF (under lab conditions). Contaminant selection was based on hydrophobicity and reactivity with hydroxyl radicals (Table 1-1).

Regenerant solution was recirculated continuously during each 30-hour experiment. Hydrogen peroxide was added at 1-hour intervals during hours 0-6 and 23-28 (Figure 6.1-1). At each point of addition, 150 mL of a 50% H_2O_2 stock solution was added to the 7 L recirculation reservoir. Since H_2O_2 was essentially exhausted at each addition point, the H_2O_2 concentration immediately after addition was about 0.38 M.

Carbon was periodically withdrawn from the top and bottom of the reactor for extraction and measurement of residual contaminants. Methylene chloride was essentially gone (full recovery) after 6-7 hours of operation. After 30 hours, just 6% of the original CF loading (125 mg CF/g carbon) remained on the GAC. The cost of recovery ranged from $2.5/kg to $6.6/kg GAC treated for the target contaminants studied. When multiple contaminants are simultaneously adsorbed to GAC, the compound with slowest recovery would determine the overall cost. Little was done in these experiments to limit the non-productive consumption of H_2O_2. That is, neither the configuration of the recovery system nor the schedule of H_2O_2 additions was designed to reduce H_2O_2

consumption/radical production that did not result in MC or CF destruction. Further discussion of this point is provided below.

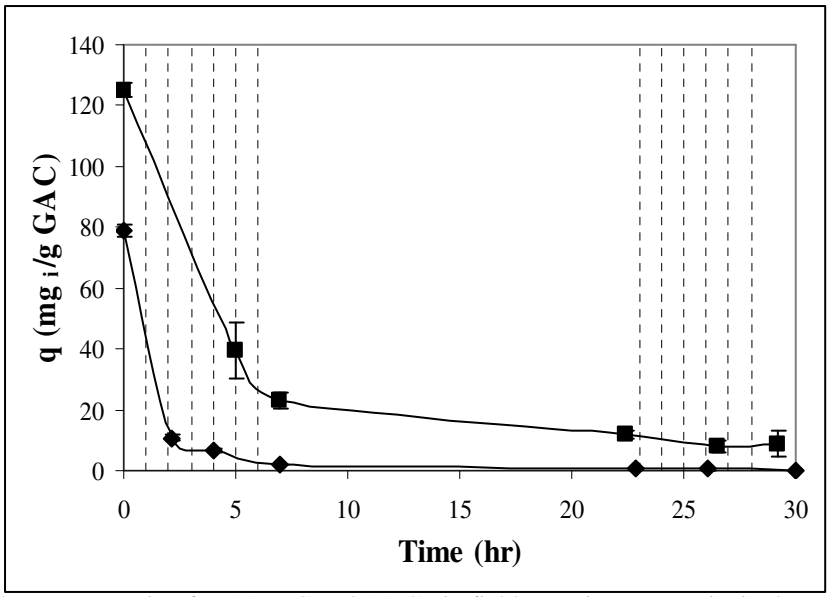

Figure 6.1-1. Carbon regeneration for (♦) MC and (■) CF in field experiments. Units in the y-axis are "mg VOC/g GAC". Degradation to below detection limit and 93% for MC and CF, respectively, was achieved after a 30-hour regeneration period. Reservoir concentrations: 10 mM iron, 0.15 M average H_2O_2, pH = 2.0. Dotted lines indicate times of 150 mL hydrogen peroxide additions. Error bars indicate difference in concentrations measured for samples taken from the top and bottom of the carbon bed.

6.2 Sequential Adsorption/Regeneration Experiments

The feasibility of carbon regeneration depends on both the acceptability of regeneration costs (primarily H_2O_2 consumption) and maintenance of carbon adsorption capacity through multiple degradation steps. Here, carbon adsorption capacity was tested before and after each of three surface regenerations. The work discussed in this section is part of a publication (De Las Casas et al., 2006).

Carbon was loaded with 100-110 mg TCE/g GAC in a batch reactor in the lab, then transferred to the field site for regeneration in the field column. GAC (100 g, dry weight)

was suspended in 1 L of pure water that was pre-saturated with TCE at room temperature (initial TCE concentration ≈ 1100 mg/L). After 3 days, the distribution of TCE between carbon and liquid was near equilibrium with more than 99% of the contaminant on the carbon surface. The process was repeated twice, after field regeneration, using the same carbon sample to determine whether TCE adsorption was adversely affected by Fenton-driven regeneration. During regeneration periods, 0.7±0.2 g carbon samples were periodically withdrawn from the top and bottom of the column and extracted in ethyl acetate for determination of residual TCE. The regenerant solution containing 10 mM total Fe (pH 2) was recirculated at a rate that produced 50% GAC bed expansion. To initiate regeneration, 150 mL of 50% H_2O_2 was added to the 7 L regenerant volume to produce an initial H_2O_2 concentration of 0.38 M. Thereafter, the schedule of H_2O_2 additions was as indicated in Figure 6.2-1. At each point, an additional 150 mL of the 50% H_2O_2 stock solution was added to the regenerant reservoir.

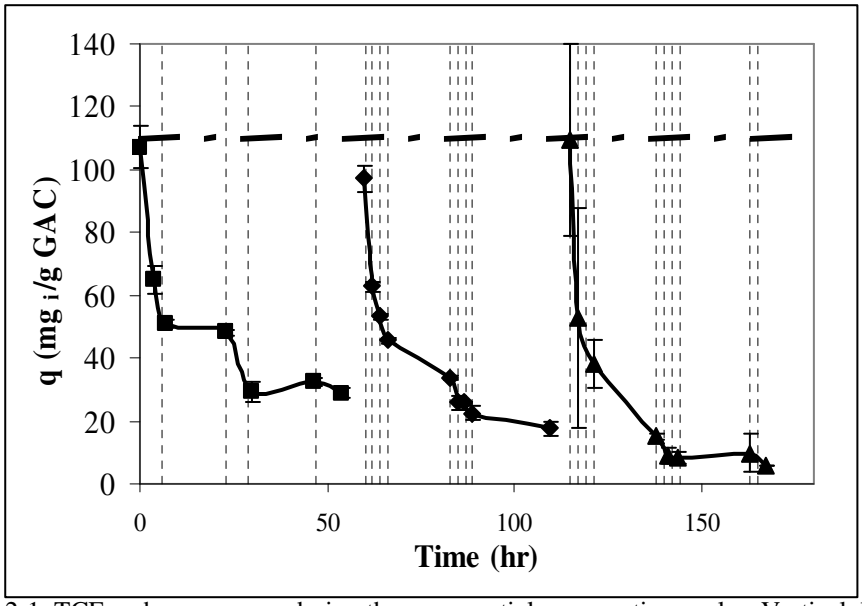

Figure 6.2-1. TCE carbon recovery during three sequential regeneration cycles. Vertical dotted lines indicate points of hydrogen peroxide addition. The horizontal dashed line represents the TCE load (107 mg/g GAC) at the start of the first carbon recovery procedure. TCE degradation of 73% (■), 82% (♦), and 95% (▲) was obtained for the three, consecutive, regeneration cycles. Error bars indicate the difference between the carbon extraction values from top and bottom of the column.

In each phase of the experiment, carbon recovery was initially fast with 50% TCE loss from the carbon surface in 4 hours or less. Thereafter, recovery was much slower so that final (60-hour) TCE recoveries were 73, 82 and 95% during the sequential regenerations. Improvement in the later regeneration cycles was probably a consequence of more frequent H_2O_2 addition rather than a treatment-derived change in the physical characteristics of the URV-MOD1 carbon. Most important was the maintenance of TCE adsorption capacity after the 180-hour experiment (Figure 6.2-1). This finding is supported by previous investigations involving *N*-nitrosodimethylamine (Kommineni *et al.*, 2003) and methyl *tert*-butyl ether (Huling *et al.*, 2005a) adsorption/regeneration on GAC.

Huling et al. (2005a) discussed two mechanisms that could adversely affect the performance of the activated carbon regenerated via an aggressive oxidative treatment such as the Fenton's reaction. In the study, the authors discussed possible chemical and physical alterations to GAC due to oxidative treatment. In a previous study, Huling et al. (2005b) reported reduction in surface area, microporosity, total porosity and sorptive capacity as a result of repeated (10-15) regeneration treatments to the GAC. In addition, incomplete transformation of the target compound(s) may affect the performance of the GAC by accumulating reaction intermediates on sorption sites and in this way diminishing the availability of sites for the target compounds. Other studies have also reported no loss of carbon sorption capacity under aggressive oxidative conditions (Toledo et al., 2003).

TCE was measured periodically in the regenerant reservoir to gauge the adequacy of the H_2O_2 addition schedule. Comparison of regenerant TCE concentrations with (calculated) aqueous-phase concentrations in equilibrium with residual sorbed TCE concentrations (Figure 6.2-2) suggests that less frequent H_2O_2 could have produced similar recovery kinetics while reducing H_2O_2 consumption.

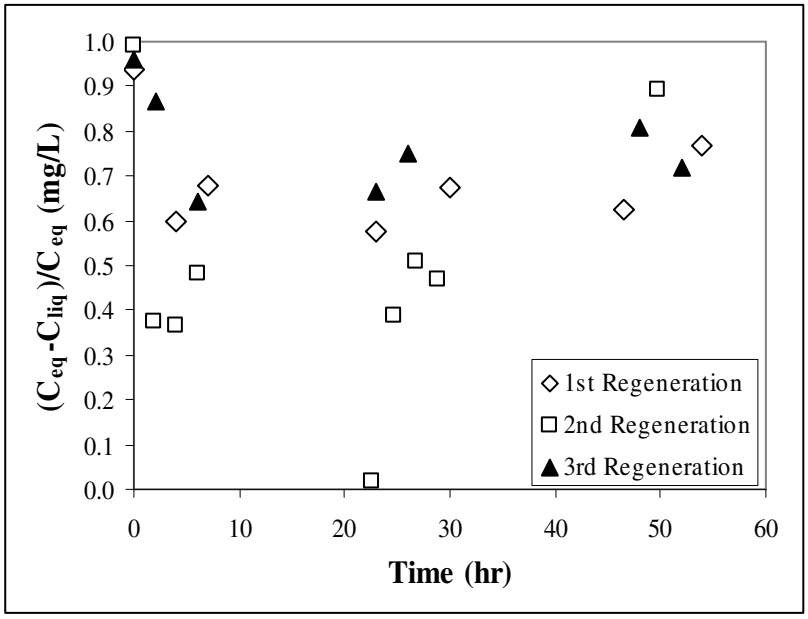

Figure 6.2-2. Ratio of ΔC_l ($C_{eq} - C_{liq}$) to C_{eq}, where C_{eq} is the aqueous-phase TCE concentration in equilibrium with the residual adsorbed concentration (q) and C_{liq} is the measured, liquid phase concentration. Results for three consecutive regeneration periods are superimposed. Equilibrium concentrations were calculated using measurements of residual adsorbed TCE (Figure 6.2-1) and TCE isotherm parameters (Table 2.4.3-1). Note: t = 0 marks the beginning of each recovery cycle.

Were liquid levels to approach equilibrium with residual adsorbed TCE between peroxide additions, reactor performance could be improved significantly by increasing the frequency of H_2O_2 additions. Conversely, if aqueous-phase concentrations remain low relative to equilibrium levels calculated on the basis of adsorbed mass, then the period of H_2O_2 addition could be extended to lower operational costs. The data (Figure 6.2-3) suggest that dissolved TCE was quickly destroyed following each H_2O_2 addition to the regenerant. However, aqueous-phase TCE concentrations also recovered quickly after H_2O_2 was exhausted. There was apparently little to gain by decreasing the frequency of H_2O_2 addition in this experiment.

Temperature was measured in the regenerant solution during the experiment. Overall, temperature increased from ambient (~30°C) to 55-60°C during the 180-hour procedure. This is consistent with the exothermic nature of the Fenton's reaction. Temperature decreased slowly following H_2O_2 exhaustion (1-2°C/hr). Greater temperature increases might be expected in larger reactors although more judicious application of H_2O_2 or reduction in regenerant iron levels would tend to mitigate temperature rise. Because TCE mass transport and reaction kinetics are favorably affected by higher temperature, the exothermic decomposition of H_2O_2 via reaction with iron might, if handled carefully, increase carbon recovery rates and lower overall costs for carbon surface regeneration.

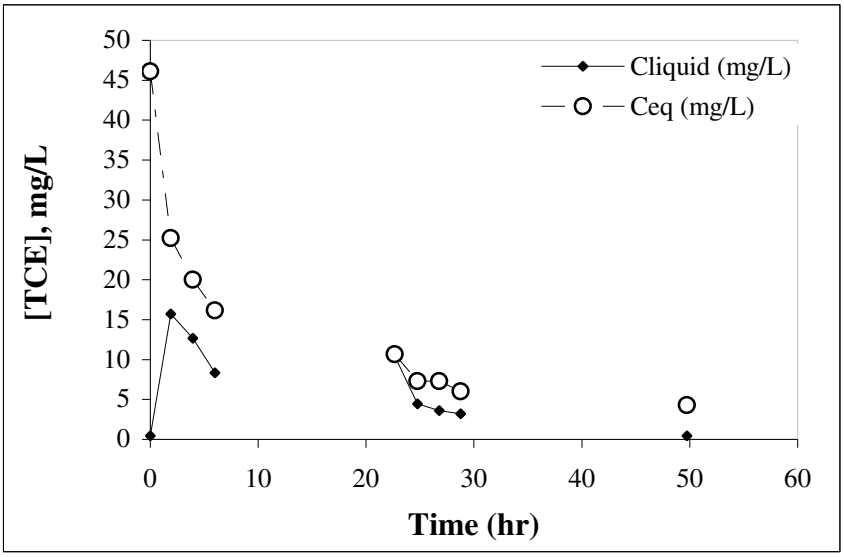

Figure 6.2-3. Comparison between Ceq (aqueous-phase TCE concentrations in equilibrium with the residual adsorbed concentration (q) and Cliq (measured, liquid phase concentration). Original data from Figure 6.2-1. Equilibrium concentrations were calculated using measurements of residual adsorbed TCE (Figure 6.2-1) and TCE isotherm parameters (Table 2.4.3-1). Note: t = 0 marks the beginning of the recovery cycle.

6.3 Loading Carbon with SVE Gases

Vadose zone gases from the soil vapor extraction system at the Park-Euclid (Arizona) state Superfund site containing primarily PCE, TCE and light diesel components as contaminants were used to load URV-MOD 1 GAC in a final set of field experiments.

It is likely that gas-phase contaminants experience more facile access to adsorption sites in carbon micropores, so that the contaminant mass removed prior to apparent breakthrough may be greater in gas-phase applications. Nevertheless, a water film is almost always present on the carbon surface in such situations, so that, ultimately, the adsorption capacity is dictated by the heterogeneous equilibrium between the adsorbed and liquid-phase chemical. If Henry's Law limits the liquid-phase chemical concentration, the carbon load at breakthrough should be indifferent to the form in which the contaminant is applied. That is, gas-phase treatment should yield the same loading as treatment of a liquid that is in Henry's Law equilibrium with that gas. Crittenden et al. (1988) suggested that 45% relative humidity represents a critical cutoff point, in that a liquid film is fully developed on the carbon at sustained relative humidity greater than 45%. Gas removed from surface solids should be near saturation levels with water vapor (at the soil temperature). For this reason, a moisture knockout box is usually included in SVE designs.

The GAC was loaded for approximately 72 hours using a 4-cfm SVE side-stream. Effluent gases were pumped back into the system of extraction wells. To determine the carbon loading, GAC samples were taken from the top and bottom of the column, extracted in ethyl acetate and analyzed with GC-ECD. Initial, 6-hour regeneration trials

produced 80% reduction in the adsorbed TCE concentrations, but only a 30% loss of adsorbed PCE (Figure 6.3-1). As in the previous field trials, degradation was initiated by adding 150 mL of the 50% H_2O_2 stock to the regenerant solution (total volume 7 L). Subsequently, 50 mL of the stock H_2O_2 solution was added every 15-30 minutes to replenish the initial H_2O_2 concentrations throughout the regeneration period. This procedure led to excessive H_2O_2 utilization and attendant cost.

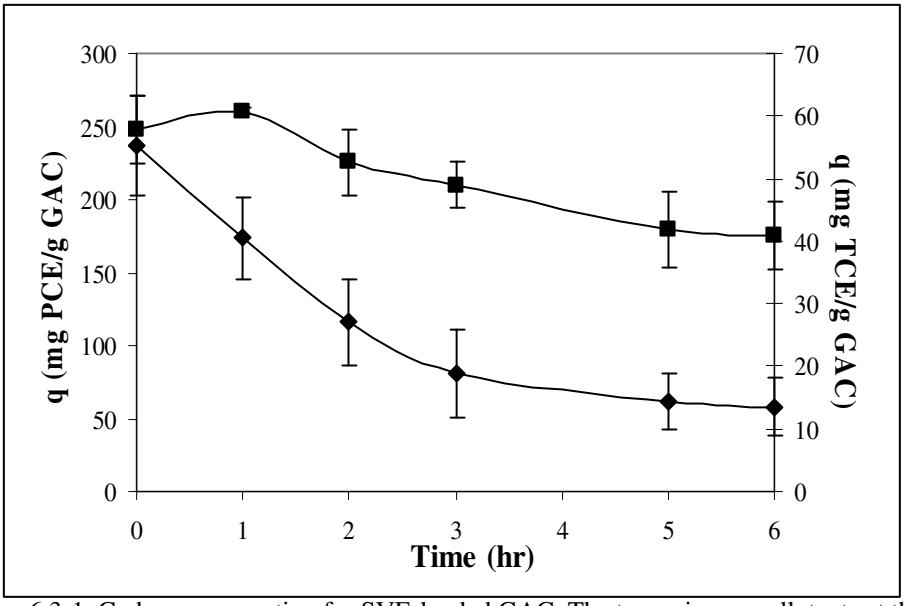

Figure 6.3-1. Carbon regeneration for SVE-loaded GAC. The two primary pollutants at the site are PCE and TCE. Overall, 30% and 80% degradation for PCE (■) and TCE (♦) were achieved during the 6-hour regeneration period. Reagent concentrations were 10 mM iron, 0.15 M H_2O_2 (average), at pH = 2.0. Error bars indicate the difference between the carbon samples from top and bottom of the column.

A total of 1.1 L of 50% H_2O_2 was consumed to destroy 7.0 g of PCE and 4.0 g TCE. This gives a molar yield of 2.2×10^{-3} and 1.6×10^{-3} for PCE and TCE, respectively. Pulsed addition of H_2O_2 with intervening periods in which H_2O_2 was exhausted (for contaminant transport to the bulk regenerant phase) might have produced comparable recoveries using a fraction of the oxidant. Peroxide costs could also be lowered significantly by reducing

the volume of regenerant in the system. In the presence of Fenton's reagents, aqueous-phase concentrations of contaminants were generally near zero. Because the rate of H_2O_2 consumption is independent of the contaminant concentration, however, H_2O_2 use continued during such periods without affecting contaminant transport out of the carbon particles. Under all circumstances, H_2O_2 consumption was proportional to the total regenerant volume, including the volume in the recirculation tank, where little or no contaminant was consumed under conditions of the field test. Consequently, future field experiments using similar conditions could further reduce the recirculation tank volume to lower reagent costs.

6.4 Economic Analysis

The cost of an in-place GAC recovery system based on Fenton's mechanism would include reagent (H_2O_2) consumption, power requirements to circulate regenerant, replacement of carbon that is lost due to abrasion and chemical (treatment) inactivation/destruction, capital expenses associated with the regeneration system itself (pumps, pipes and tanks) and the additional capacity necessary for temporary column retirement for regeneration. Here, it is assumed that H_2O_2 costs dominate the additional cost for an in-place Fenton carbon recovery system (see subsequent, detailed GAC Economic Analysis for a more complete cost estimate supporting this assumption). The primary sinks for •OH are H_2O_2 itself, due to concentration effects (Table 4.3.3-1) and possibly (as regeneration cycles progress) free chloride ion. Thus, free radical concentrations (and H_2O_2 consumption rates necessary to maintain those levels) are

essentially independent of the identity or concentration of the target compounds. This is not to say, however, that H_2O_2 costs are independent of contaminant identity. Compounds that desorb slowly from GAC require significantly greater time to achieve comparable degrees of recovery and, hence, greater recovery costs (Table 6.4-1).

Table 6.4-1. Cost Estimates at the Bench and Field Scales

	Cost ($/kg GAC)[b]	
Compound	Bench- Scale T= 32°C[a]	Field-scale
MC	4.6	6.63 (100%) 3.57 (97%)
1,2-DCA	N/A	N/A
1,1,1-TCA	N/A	N/A
CF	3.50 (93%)	6.63 (93%)
CT	N/A	N/A
TCE	5.14 (52%)	2.55(73%) 4.53(82%) 6.54(95%)
PCE	2.63(35%)	6.54(50%)

NOTE: [a]Bench-scale regeneration column experiments at 32°C (Figure 5.2.1-1). [b]Cost is based on hydrogen peroxide consumption for spent GAC regeneration. The number in parenthesis indicates the percentage GAC recovery for each trial.

When multiple contaminants are present simultaneously, the compound most resistant to Fenton-driven recovery, in this case PCE, is likely to dominate recovery costs. Consequently, PCE degradation was used to estimate overall carbon regeneration costs. Other assumptions and economic or operational factors were:

Unit cost of H_2O_2	\$0.34/L (Kommineni *et al.*, 2003)
(50% solution, 1.18 g/mL)	(transportation cost not included)
H_2O_2 utilization for carbon recovery	95-232 mL (bench-scale column)
	1-2 L (field column)
Carbon in experimental columns	10-16 g (bench-scale column)
	78-100 g (field column)
Carbon purchase cost (EPA, 2000)	\$1.54-2.64/kg virgin coal carbon
	\$1.10-1.72/kg regenerated carbon
Carbon change out/disposal	\$0.66/kg (soiltherm.com, 2006)

Costs for carbon recovery/replacement alternatives are compared in Table 6.4-2. The comparison is necessarily simplistic. The mechanism, rate limitation and kinetics of PCE recovery on GAC are poorly known, certainly not well enough to produce a most refined economic analysis. In-place oxidations of all other contaminants tested were significantly faster than that of PCE and, therefore, more economically attractive. Nevertheless, PCE was among the important contaminants in this application and should be considered when assessing the utility of the technology locally.

Table 6.4-2. Comparison of GAC Replacement vs. Regeneration Costs

Option	*Cost/kg*	*Critical assumptions/parameters*
1. Replacement	$3.30	$2.64/kg purchase cost $0.66/kg disposal of spent carbon
2. Thermal Regeneration	$2.64	$1.65/kg regeneration cost $0.66/kg transportation $0.33/kg carbon replacement
3. Fenton-based, in-place recovery		Peroxide costs dominate (0.34/L) PCE recovery dictates treatment time
a. Lab column	$2.69	95 mL H_2O_2/12 g GAC
b. Field column	$6.54	1.5 L H_2O_2/78 g GAC

Methods for increasing the efficiency of H_2O_2 use have been discussed to some extent. The mixing reservoir allowed the Fenton reaction to take place and H_2O_2 to be consumed without oxidation of the target contaminants. Based on the dimensions of the pilot-scale column, and assuming a porosity of 0.5 of the GAC, the pore volume within the column is approximately 0.3 L. The total liquid volume of the reactor system was 7 L. This suggests that more than 95% of the H_2O_2 applied to this system was consumed outside of the column (i.e. 0.3 L/7 L). Although we assume that the Fenton reaction (in our system) occurred predominantly in the reservoir, limiting the H_2O_2 reaction outside the mixing reservoir would economize H_2O_2. It may be possible to immobilize iron on the carbon surface and run regenerations in a pH range to avoid iron dissolution during recovery operations. The feasibility of such a scheme depends on selection of iron loadings that allow degradation reactions to proceed without blocking the carbon surface or interfering with contaminant access to carbon pores. Preliminary tests of Fenton-driven recovery in such iron-mounted systems have been discussed in a previous section. The potential advantage lies in localization of H_2O_2-consuming reactions and radical generation in the vicinity of the carbon surface. Bulk-aqueous-phase Fenton reactions can

be minimized (i.e. sizing down reservoir) so that non-productive H_2O_2 consumption (that which destroys no contaminants) is greatly diminished.

6.5 Cost estimation based on iron-amended GAC regeneration.

The cost of carbon recovery in the field-scale reactors using iron-mounted on the surface of the GAC is discussed here by considering the scale-up factors and issues for going from bench to field scale. The field-scale set-up is approximately seven times bigger than the bench-scale, in which experiments with iron-amended carbon were actually run (based on g GAC and reservoir size). This factor was used to roughly scale costs to the field-scale. Table 6.5-1 summarizes the results from the bench-scale trials, discussed previously (see bench-scale section). The last column shows the estimated demand for H_2O_2, scaled-up to field dimensions. If the iron-amended GAC were employed in field trials, attendant costs will be significantly lower that those actually encountered. For example, if we regenerate 100 g GAC, it is estimated that 181 mL H_2O_2 will be consumed. Actual field trials utilized 1-2 L H_2O_2 when iron was provided. That is at least 8 times higher than the amount to be used if an iron-amended GAC system were implemented. In the field site studied, the SVE stream contains mainly TCE and PCE. However, the presence of other organic compounds can increase the demand for H_2O_2. Nevertheless, for ease of calculations it is assumed that the same amount of H_2O_2 will be applied in the recovery of the spent GAC when both TCE and PCE are present. Consequently, the cost of GAC regeneration for SVE-loaded GAC will be the same for both compounds, and estimations based on TCE regeneration will be applied to estimate

the field-scale cost. If the iron-mounted GAC is 10 times more efficient than the soluble iron system, then the peroxide cost would be $0.62/kg GAC ($0.28/lb GAC). Under these circumstances, the iron-amended GAC regeneration is probably less expensive than replacement of spent GAC (Table 6.5-1). A more complete economic analysis follows.

Table 6.5-1. Cost Evaluation Based on Bench-Scale Results Using TCE-Loaded and Iron-Amended GAC.

GAC type	Iron Content	C/Co (TCE)	H_2O_2 (mL)	H_2O_2 (mL) scaled-up to field dimensions (estimate)
Iron-amended GAC	7.4mgFe/gGAC (5 mM)	47%	25.8	181 ($0.62/kg GAC)$^+$
Iron in Solution, pH 2	10 mM	50%	160-224	1.6*

*Actual field scale trials employed 1-2 L H_2O_2 for experiments using iron in solution.
Field-scale is approximately 7x bigger than bench-scale experiments.
Costs can be easily calculated using the cost of H_2O_2 ($0.34/L). Field scale reservoir can be reduced in size as it was done with the bench-scale trials, reducing costs by half.
$^+$ Costs calculated for 181 mls H_2O_2 to regenerate 100 g GAC.
Both background GAC and iron-amended GAC trials employed a 400 ml-size reservoir (less than half the size of the iron in solution experiment (1 L reservoir).

6.6 GAC Economic Analysis

The economic analysis conducted here was designed to compare alternative carbon replacement/regeneration strategies in processes using activated carbon for contaminant adsorption. In scenario #1, spent carbon is replaced with new activated carbon, and the waste carbon is disposed of as a hazardous waste. Scenario #2 differs in that carbon is periodically regenerated or, at least, partially regenerated using Fenton's reagents to destroy the adsorbed contaminants. The economic analysis was carried out by comparing costs that are unique to each scenario on both a present worth and an annual cost basis. Most of the costs from activated carbon adsorption for treatment of gas-phase streams derived from SVE (the basic scheme for both scenarios) are common to both alternatives.

As such they are omitted from the analysis. These include energy costs for the SVE system, capital costs for the carbon adsorption unit, initial carbon costs and some maintenance and other labor activities. A description of the costs that are unique to each alternative follows:

	Scenario #1	Scenario #2
Carbon costs	GAC replacement cost GAC cost = $1.60/lb Disposal cost = $1.00/lb	5% loss/regeneration cycle GAC cost = $1.60/lb No disposal costs
H_2O_2 consumption	Not Applicable	$0.345/lb H_2O_2 plus transportation from Houston $3.50/mi, 1067 miles
Incremental capital for chemical dosing/storage	Not Applicable	Dosing pumps, H_2O_2 storage tanks

The scenarios were built in part from field experience in this project (H_2O_2 dosing and time to recovery) and in part based on engineering rules of thumb or professional judgment. Cost comparisons were carried out for carbon recovery when (i) PCE and (ii) methylene chloride were the target contaminants. The behaviors of these compounds during carbon regeneration were diametrically opposed. PCE provides a challenging recovery problem, presumably because of its affinity for the carbon surface and consequent slow desorption rate. Carbon recovery following methylene chloride breakthrough is remarkably fast, probably due to its low affinity for the carbon surface.

Other assumptions or data used to support the economic comparison were:

- bulk GAC density = 0.5 kg/L
- gas-flow rates during SVE = 10, 100 cfm (2 distinct analyses)
- equilibrium is assumed to exist among gas, liquid and solid phases at breakthrough during SVE
- T = 25°C

- The concentration of contaminant (PCE or MC) in the gas treated by SVE is 100 ppmv.
- GAC column diameter = 1 m
- The mass of carbon in the column is irrelevant since carbon wastage rates are calculated on the same basis for each scenario investigated
- The pump efficiency during recirculation of Fenton's reagents is 0.70.
- The economic discount operator of 0.08 was assumed
- Equipment for H_2O_2 dosing and storage has a service life of 20 years
- GAC disposal cost ($1.00/lb) is an engineering estimate
- All GAC costs are in year 2000 dollars and all other cost are in 2006 dollars

Details for the analysis, including calculations, are provided in Appendix B. Additional assumptions are exposed in the appendix. The following summary represents the annualized costs that are unique to each alternative (Table 6.6-1). Annual costs are provided for hypothetical SVE systems treating gas flows of 10 and 100 cfm for removal of PCE or methylene chloride. Alternative #2 consists of in-place recovery using the Fenton-driven method investigated here.

The analysis shows that the chemical costs are in fact the dominant expense in Scenario #2 (Appendix B). The following analysis was added to this section and to Appendix B to highlight the importance of H_2O_2 purchase to the total cost in Scenario #2.

Table 6.6-1. Cost estimates comparing hazardous waste disposal of spent GAC (#1) and virgin carbon replacement versus Fenton's reagent regeneration of GAC (#2).

Target Contaminant / SVE Flow	PCE	MC
10 cfm	#1: $2,545 #2: $25,212	#1: $1.1M #2: $0.83M
100 cfm	#1: $25,416 #2: $239,745	#1: $11.1 M #2: $8.2M

Note: Option 1: GAC cost = $2.60/lb. Option 2: GAC cost = $1.60/lb (no disposal), H_2O_2 cost (purchase and transportation), additional process energy, labor, and capital (recirculation pumps, chemical storage tanks).

6.6.1 Cost of H_2O_2 consumption in Fenton's system

The following table (6.6.1-1) contains both total costs for each treatment alternative and the associated H_2O_2 cost in order to illustrate the importance of reagent costs to overall process economics.

Table 6.6.1-1. Summary of estimated H_2O_2 cost contribution to total cost of Fenton's regeneration.

Compound	Total H_2O_2 Cost for GAC regeneration ($/yr)		Total Annual Cost ($/yr)		Fraction of H_2O_2 Cost for GAC regeneration ($/yr)	
	Q_{air} =10 cfm	Q_{air} =100 cfm	Q_{air} =10 cfm	Q_{air} =100 cfm	Q_{air} =10 cfm	Q_{air} =100 cfm
PCE	17,966	179,495	25,212	239,745	71%	75%
MC	0.75M	7.4M	0.83M	8.2M	90%	90%

Note: All values were obtained from Appendix B.

6.6.2 Engineering considerations

A number of practical considerations that may affect operation of a Fenton-driven carbon recovery system have been neglected to this point. Chief among these is (i) the generation of molecular oxygen from the decomposition reactions of H_2O_2 in the presence of iron and (ii) the exothermic character of the same reactions. In this section, each of these is analyzed using engineering tools in order to gain perspective on the magnitude of related operational difficulties.

In the case of gas-phase O_2 generation, field data on H_2O_2 consumption are combined with operational flow rates and hydrogen peroxide decomposition stoichiometry to determine the probable oxygen volume rate of flow during regeneration. For perspective, this is compared to the volume rate of flow of the regenerant stream that is necessary to expand the carbon bed during regeneration. The analysis can go only so far, however, since the effects of oxygen generation in carbon pores cannot be adequately addressed without much more study.

The engineering analysis of heat generation/transport is again based on the H_2O_2 consumption data and regenerant flow using the (known) heat of hydrogen peroxide decomposition. In this case, the regenerant flow and specific heat of water allow us to calculate the regenerant temperature rise necessary to balance the rate of heat liberation due to reaction during one pass of regenerant through the reactor during recovery. Then, based on the volume of regenerant in the storage tank and regenerant flow rate it is possible to predict the rate and extent of fluid temperature rise during recovery operations.

The methods and calculations are fully explained below.

6.6.2.1 Hydrogen Peroxide stability

The main factors affecting H_2O_2 decomposition during storage include: increasing temperature, pH (pH > 6-8); impurities (i.e. transition metals such as copper, manganese or iron); and exposure to ultraviolet light. Overall, pH and contamination are the dominant factors (US Peroxide, 2006)http://www.h2o2.com/intro/faq.html. Generally, 50% hydrogen peroxide loses less than 1% per year when stored properly (http://www.h2o2.com/h2o2update/volume2/hypochlorite.html). During Fenton's based reactions, of course, H_2O_2 decomposition is exactly what is to be promoted.

Hydrogen peroxide often decomposes exothermically into water and oxygen gas spontaneously:

$$2H_2O_2 \rightarrow 2H_2O + O_2 + \text{Energy} \qquad (68)$$

This process is very energetically favorable; with a $\Delta H°$ of –98.2 KJ/mol, a $\Delta G°$ of -19.2 KJ/mol and a ΔS of 70.5 J/mol °K. The H_2O_2 decomposition rate is dependent on the temperature, H_2O_2 concentration, pH and the presence of transition metals and stabilizers (Wikipedia, http://en.wikipedia.org/wiki/Hydrogen_peroxide#Decomposition). Even though pure H_2O_2 is quite stable, it can decompose to produce water and oxygen when heated above 80°C. http://www.infoplease.com/ce6/sci/A0824724.html

6.6.2.2 The heat of H_2O_2 decomposition

Accumulation of heat in the regenerant and, as a consequence, in the carbon bed from the exothermic decomposition of H_2O_2 could be beneficial within manageable limits, but would be a problem if excessive. However, moderate heat generation and consequent temperature increases could aid the recovery process by increasing radical generation rates and the rates of temperature dependent mass transfer processes. An energy balance was used to estimate the temperature increase in the regenerant. In the balance, the average rate of heat generation by hydrogen peroxide decomposition was exactly balanced by the rate of heat loss in advective flow through the column. That is

$\Delta H^{\circ}_{rxn}\, \dot{m}_{H_2O_2} = \rho Q C_p \Delta T$ where

$\Delta H^{\circ}_{rxn}\, \dot{m}_{H_2O_2}$ = average rate of heat generation from the H_2O_2 decomposition (J/min)

ρ = density of the solution (g/mL)

Q= flowrate through the column (mL/min)

C_p = specific heat (cal/g $^{\circ}$C)

ΔT = temperature change = $T_f - T_i$ ($^{\circ}$C)

It should be noted that $\dot{m}_{H_2O_2}$ is taken here as the average rate of H_2O_2 use during experiments that comprised the field demonstration project. H_2O_2 was unevenly applied and consumed during those experiments, however. Consequently, there will be periods in which heat is generated more rapidly and more slowly than estimated here. The average rate of heat generation provides an adequate estimate of temperature rise as long as that rate is not so rapid as to become dangerous during particularly fast reaction periods

(immediately following addition of H_2O_2 to the regenerant). In fact, predicted and (field) observed rates of regenerant temperature rise proved to be modest (see below).

Furthermore, it was assumed that:

The heat capacity of the carbon and column materials could be ignored;

Radiative heat losses were comparatively small;

1. There was no cumulative heat energy in the regenerant or carbon bed (one-pass analysis);
2. Excursions from the average rate of H_2O_2 consumption and heat generation could be ignored for convenience; and
3. All reactions involving H_2O_2 other than its breakdown to water and molecular oxygen could be ignored.

Heat production:

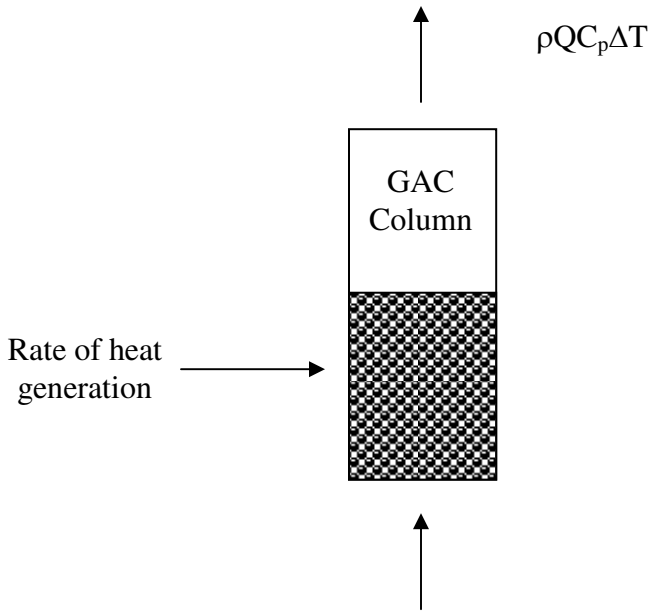

ΔH°_{rxn} is the heat of reaction at constant pressure and standard conditions

C_p=1.00 cal/g $^{\circ}$C and $\rho_{solution}$ = 1 kg/L

1 cal=4.184 J

For the reaction:

$2H_2O_{2\,(l)} \rightarrow 2H_2O_{\,(l)} + O_{2\,(g)}$ ΔH_{rxn}° (KJ/mol) = 2(-286)+0-2(-187.8)= -196.4

	ΔH_f° (KJ/mol)
H_2O_2 (l)	-187.8
H_2O (l)	-286
O_2 (g)	0

Source: Fundamentals of Chemistry. Brady, J. and Holum, J. 3rd ed. John Wiley & Sons. NY:1988.

Since 2L of 50% wt/wt H_2O_2 in water (ρ = 1.2 g/ml) were used to regenerate the pilot column over a 54-hour period, the mass of H_2O_2 consumed was

$$\frac{0.50g}{g_{solution}} \times \frac{1.2g_{solution}}{mL_{solution}} \times \frac{1000mLs}{1L} \times \frac{1mol}{34g_{H2O2}} = 17.65\frac{mol}{L}$$

$$17.65\frac{mol}{L} \times 2L = 35.30molH_2O_2$$

Thus, the average rate of H_2O_2 consumption was

$$\frac{35.30molesH_2O_2}{54hrs} \times \frac{1hr}{60\min} = 1.09x10^{-2}molesH_2O_2/\min$$

and the average rate of heat generation from the reaction was:

$$\frac{1.09x10^{-2}molesH_2O_2}{\min} \times \frac{196.4KJ}{2molH_2O_2} \times \frac{1000J}{1KJ} = 1.07x10^3 J/\min$$

The rate of regenerant flow through the column was estimated at 8 L/min (field data), so that the average increase in regenerant temperature to balance the rate of heat generation was:

$$\frac{1.07x10^3 J}{\min} \times \frac{1\min}{8000mL} \times \frac{1cal}{4.184J} \times \frac{1mL}{1g} \times \frac{g^\circ C}{1cal} = 0.032^\circ C$$

This is the temperature increment in regenerant fluid per single pass through the carbon column due to the regeneration reaction. The average detention time in the regenerant tank was about 1 minute, so that there were opportunities for heat energy to accumulate in the regenerant, immediately after one of the H_2O_2 pulses, when the decomposition reaction was most rapid. In fact, however, the reservoir temperature never exceeded 52°C, after an overnight low of 36°C, suggesting that the regeneration system can be conveniently regulated through management of the H_2O_2 addition rate.

In an hour, without any regenerant cooling, the temperature rise would be

$$\Delta T_{1hr} = \frac{60\min}{hr} \times \frac{8L/\min}{7L} \times 0.032^\circ C = 2.2^\circ C$$

The field reaction was operated for 7-hour periods with consequent temperature changes of about 16°C, or 2.2°C/hr, suggesting that the analysis is valid. However, the rate of H_2O_2 use during the 7-hr daylight periods was about 3x the average daily rate, so that perhaps two-thirds of the heat generated is unaccounted for in the regenerant fluid.

6.6.2.3 Oxygen formation via Fenton's reactions:

The mechanism proposed by De Laat and Gallard (1999) describes in detail the reactions that result in oxygen formation. Depending on the pH of the solution, $HO_2\bullet$/ $O_2\bullet^-$ will react with iron to generate oxygen.

$Fe(III) + HO_2\bullet \rightarrow Fe^{2+} + O_2 + H^+$	$k_{11a} < 2 \times 10^3\ M^{-1}\ s^{-1}$
$Fe(III) + O_2\bullet^- \rightarrow Fe^{2+} + O_2$	$k_{11b} = 5 \times 10^7\ M^{-1}\ s^{-1}$
$HO_2\bullet + HO_2\bullet \rightarrow H_2O_2 + O_2$	$k_{13a} = 8.3 \times 10^5\ M^{-1}\ s^{-1}$
$HO_2\bullet + O_2\bullet^- + H_2O \rightarrow H_2O_2 + O_2 + OH^-$	$k_{13b} = 9.7 \times 10^7\ M^{-1}\ s^{-1}$
$\bullet OH + HO_2\bullet \rightarrow H_2O + O_2$	$k_{14a} = 0.71 \times 10^{10}\ M^{-1}\ s^{-1}$
$\bullet OH + O_2\bullet^- \rightarrow OH^- + O_2$	$k_{14b} = 1.01 \times 10^{10}\ M^{-1}\ s^{-1}$

Given the typical conditions under which these reactions occur, however, radical-radical recombination reactions are not a significant source of oxygen. Consequently, oxygen production is estimated according to the overall hydrogen peroxide decomposition reaction (above) resulting in liquid water and oxygen gas formation. This analysis ignores

1. Compressibility effects
2. Dissolved oxygen transport in the regenerant
3. Temperature effects

Stoichiometrically, $2H_2O_2$ molecules generate one molecule of oxygen during decomposition:

$$2H_2O_{2\,(l)} \rightarrow 2H_2O_{\,(l)} + O_{2\,(g)}$$

From previous calculations based on the average rate of H_2O_2 decomposition, 2L of 50% wt/wt H_2O_2 in water were used to regenerate the pilot column over each 54-hour period. The average rate of O_2 production was therefore

$$\frac{35.30 moles H_2O_2}{54 hrs} \times \frac{1 mol O_2}{2 mol H_2O_2} \times \frac{1 hr}{60 \min} = 5.45 x 10^{-3} moles O_2 / \min$$

Normalized to the rate of flow of water:

$$\frac{5.45 x 10^{-3} moles O_2}{\min} \times \frac{32000 mg O_2}{mol O_2} \times \frac{\min}{8 L} = 21.8 mg O_2 / L$$

Now, the solubility of oxygen in water can be calculated as follows:

$$P_{O2} = 1 atm$$

Using the Henry's law, the concentration of oxygen dissolved in water is

$$[O_2] = K_H P_{O2}$$

where K_H = Henry's law constant =0.0012630 M·atm (From Table 2.4 at T=25°C. Introduction to Environmental Engineering and Science. 2nd Ed. Masters, G. Prentice Hall. New Jersey, 1998.)

$$[O_2] = 0.0012630 M \cdot atm \times 1 atm = 0.0012630 M \times \frac{32000 mg}{mol} = 40.4 mg / L$$

$[O_2] = 40.4 mg / L$ (at equilibrium with pure O_2 gas at a total pressure of 1 atm.).

The concentration of oxygen for a pure oxygen saturated solution at 25°C is about 40 mg/L, which means that the oxygen concentration produced from the decomposition of

hydrogen peroxide does not exceed (21.8mg/L < 40 mg/L) the solubility of oxygen in water.

The oxygen concentration was calculated for the 54-hour period of regeneration. In general, the hydrogen peroxide was added over short periods (30 min) followed by longer periods (6 hours) in which hydrogen peroxide was exhausted and the target compound was allowed to desorb from the GAC. Thus, oxygen formation rates were considerably higher during those short periods. The likely formation of O_2 gas bubbles, which was actually observed in the lab and field experiments, indicates that course media should be used and that the GAC bed should be expanded during regeneration to aid in the release of gas bubbles from the column.

6.7 Field-Scale Regeneration Trials - Summary

- The data and analysis suggest that intraparticle diffusion or desorption from the solid phase of the contaminant is a limiting factor in the second, slow phase of degradation.
- The following table contains bench- and field-scale recovery data that reflect the ease or speed of column recovery when respective compounds have initially saturated carbon adsorption sites. The consensus of the study group regarding the source of rate limitation during the recovery process is as indicated (Table 6.7-1).

Table 6.7-1. Summary of efficiency results for Fenton's reagent regeneration of GAC in bench and field trials.

Compound	Percentage Removed from GAC (%) Bench-scale (14 hrs @ 32C)	Field scale (7-54 hours)	Controlling Mechanism
Methylene Chloride (MC)	99	98 (7 hrs) 99 (30 hrs)	Radical Reaction rate
1,2-DCA	98	N/A	Radical Reaction rate
1,1,1-TCA	67	N/A	Desorption or pore diffusion
Chloroform (CF)	93	82 (7 hrs) 93 (29 hrs)	Radical Reaction rate
Carbon Tetrachloride (CT)	73 @25C	N/A	Desorption or pore diffusion
Trichloroethylene (TCE)	52	73-95 (50-54 hrs)*	Desorption or pore diffusion
Perchloroethylene (PCE)	35	50 (52 hrs)	Desorption or pore diffusion

*depending on H_2O_2 application frequency (see Field-scale Results Section).

- GAC was preloaded with methylene chloride (MC) and chloroform (CF) for field-scale regeneration experiments. H_2O_2 was added hourly between hours 0-6 and 23-28. The reduction of solid-phase CF was 93% after 30 hours. Residual MC could not be detected.

- GAC was loaded with trichloroethylene (TCE) in the laboratory and regenerated in the field in three successive loading/regeneration cycles. In each cycle, the solid-phase TCE concentration decreased by >50% in the first 4 hours. After 60 hours, however, carbon recoveries ranged from 73-95%. No loss of adsorption capacity was observed during the overall period of the experiment. H_2O_2 was added intermittently during regeneration. By allowing the bulk aqueous-phase contaminant concentration to approach equilibrium levels prior to H_2O_2 addition, it may be possible to minimize H_2O_2 costs. Since recovery appears to be limited by compound desorption at least in some cases,

accumulation of the target in the aqueous phase prior to H_2O_2 addition is likely to minimize chemical costs.

- Temperature in the field reactor was observed to increase from an ambient value of about 30°C to 55-60°C during a 60-hour regeneration period. Because VOC mass transport and reaction kinetics are favorably affected by higher temperatures, the exothermic decomposition of H_2O_2 could, if handled carefully, increase carbon recovery rates and lower overall costs for carbon surface regeneration.

- PCE, TCE and light diesel contaminants from the field site soil vapor extraction system were used to load URV-MOD 1 GAC in a final set of field experiments. A 6-hour regeneration trial reduced the adsorbed TCE concentration by 80%, but PCE by only 30%. H_2O_2 was added periodically but without any attempt to minimize chemical consumption.

- A scoping-level economic analysis was conducted, based on regeneration of PCE-loaded GAC. PCE presents the most challenging recovery situation in terms of recovery kinetics. The cost for Fenton-based regeneration, determined from results of bench-scale studies (~$2.70/lb), was comparable to that of conventional thermal regeneration (~$2.60/lb) and new carbon replacement (~$3.30/lb). The cost of Fenton regeneration based on the field trials was higher (~$6.50/lb), but this cost may not represent operational cost following optimization of chemical addition frequency. There was no attempt to minimize H_2O_2 consumption, the primary cost-driver, in the field trial. Further study in this are is recommended.

- It may be possible to both minimize unproductive H_2O_2 consumption and to shift the operational pH range for carbon recovery by precipitating iron on the carbon surface prior to use in adsorption/recovery operations. The feasibility of such a scheme depends on selection of iron loadings that allow degradation reactions to proceed without blocking carbon pores, interfering with contaminant access. Bench-scale trials were carried out. Although field-scale trials using iron-amended GAC were not conducted, a first-cut, estimate of H_2O_2 cost ($0.34/L) was undertaken. The analysis suggests that iron-amended GAC regeneration costs would be ~$0.28/lb GAC, or about 10-fold lower than the cost of thermal carbon regeneration or GAC replacement.

7. SUMMARY AND RECOMMENDATIONS FOR ADDITIONAL STUDY

7.1 General Observations

Data suggest that a single mechanism does not control the rate of VOC-loaded carbon regeneration by Fenton's mechanism for all contaminants and conditions. Weakly adsorbed compounds with relatively low reactivity with •OH, like chloroform, can be limited by reaction in the bulk aqueous phase. Less soluble, more reactive compounds, like TCE, are limited by intraparticle transport. The desorption reaction rate may also play a role in the most strongly bound compounds (e.g., PCE). For compounds with limited solubility intraparticle aqueous concentrations of the sorbate may be much lower than their equilibrium levels. Under these circumstances, surface diffusion may be the predominant mechanism of sorbate transport to the particle exterior. Surface effects resulting from the pore volume distribution may prove to be significant as well. As pore dimensions approach the molecular size of the contaminant, it is anticipated that surface diffusion mechanisms limit transport kinetics. It is known from literature that in micropores found in zeolites (Ruthven, 1984), surface diffusion is the dominant transport mechanism, while pore diffusion dominates in macropores (Ma *et al.*, 1996). The results lead the investigators to conclude that mass transport mechanisms limit the effectiveness of Fenton's reaction for carbon recovery, at least for slightly soluble compounds that are otherwise reactive with Fenton's reagents. Therefore, optimal design of this type of treatment would maximize contaminant flux from the sorbent while minimizing the use of H_2O_2, the primary contributor to process cost. Just how this is done will probably be

compound specific. Pulsed addition of H_2O_2 probably offers advantages over continuous maintenance of a target H_2O_2 concentration when mass transport governs the carbon recovery rate. Temperature management may be an essential issue inasmuch as the rates of physico-chemical processes that determine recovery rate are temperature dependent and the Fenton reactions are exothermic. Fenton-based carbon regeneration was shown to be cost competitive for VOCs of modest binding strength on GAC, but was not clearly cost effective for strongly binding VOCs. However, the cost efficiency can be improved substantially by implementing the design/operational changes discussed. Additional cost saving may be possible by directing radical-generating reactants to the carbon surface although additional research is needed to evaluate this strategy. Selection of carbon (or other sorbents) with a pore size distribution that minimizes mass transfer limitations should be considered as a means to minimize intraparticle mass transfer limitations.

The specific project findings follow on which this summary discussion is based.

7.2 Homogeneous, Bench-Scale Experiments

- Tetrachloroethylene (PCE) degradation followed first order kinetics in which the rate constant was a function of total iron in the Fenton system. The reaction proceeds with essentially no lag following the addition of H_2O_2, indicating that near steady concentrations of iron species and hydroxyl radical are established quickly.
- Quinones are known electron shuttles that can facilitate iron reduction. 1,4-hydroquinone (HQ), 1,4-benzoquinone (BQ) and 9,10-anthraquinone-2,6-

disulfonic acid all initially increased PCE degradation in Fenton's system. The increase was proportional to quinone concentration. However, as with hydroxylamine addition, the rate enhancement was not sustained, probably reflecting the gradual destruction of the quinone. After quinine addition, the PCE degradation rate eventually stabilized at a rate that was slower than that of the unamended Fenton's system, suggesting that the by-products of quinone degradation retarded the contaminant degradation rate.

- PCE degradation ceases if Cu(II) replaces Fe(III) in the Fenton's system. However, if both copper and iron are present in a Cu:Fe ratio of 2, the rate of PCE degradation increases by a factor of 4.3. This accelerated rate was steady over the course of the experiments. Among the possible mechanistic explanations, Cu(II) may be reduced to Cu(I) via H_2O_2 consumption after which the conversion of Cu(I) to Cu(II), Cu(I) reduces Fe(III) to Fe(II). The hypothesized mechanism may provide a more rapid pathway for iron reduction than reaction of Fe(III) with H_2O_2 in the Fenton system. Although the ability of copper to accelerate PCE degradation is modest, Cu(II) solubility is greater than that of iron, and copper may provide greater benefit in the pH range where the iron concentration solubility in Fenton's system is limited.
- The first-order rate constant for PCE degradation increased more rapidly with temperature in the copper:iron system than in the Fe-only Fenton system. Thus, the benefit of copper addition will be increased for Fenton's reactor systems operating above ambient temperature.

- A homogeneous-phase kinetic model was formulated based on earlier work by De Laat and Gallard (1999), in which the rate constant for Fe(III)-hydroperoxy complex reduction is the sole fitted parameter. Although model simulations were in qualitative agreement with results generated here, there were several noteworthy quantitative departures between model and experiment. It is suspected that the fitted rate constant requires revision based on the substantially lower ionic strength in the present work and the insensitivity of the fitted rate constant to pH in the De Laat and Gallard case.
- As chlorinated VOCs are degraded in a Fenton's system, chloride anions build up in the regenerant solution. Literature rate constants for the reaction of the hydroxyl radical and chloride indicate that chloride accumulation should significantly retard VOC degradation rates. However, model simulations using the literature rate constant overestimate the chloride impact observed in the experimental trials. Additional modeling efforts using a fitted rate constant for the $\bullet OH/Cl^-$ reaction are in progress
- The rate of PCE degradation by Fenton's system increases with increasing pH in the range 1 to 3. Above pH 3, decreased iron solubility limits free iron availability and, consequently, limits the rate of degradation. Measured PCE degradation rates at $0.9<pH<3.0$ were not in good agreement with the model results although predicted and observed trends in pH-dependent data are similar. At every pH (except pH = 0.9), the model over-predicts the PCE transformation rate.

- The rate of carbon tetrachloride (CT) degradation was increased by the addition of isopropanol (IP), a •OH scavenger. The work strongly suggests CT degradation occurs via superoxide radical (O_2•$^-$) attack in Fenton's system. Literature studies suggest the increase in rate may be due to a co-solvency effect due to IP addition that increases O_2•$^-$ activity.

7.3 Heterogeneous, Bench-Scale Experiments

- Ethyl acetate was the best solvent tested for solid:liquid extraction of PCE from GAC. An extraction duration of 12 hours provided practically complete extraction.
- Contaminant degradation kinetics in a heterogeneous Fenton's system (VOC loaded on GAC) follows bi-phasic, first-order kinetics. A fast initial phase was followed (after 1-3 hours) by a slower second phase. The fraction of total contaminant degraded in the rapid initial phase increased with the aqueous-phase solubility of the contaminants. The data and analysis suggest intraparticle diffusion or desorption of the contaminant is a limiting factor in the second, slow phase of degradation.
- When chloroform (CF) -loaded GAC was rapidly flushed with fresh water, the rate of CF loss increased as the size of the GAC particles on which it was adsorbed decreased. These results suggest that pore and/or surface diffusion, affect the overall removal kinetics.

- Based on experimental results, it is concluded that mass transport mechanisms limit the effectiveness of Fenton's reaction for carbon recovery, at least for slightly soluble compounds (e.g., PCE) that are reactive with Fenton's reagents. Therefore, optimal design for this type of treatment would maximize contaminant flux from the sorbent while minimizing the use of H_2O_2, the primary contributor to process cost.
- Trials were conducted using Calgon URV-MOD 1 carbon on which iron had been precipitated onto the pore and outer surfaces. No iron was added to the bulk regenerant (Fenton's solution). This was to localize the Fenton's-driven radical generation near the GAC surface and the desorbing VOC targets, to minimize the rate limitation due to desorption or pore and surface diffusion. However, negligible improvement in the rate of carbon recovery was observed compared to the rate observed using non-iron-amended carbon. The rate of H_2O_2 usage, the primary driver in operating cost of the system, was decreased by about three-fold in the iron-amended system.

7.4 Field-Scale Regeneration Trials

- GAC was preloaded with methylene chloride (MC) and chloroform (CF) for field-scale regeneration experiments. H_2O_2 was added hourly between hours 0-6 and 23-28. The reduction of solid-phase CF was 93% after 30 hours. Residual MC could not be detected.

- GAC was loaded with trichloroethylene (TCE) in the laboratory and regenerated in the field using Fenton's reagents through three loading/regeneration cycles. In each regeneration cycle, an initial loss of over 50% of the TCE occurred in the first 4 hours, and after 60 hours TCE recovery was 73-95%. No loss of adsorption capacity was observed after three GAC regenerations. H_2O_2 was added intermittently during regeneration. Analysis indicates H_2O_2 additions timed to allow the bulk aqueous contaminant concentration to reach near-equilibrium levels would minimize H_2O_2 cost.
- Temperature in the field reactor increased from an ambient value of about 30°C to 55-60°C during a 60-hour regeneration period. Because VOC mass transport and reaction kinetics are favorably affected by higher temperatures, the exothermic decomposition of H_2O_2 could increase carbon recovery rates and lower overall costs for carbon surface regeneration.
- PCE, TCE and light diesel contaminants from the field site soil vapor extraction system were used to load URV-MOD 1 GAC in a final set of field experiments. A 6-hour regeneration trial reduced adsorbed TCE by 80%, but PCE recovery was only 30%.
- A scoping-level economic analysis was conducted, based on regeneration of PCE-loaded GAC (the most challenging case investigated). The cost for Fenton Reagent regeneration based on the bench-scale studies (~$2.70/lb) was comparable to that for conventional thermal regeneration (~$2.60/lb) and new carbon replacement (~$3.30/lb). The cost of Fenton regeneration based on the field trials was higher

(~$6.50/lb), but this may be a considerable overestimate since the primary cost driver, H_2O_2 consumption, was not optimized to any extent in the field trial. Further tests in this regard are needed.

- It may be possible to immobilize iron on the carbon surface and regenerate in a pH range to avoid iron dissolution during recovery operations. The feasibility of such a scheme depends on selection of iron loadings that allow degradation reactions to proceed without blocking the carbon surface or interfering with contaminant access to carbon pores. Field-scale trials using iron-amended GAC were not conducted. The results of bench-scale experiments were used to estimate recovery costs in the iron-amended carbon systems. Projected regeneration costs, ~$0.28/lb GAC, were approximately 10-fold lower than the cost of thermal regeneration or GAC replacement.

7.5 Data Quality and Limitations

The data presented in this report was gathered using the procedures and tools detailed in the Quality Assurance Project Plan (QAPP) submitted prior to project initiation. None of the procedures detailed in the QAPP were required to be modified during the subsequent execution of the project. Consequently, there are no limitations on the use of the data related to its original intended application beyond the following specific instances considerations.

- Considerable work was undertaken in modeling the homogeneous system degradation of VOCs by Fenton's reagents. This work is largely beyond the

original scope of the project and was undertaken as a no cost extension of benefit to the project. Quality control and assurance for the modeling approach was not detailed in the QAPP. In an effort to validate the homogeneous model functioning, the project model was used to simulate the data and model fit from the study by De Laat and Gallard (1999). The De Laat and Gallard study was conducted in a much higher ionic strength and lower iron environment than the current work. The project model was successful in simulating the literature study data, yet when the model when it was used to simulate data generated in the conditions of interest in this project, the agreement was not nearly as good. Several efforts that were made to reconcile the issue are detailed earlier, including temperature corrections, ionic strength corrections, sulfate and chloride concentration adjustments. Although the fit improved with these revisions, the model is still not considered ready for use as a predictive tool and should not be applied unless first validated for a data set with the appropriate water composition conditions as will be used in the model. Recommendations for addressing this shortcoming are given later in this section.

- The economic analysis reported was based (unless otherwise specified) on the results from the pilot-scale treatment unit deployed in the field. Only very limited efforts were made to optimize this system, particularly with respect to H_2O_2 use, which is the primary driver of the technology's cost. This fact coupled with the observation that H_2O_2 use in the field was greater than 5-fold

higher (per mass of carbon regenerated) than in the lab trials, suggests that the cost estimates for the Fenton's based system over-estimate the real cost of the technology deployment.

7.6 Research Recommendations

Based on this work and the perspective provided by other investigators it is possible to recommend additional, follow-on research in a number of areas. These are:

1. Despite the contributions of De Laat and co-workers, uncertainties remain in details of both the Fenton mechanism itself and its application for destruction of organic contaminants. The primary uncertainties from the perspective of advanced oxidation processes include (i) the respective roles of hydroxyl and superoxide radicals in transforming specific halogenated contaminants (e.g. CCl_4 and PCE) and (ii) matrix effects on process kinetics and efficiency – that is, those imposed by non-target organics, partial degradation products and reactive anions like Cl^- and SO_4^{2-}. Extension of the De Laat kinetic model to more chemically complex waters depends on reasonable representation of radical reaction kinetics with a variety of chemical species that are usually omitted for simplicity. Difficulty in matching chloride-dependent reaction kinetics with model predictions using published rate constants is apparent in this work. This is unfortunate in light of the obvious importance of chloride ion concentrations in the context of our investigation.

2. A reinforced De Laat chemical model can be used to help understand the accelerating effects of copper and isopropanol additions that were observed in this work. In neither case are we able to offer a convincing mechanism for compound-dependent changes in reaction kinetics, and explanations remain speculative. Without additional work, the potential benefits of copper and cosolvent addition in Fenton-based advanced oxidation systems are unlikely to be realized.
3. Certain other minor additions to the homogeneous Fenton model would be helpful. In particular, an easy way to incorporate effects due to solution ionic strength and temperature could be important.
4. Field operations provide yet another level of uncertainty that has not yet been fully evaluated. It is evident that process economic feasibility depends on the efficient use of H_2O_2 for contaminant destruction, but additional work is necessary to find a target-dependent H_2O_2 feed rate to promote such efficiency. A systems approach to H_2O_2 scheduling and additional verifying experiments seem warranted.
5. Provision of Fe on the carbon surface provides operational possibilities (pH>3.0, soluble Cu(II) provision to enhance kinetics, cosolvent effects) that have not yet been investigated. Much more effort here is warranted.
6. The full breadth of compounds that can be destroyed in place following carbon adsorption has not yet been identified. Reactivity with •OH seems not to be the most important issue, as indicated by the relative success in previous NDMA

experiments and the apparent stubbornness of PCE to Fenton-based recovery. A through examination of compound parameters that affect the recovery kinetics for specific compounds would be useful.

7. The presence of reactive co-contaminants on carbon to be regenerated using the propanol Fenton-based technology may have consequences that have not yet been investigated.

APPENDIX A. SUPPORTING INFORMATION FOR THE HOMOGENEOUS MODEL

A.1. Ionic Strength Corrections

The effect of all ions in solution can be quantified in terms of the ionic strength (I), which can be defined as follows:

$$I = \frac{1}{2} \sum_{allions} c_i z_i^2 \qquad [A.1\text{-}1]$$

where c_i is the concentrations of *i* in M and z_i is the charge of the ion *i*. The ionic strength is a key parameter controlling the reactivity of dissolved ions in solution. Here, reactivity refers to the overall tendency for the chemical to participate in reactions, which will be affected by system-specific chemical factors such as temperature, pressure, in addition to the substance's concentration. In general the reactivity of any chemical should be proportional to its concentration in the phase wherein it is found.

Equilibrium constants are a function of the activity of each substance and not concentrations. The activity of a substance is defined as the ratio of the actual reactivity to the reactivity in the standard state. The activity coefficient (γ_A) is expressed as the ratio of the activity to the concentration of the substance:

$$\gamma_A = \frac{a_A}{C_A} \qquad [A.1\text{-}2]$$

Therefore, activity coefficients can be used to make corrections for variations in the ionic strength in the solution and the corresponding reactivity of the substance. The basis for the relationship between ionic strength and activity coefficients is that dissolved ions

attract oppositely charged ions and repel like-charged ions. The activity coefficient of dissolved species can be estimated from theory. In all the equations used, the activity coefficient of an ion depends strongly on that ion's charge and the ionic strength characterizes the ionic composition of the solution.

Here, the Davies equation is used to predict the activity coefficient in aqueous solution.

$$\log \gamma_{Davies} = -Az^2\left(\frac{I^{1/2}}{1+I^{1/2}} - 0.2I\right) \qquad \text{Applicable at I<0.5M} \qquad \text{[A.1-3]}$$

where $A = 1.82x10^6(\varepsilon T)^{-3/2}$, and ε is the dielectric constant of the medium. For water at 25°C, A =0.51 (Benjamin, M., 2002). The following table shows the ε, and corresponding A values at 25 and 30°C.

Table A.1-1. Parameters used in the Davies equation

T(°C)	T(°F)	ε*	A
25	77	78.54	0.51
30	86	76.75	0.51

Source: *Stumn and Morgan, 1996

Neutral species are generally assumed to have an activity coefficient equal to 1.0, as they are predicted to behave ideally because they are uncharged. Even though empirically the activity coefficients of neutral species generally increase with ionic strength, their dependence is quite weak and the error associated with assuming $\gamma_{neutral}$ = 1.0 is small (Benjamin, 2002).

In addition to activity coefficient corrections due to ionic strength, a charge balance is necessary to express the electrical neutrality of all solutions, given by:

$$\sum_i c_i z_i = 0 \qquad \text{[A.1-4]}$$

where c_i is the concentration of a species *i* in solution and z_i is the ionic charge of species *i*, including the sign. The summation must include all charged species in solution. The charge balance is generally expressed as the sum of all cations equal to the sum of all anions as

$$\sum_{cations} (c_i|z_i|) = \sum_{anions} (c_i|z_i|) \qquad \text{[A.1-5]}$$

To calculate the ionic strength of the solution, it is necessary to account for all the iron species. Iron species were calculated with the excel solver using the iron total, I_1 and I_2 species equations equal to 0 and solving for Fe^{3+}, I_1 and I_2 species.

$$\left[Fe^{3+}\right] + K_1\frac{[Fe^{3+}]}{[H^+]} + K_2\frac{[Fe^{3+}]}{[H^+]^2} + 2K_{2,2}\frac{[Fe^{3+}]^2}{[H^+]^2} + K_{I1}\frac{[Fe^{3+}][H_2O_2]}{[H^+]} + K_{I2}K_1\frac{[Fe^{3+}][H_2O_2]}{[H^+]^2} + Fe^{2+} - Fe_{TOT} = 0 \qquad \text{[A.1-6]}$$

$$K_{I1}\frac{[Fe^{3+}][H_2O_2]}{[H^+]} - I_1 = 0 \qquad \text{[A.1-7]}$$

$$K_{I2}K_1\frac{[Fe^{3+}][H_2O_2]}{[H^+]^2} - I_2 = 0 \qquad \text{[A.1-8]}$$

For the following initial conditions,

$[Fe(III)]_{TOT}$ = 0.1mM, $[H_2O_2]_o$ = 0.1M, pH = 2.0 and constants from Table 4.2.1-1, we obtain the following iron species distribution:

$[Fe^{3+}]$	$[FeOH^{2+}]$	$[Fe(OH)_2^+]$	$[Fe(OH)_2^{4+}]$	I_1	I_2
7.52×10^{-5}	2.18×10^{-5}	5.73×10^{-7}	4.52×10^{-8}	2.33×10^{-6}	4.36×10^{-8}

Note: $[Fe(III)]_{TOT} = 9.9955\times10^{-5}$M.

The ionic strength of the system can then be calculated by substituting the concentration of the iron species, pH and total sulfate in solution and their respective charge into equation 1-1.

$[H^+]^1$	$[OH^-]$	$[SO_4^{2-}]^2$	$\Sigma c_a\|z_a\|$	$\Sigma c_c\|z_c\|$	I (M)
$1.0x10^{-2}$	$1.0x10^{-12}$	$5.14x10^{-3}$	$1.03x10^{-2}$	$1.03x10^{-2}$	$1.56x10^{-2}$

Note: [1]pH, [2]Sulfate from iron salt added as $Fe_2(SO_4)_3 \cdot 5.6H_2O$: (3/2)$[Fe(III)]_{TOT}$, and H_2SO_4 for pH adjustment.

$$I = \frac{1}{2}\left[\begin{array}{l}(7.52x10^{-5})(3)^2 + (2.18x10^{-5})(2)^2 + (5.73x10^{-7})(1)^2 + (4.52x10^{-8})(4)^2 + \\ (2.33x10^{-6})(2)^2 + (4.36x10^{-8})(1)^2 + (1.0x10^{-2})(1)^2 + (1.0x10^{-12})(-1)^2 + \\ (5.14x10^{-3})(-2)^2\end{array}\right]$$

$$I = 1.56x10^{-2} M$$

Once the ionic strength of the solution is determined, the activity coefficients for all the species listed can be calculated to adjust for ionic strength variations. For example, in the following equilibrium reaction

$$Fe^{3+} + H_2O \leftrightarrow FeOH^{2+} + H^+ \qquad K_1=2.9x10^{-3}\ M \qquad [A.1\text{-}9]$$

$$K_1 = \frac{[FeOH^{2+}][H^+]}{[Fe^{3+}]} \qquad [A.1\text{-}10]$$

K_1 depends on the activities of $FeOH^{2+}$, H^+ and Fe^{3+}, hence we need to calculate the activity coefficients of all these species.

$$\log \gamma_{Davies} = -Az^2\left(\frac{I^{1/2}}{1+I^{1/2}} - 0.2I\right) \qquad [A.1\text{-}11]$$

$$\log \gamma_{Fe^{3+}} = -0.51(3)^2\left(\frac{(1.56x10^{-2})^{1/2}}{1+(1.56x10^{-2})^{1/2}} - 0.2(1.56x10^{-2})\right) = -0.496 \qquad \text{[A.1-12]}$$

$$\gamma_{Fe^{3+}} = 0.319$$

$$\log \gamma_{FeOH^{2+}} = -0.51(2)^2\left(\frac{(1.56x10^{-2})^{1/2}}{1+(1.56x10^{-2})^{1/2}} - 0.2(1.56x10^{-2})\right) = -0.220 \qquad \text{[A.1-13]}$$

$$\gamma_{FeOH^{2+}} = 0.602$$

$$\log \gamma_{H^{+}} = -0.51(1)^2\left(\frac{(1.56x10^{-2})^{1/2}}{1+(1.56x10^{-2})^{1/2}} - 0.2(1.56x10^{-2})\right) = -0.055 \qquad \text{[A.1-14]}$$

$$\gamma_{H^{+}} = 0.881$$

$$\frac{\gamma_{FeOH^{+}}\gamma_{H^{+}}}{\gamma_{Fe^{3+}}} = \frac{0.602 * 0.881}{0.319} = 1.66 \qquad \text{[A.1-15]}$$

$$K_1\left(I = 1.56x10^{-2}\,M\right) = \frac{K_1(I = 0M)}{1.66} = \frac{6.58x10^{-3}}{1.66} = 3.96x10^{-3}\,M \qquad \text{[A.1-16]}$$

The equilibrium constant for the reaction can be calculated by dividing the intrinsic constant (at I = 0 M) by the product of the activity coefficients of the species involved. The new constant corrected for the ionic strength of the solution can be used in the computer model.

A.2. Sulfate effect

Addition of sulfate ion in the Fenton's reactions affects the distribution of the iron species by forming complexes with iron. Under our experimental conditions, nearly 14% of the total iron is in the form $FeSO_4^+$ and 53% of the total sulfate is as SO_4^{2-}. Sulfate ions also affect the Fenton's reaction by scavenging hydroxyl radicals to form sulfate radicals. These radicals may react with Fe(II) species in a non-productive way. See table A.2-1 for additional reactions in the presence of sulfate.

TABLE A.2-1. Additional Reactions for the Fenton's Reaction in the Presence of Sulfate

No.	Reactions	Constants (I=0.1M, 25°C)
(16)	$H^+ + SO_4^{2-} \leftrightarrow HSO_4^-$	$K_{16} = 3.47x10^1\ M^{-1}$
(17)	$Fe^{3+} + SO_4^{2-} \leftrightarrow FeSO_4^+$	$K_{17} = 3.89x10^2\ M^{-1}$
(18)	$Fe^{3+} + 2SO_4^{2-} \leftrightarrow Fe(SO_4)_2^-$	$K_{18} = 4.47x10^3\ M^{-2}$
(19)	$Fe^{2+} + SO_4^{2-} \leftrightarrow FeSO_4$	$K_{19} = 2.29x10^1\ M^{-1}$
(20)	$HSO_4^- + \bullet OH \rightarrow SO_4\bullet^- + H_2O$	$k_{20} = 3.5x10^5\ M^{-1}\ s^{-1}$
(21)	$SO_4\bullet^- + H_2O \rightarrow H^+ + SO_4^{2-} + \bullet OH$	$k_{21} = 6.6x10^2\ s^{-1}$
(22)	$SO_4\bullet^- + OH^- \rightarrow SO_4^{2-} + \bullet OH$	$k_{22} = 1.4x10^7\ M^{-1}\ s^{-1}$
(23)	$SO_4\bullet^- + SO_4\bullet^- \rightarrow S_2O_8^{2-}$	$k_{23} = 2.7x10^8$
(24)	$SO_4\bullet^- + H_2O_2 \rightarrow SO_4^{2-} + H^+ + HO_2\bullet$	$k_{24} = 1.2x10^7\ M^{-1}\ s^{-1}$
(25)	$SO_4\bullet^- + HO_2\bullet \rightarrow SO_4^{2-} + H^+ + O_2$	$k_{25} = 3.5x10^9\ M^{-1}\ s^{-1}$
(26)	$SO_4\bullet^- + O_2\bullet^- \rightarrow SO_4^{2-} + O_2$	$k_{26} = 0$
(27)	$FeSO_4 + H_2O_2 \rightarrow Fe^{3+} + SO_4^{2-} + \bullet OH + OH^-$	$k_{27} = 78$
(28)	$FeSO_4 + \bullet OH \rightarrow Fe^{3+} + SO_4^{2-} + OH^-$	$k_{28} = 2.7x10^8$
(29)	$FeSO_4 + HO_2\bullet \rightarrow Fe^{3+} + SO_4^{2-} + HO_2^-$	$k_{29} = 1.2x10^6$
(30)	$FeSO_4 + O_2\bullet^- \rightarrow Fe^{3+} + SO_4^{2-} + O_2^{2-}$	$k_{30} = 5x10^8$
(31)	$Fe^{2+} + SO_4\bullet^- \rightarrow Fe^{3+} + SO_4^{2-}$	$k_{31} = 3.0x10^8\ M^{-1}\ s^{-1}$
(32)	$FeOH^+ + SO_4\bullet^- \rightarrow Fe^{3+} + SO_4^{2-}$	$k_{32} = 3.0x10^8\ M^{-1}\ s^{-1}$
(33)	$FeSO_4 + SO_4\bullet^- \rightarrow Fe^{3+} + 2SO_4^{2-}$	$k_{33} = 3.0x10^8\ M^{-1}\ s^{-1}$
(34)	$FeSO_4^+ + HO_2\bullet \rightarrow Fe^{2+} + SO_4^{2-} + O_2 + H^+$	$k_{34} < 1x10^3$
(35)	$FeSO_4^+ + O_2\bullet^- \rightarrow Fe^{2+} + SO_4^{2-} + O_2$	$k_{35} < 1x10^3$
(36)	$Fe(SO_4)_2^- + O_2\bullet^- \rightarrow Fe^{2+} + SO_4^{2-} + O_2$	$k_{36} < 1x10^3$

SOURCE: De Laat and Le Truong, 2005.

The following equations can be added to the system of nonlinear ordinary differential equations (described in chapter 4) to obtain the distribution of the iron species in the presence of sulfate. Steady-state conditions were assumed for the rate of radical species ($d[\bullet OH]/dt = d[HO_2\bullet]/dt = d[O_2\bullet^-]/dt = dSO_4\bullet^-/dt = 0$) and the resulting system of nonlinear equations can be solved using the Gaussian elimination method.

$$dSO_4\bullet^-/dt = k_{32}[HSO_4^-][\bullet OH] - k_{33}[SO_4\bullet^-] - k_{34}[SO_4\bullet^-][OH^-] - 2k_{35}[SO_4\bullet^-]^2 - k_{36}[SO_4\bullet^-][H_2O_2] - k_{37}[SO_4\bullet^-][HO_2\bullet] - k_{38}[SO_4\bullet^-][O_2\bullet^-] - k_{43}[Fe^{2+}][SO_4\bullet^-] - k_{44}[FeOH^+][SO_4\bullet^-] - k_{45}[FeSO_4][SO_4\bullet^-]$$

$$[SO_4^{2-}]_{TOT} = [SO_4^{2-}] + [HSO_4^-] + [FeSO_4^+] + [Fe(SO_4)_2^-] + [FeSO_4]$$

$$[SO_4^{2-}]_{TOT} = [SO_4^{2-}] + K_{28}[SO_4^{2-}][H^+] + K_{29}[Fe^{3+}][SO_4^{2-}] + K_{30}[Fe^{3+}][SO_4^{2-}]^2 + K_{31}[Fe^{2+}][SO_4^{2-}]$$

A.3. Chloride production from PCE dechlorination

The problem is to determine the [Cl^-] in the regeneration water produced from PCE dechlorination during Fenton's reaction and then predict its impact. The solution strategy was to calculate the ΔCl^- concentration attributable to one regeneration of the spent carbon and compare that concentration to Cl^- levels shown to impair Fenton-dependent process performance. Conditions were selected to mimic observations in field-scale experiments. Those conditions included mass of PCE on the carbon at breakthrough, regenerant volume and fractional recovery during the regeneration event.

Assumptions:

(i) PCE concentration in the solid, C_s = 250 mg/g

(ii) 50% PCE degradation/regeneration

(iii) 4 moles of Cl^- produced/mole PCE degraded

(iv) Bulk density of GAC = 0.5 kg/L

(v) 8 L of regenerant for recovery of 1 L of (unexpanded) carbon

The mass of PCE on the carbon at saturation is

$$\frac{0.5 kgGAC}{Lbed} \times \frac{0.250 kgPCE}{kgGAC} \times \frac{1 Lbed}{8 Lwater} \times 0.5(recovery\_efficiency) = \frac{7.8 gPCE}{Lwater}$$

and the resultant fractional Cl^- mass is

$$\frac{142 gCl^- / mol}{165.83 gPCE / mol} \times \frac{7.8 gPCE}{Lwater} = \frac{6.68 gCl^-}{L} \times \frac{molCl^-}{35.5 gCl^-} = 0.19 MCl^-$$

A.4 Chloride reactions

Chloride ions, produced from the dechlorination of PCE, can accumulate in the regenerant solution and affect the rate of H_2O_2 and organic target degradation. Chloride ions can affect the distribution of the iron species by forming complexes with iron and by scavenging hydroxyl radicals to form halogen radicals. At low chloride concentrations (i.e. 2.4 mM), more than 99% of the chloride is in the free form. The halogen radicals produced may react with Fe(II) species in a non-productive way. However, as the chloride levels increase chloride starts complexing with iron affecting the distribution of the iron species. See table A.4-1 for additional reactions in the presence of chloride.

The following equations can be added to the system of nonlinear ordinary differential equations (described in chapter 4 and appendix A.2) to obtain the distribution of the iron species in the presence of sulfate and chloride. Steady-state conditions were assumed for the rate of radical species ($d[\bullet OH]/dt = d[HO_2\bullet]/dt = d[O_2\bullet^-]/dt = dSO_4\bullet^-/dt = dClOH\bullet^-/dt = dCl\bullet/dt = dCl_2\bullet/dt = 0$) and the resulting system of nonlinear equations can be solved using the Gaussian elimination method.

$$dClOH\bullet^-/dt = k_{40}[Cl^-][\bullet OH] - k_{41}[ClOH\bullet^-] - k_{42}[ClOH\bullet^-][H^+] + k_{43}[Cl\bullet] + k_{46}[Cl_2\bullet^-]$$

$$dCl\bullet/dt = k_{42}[ClOH\bullet^-][H^+] - k_{43}[Cl\bullet] - k_{44}[Cl\bullet][Cl^-] + k_{45}[Cl_2\bullet^-] - k_{47}[Cl\bullet][H_2O_2] - k_{52}[Cl\bullet][Fe(II)]$$

$$dCl_2\bullet/dt = k_{44}[Cl\bullet][Cl^-] - k_{45}[Cl_2\bullet^-] - k_{46}[Cl_2\bullet^-] - k_{48}[Cl_2\bullet^-][H_2O_2] - k_{49}[Cl_2\bullet^-][HO_2\bullet] - k_{50}[Cl_2\bullet^-][O_2\bullet^-] - k_{53}[Cl_2\bullet^-][Fe(II)]$$

$$[Cl^-]_{TOT} = [Cl^-] + [FeCl^+] + [FeCl^{2+}] + [FeCl_2^+]$$

$$[Cl^-]_{TOT} = [Cl^-] + K_{37}[Fe^{2+}][Cl^-] + K_{38}[Fe^{3+}][Cl^-] + K_{39}[Fe^{3+}][Cl^-]^2$$

TABLE A.4-1. Additional Reactions for the Fenton's Reaction in the Presence of Chloride

No.	Reactions	Constants (I=0.1M, 25°C)
(37)	$Fe^{2+} + Cl^- \leftrightarrow FeCl^+$	$K_{37} = 2.88\ M^{-1}$
(38)	$Fe^{3+} + Cl^{--} \leftrightarrow FeCl^{2+}$	$K_{38} = 6.61\ M^{-1}$
(39)	$Fe^{3+} + 2Cl^- \leftrightarrow FeCl_2^+$	$K_{39} = 10.5\ M^{-2}$
(40)	$Cl^- + \bullet OH \rightarrow ClOH\bullet^-$	$k_{40} = 4.2x10^9\ M^{-1}\ s^{-1}$
(41)	$ClOH\bullet^- \rightarrow Cl^- + \bullet OH$	$k_{41} = 6.0x10^9\ s^{-1}$
(42)	$ClOH\bullet^- + H^+ \rightarrow Cl\bullet + H_2O$	$k_{42} = 2.4x10^{10}\ M^{-1}\ s^{-1}$
(43)	$Cl\bullet + H_2O \rightarrow ClOH\bullet^- + H^+$	$k_{43} = 1.8x10^5\ s^{-1}$
(44)	$Cl\bullet + Cl^- \rightarrow Cl_2\bullet^-$	$k_{44} = 7.8x10^9\ M^{-1}\ s^{-1}$
(45)	$Cl_2\bullet^- \rightarrow Cl\bullet + Cl^-$	$k_{45} = 5.7x10^4\ s^{-1}$
(46)	$Cl_2\bullet^- + H_2O \rightarrow ClOH\bullet^- + H^+ + Cl^-$	$k_{46} = 1.3x10^3\ s^{-1}$
(47)	$Cl\bullet + H_2O_2 \rightarrow HO_2\bullet + Cl^- + H^+$	$k_{47} = 1.0x10^9\ M^{-1}\ s^{-1}$
(48)	$Cl_2\bullet^- + H_2O_2 \rightarrow HO_2\bullet + 2Cl^- + H^+$	$k_{48} = 1.4x10^5\ M^{-1}\ s^{-1}$
(49)	$Cl_2\bullet^- + HO_2\bullet \rightarrow 2Cl^- + H^+ + O_2$	$k_{49} = 3.1x10^9\ M^{-1}\ s^{-1}$
(50)	$Cl_2\bullet^- + O_2\bullet^- \rightarrow 2Cl^- + O_2$	$k_{50} = 2.0x10^9\ M^{-1}\ s^{-1}$
(51)	$FeCl^+ + H_2O_2 \rightarrow Fe^{3+} + Cl^- + \bullet OH + OH^-$	$k_{51} = 55\ M^{-1}\ s^{-1}$
(52)	$Fe(II) + Cl\bullet \rightarrow Fe^{3+} + Cl^-$	$k_{52} = 5.9x10^9\ M^{-1}\ s^{-1}$
(53)	$Fe(II) + Cl_2\bullet^- \rightarrow Fe^{3+} + 2Cl^-$	$k_{53} = 5x10^6\ M^{-1}\ s^{-1}$
(54)	$FeCl^+ + HO_2\bullet \rightarrow Fe^{3+} + Cl^- + HO_2^-$	$k_{54} = 1.2x10^6\ M^{-1}\ s^{-1}$
(55)	$FeCl^+ + O_2\bullet^- \rightarrow Fe^{3+} + Cl^- + O_2^{2-}$	$k_{55} = 1.0x10^7\ M^{-1}\ s^{-1}$
(56)	$FeCl^{2+} + HO_2\bullet \rightarrow Fe^{2+} + O_2 + H^+ + Cl^-$	$k_{56} = 2x10^4\ M^{-1}\ s^{-1}$
(57)	$FeCl_2^+ + HO_2\bullet \rightarrow Fe^{2+} + O_2 + H^+ + 2Cl^-$	$k_{57} = 2x10^4\ M^{-1}\ s^{-1}$
(58)	$FeCl^{2+} + O_2\bullet^- \rightarrow Fe^{2+} + O_2 + Cl^-$	$k_{58} = 5x10^7$
(59)	$FeCl_2^+ + O_2\bullet^- \rightarrow Fe^{2+} + O_2 + 2Cl^-$	$k_{59} = 5x10^7$

SOURCE: De Laat and Le Truong, 2006.

APPENDIX B. COMPARING COSTS OF CARBON DISPOSAL VS. (FENTON) CARBON REGENERATION

The economic analysis conducted here was designed to compare alternative carbon replacement/regeneration strategies in processes using activated carbon for contaminant adsorption. In scenario #1, spent carbon is replaced with new activated carbon, and the waste carbon is disposed of as a hazardous waste. Scenario #2 differs in that carbon is periodically regenerated, or at least partially regenerated using Fenton's reagents to destroy the adsorbed contaminants. The economic analysis was carried out by comparing costs that are unique to each scenario on both a present worth and an annual cost basis. Most of the costs for activated carbon adsorption for a gas-phase streams derived from SVE (the basic scheme for both scenarios) are common to the alternatives compared. As such they are omitted from the analysis. These include energy costs for the SVE system, capital costs for the carbon adsorption unit, initial carbon costs and some maintenance and other labor activities. A description of the costs that are unique to each alternative follows:

	Scenario #1	Scenario #2
Carbon costs	GAC replacement cost GAC cost = $1.60/lb Disposal cost = $0.48/lb plus transportation to UT $3000 for 8316 lbs GAC plus $28/ton UT disposal tax	5% loss/regeneration cycle GAC cost = $1.60/lb No disposal costs
H_2O_2 consumption	Not Applicable	$0.345/lb H_2O_2 plus transportation from Houston $3.50/mi, 1067 miles
Incremental capital for chemical dosing/storage	Not Applicable	Dosing pumps, H_2O_2 storage tanks

Source: Disposal cost (email correspondence with Clean Harbors Environmental, 2004).

The scenarios were built in part on the basis of field experience in this project (H_2O_2 dosing and time to recovery) and in part based on engineering rules of thumb or professional judgment. Cost comparisons were carried out for carbon recovery when (i) PCE and (ii) Methylene chloride were the target contaminants. The behaviors of these compounds during carbon regeneration were diametrically opposite. PCE provides a challenging recovery problem, presumably because of its affinity for the carbon surface and consequent slow desorption rate. Carbon recovery following Methylene chloride breakthrough is remarkably fast, probably due to its low affinity for the carbon surface. Other assumptions or data used to support the economic comparison follow:

- bulk GAC density = 0.5 kg/L
- gas-flow rates during SVE = 10, 100 cfm (2 distinct analyses)
- equilibrium is assumed to exist among gas, liquid and solid phases at breakthrough during SVE
- T = 25°C
- The concentration of contaminant (PCE or MC) in the gas treated by SVE is 100 ppmv.
- GAC column diameter = 1 m
- The mass of carbon in the column is irrelevant since we will calculate carbon wastage rates for each scenario investigated
- The pump efficiency during recirculation of Fenton's reagents is 0.70.
- The discount generator is 0.08
- Equipment for H_2O_2 dosing and storage has a service life of 20 years

- All GAC costs are in year 2000 dollars and all other cost are current

Calculations:

Estimating time to breakthrough:

At a MC-gas phase concentration of 100 ppm, the concentration in the liquid can be calculated using the Henry's law.

From La Grega et al., (2001),

H=exp(A-B/T) where A = 6.65 and B=3.82x10^3

then the Henry's law constant can be calculated at a T = 25°C (298 K)

$$H = \exp\left(6.65 - \frac{3.82x10^3}{298}\right) = 2.09x10^{-3}\, atm \cdot m^3 / mol = 2.1 atm / M$$

$$C_{L,MC} = \frac{C_{g,MC}}{H} = \frac{100x10^{-6}\, atm}{2.1 atm / M} \times \frac{85\, g}{mol} \times \frac{1000 mg}{g} = 4.05 mgMC / L$$

At saturation, the concentration of MC in equilibrium with the solid is

$$C_{S,MC} = KC_{eq}^{\ 1/n} = 0.069(mg / g)(L / mg)^1 \times (4.05 mg / L)^1 = 0.280 mgMC / gGAC$$

where K and 1/n are the Freundlich parameters for MC and the URV-MOD1 GAC. The concentration of PCE in the solid is 250 mg/g (from the field data).

The carbon wastage rate at Q_{air} = 10 cfm,

$$\dot{m}_c\, C_s = Q_{air} C_{air} = \frac{10\, ft^3}{\min} \times \frac{7.5\, gal}{ft^3} \times \frac{3.78 L}{gal} \times \frac{1 mol}{24.465 L} \times \frac{1}{10^4} = 11.6x10^{-4}\, mol / \min$$

$$\text{so, } \dot{m}_c = \frac{\frac{11.6x10^{-4}\,mol}{\min} \times \frac{165.83x10^{3}\,mgPCE}{mol}}{250 mgPCE / gGAC} = 0.769\,gGAC/\min$$

$$\dot{m}_c = 0.769\,gGAC/\min = 439\,lbsGAC/6months = 878\,lbs/yr$$

At a gas flowrate of 10 cfm, the carbon wastage rate for PCE-loaded GAC is nearly 900lbs/yr and for MC is

$$\dot{m}_c = \frac{\frac{11.6x10^{-4}\,mol}{\min} \times \frac{85x10^{3}\,mgMC}{mol}}{0.280 mgMC / gGAC} = 356\,gGAC/\min$$

$$\dot{m}_c = 356\,gGAC/\min = 202981\,lbsGAC/6months = 405{,}961\,lbs/yr$$

The carbon wastage rate at Q_{air} = 100 cfm,

$$\dot{m}_{c,PCE} = 7.69\,gGAC/\min = 4385\,lbsGAC/6months = 8770\,lbs/yr$$

$$\dot{m}_{c,MC} = 3518\,gGAC/\min = 2{,}005{,}979\,lbsGAC/6months = 4{,}011{,}958\,lbs/yr$$

Up to this point, all calculations are common to both option 1 and 2 (See the following table).

Properties and GAC wastage rate for Methylene chloride and PCE

Compound	Form.	Initial Conc. (ppm)	H (atm/M)	C_s (mg/g) = $KC_{eq}^{1/n}$	GAC wastage rate (lbs /yr)	
					Q_{air} =10 cfm	Q_{air} =100 cfm
Methylene Chloride (MC)	CH_2Cl_2	100	2.1	0.280	405,961	4,011,958
Perchloroethylene (PCE)	C_2Cl_4			250	878	8770

Note: MC Henry's law constant calculated with the parameters A = 6.65, B=3.82x10^3 and T = 25°C. The PCE concentration in the solid is measured from field data.

For option 2, it is necessary to perform additional calculations to find out the cost of regeneration via Fenton's reaction.

Annual Cost for H_2O_2 - Option 2

SVE+TCE (aqueous phase) and MC(aqueous phase) loaded GAC-Field data

Target Comp.	$C_{s,i}$ (mg/g)	%Target degraded	GAC (g)	mass degraded (g)	H_2O_2 added (L)	Regeneration period (hrs) 7L reservoir
PCE	270	50	78 (0.17lbs)	10.5	1.5	48
MC	79	86	100 (0.22lbs)	6.8	0.30	2

Note: For PCE, H_2O_2 additions (50%) to 7-L reservoir: 150 mLs at time 0, 1,2,4,6,23,25,27,29,48 hrs. Annual hydrogen peroxide cost is for 2 regenerations/yr (assumes 50% regeneration for PCE). For MC, H_2O_2 additions (50%) to 7-L reservoir: 150 mLs at time 0, 1,2,3,4,5,6 hrs. Analysis uses (2)-150 mL H_2O_2 additions, as they are sufficient to degrade 86% of MC in 2 hrs.
Source: Field data (see section Field-scale regeneration trials).

The H_2O_2 Cost is \$0.34/lb (\$0.90/L)- US. Peroxide

$$\frac{\$0.34}{lb}\times\frac{2.2lbs}{1kg}\times\frac{1.2kg}{L}=\$0.90/L$$

In the field experiments, 1.5 L H_2O_2 were added to a 7-L reservoir to regenerate 78 g GAC-loaded with PCE (50% in 48 hrs). For MC, 0.3 L H_2O_2 were added to regenerate 100 g GAC (86% in 2 hrs).

$$78gGAC\times\frac{1kg}{1000g}\times\frac{2.2lbs}{1kg}=0.17lbsGAC \text{ for PCE}$$

$$100gGAC\times\frac{1kg}{1000g}\times\frac{2.2lbs}{1kg}=0.22lbsGAC \text{ for MC}$$

If 1000 lbs of GAC will be regenerated at a time, the H_2O_2 utilization (lbs) per pound of carbon for PCE-loaded GAC is

$$1.5LH_2O_2 \times \left(\frac{1000lbs}{0.17lbs}\right) = 8824LH_2O_2 \times \frac{1.2kgH_2O_2}{LH_2O_2} \times \frac{2.2lbsH_2O_2}{kgH_2O_2} = 23{,}295lbsH_2O_2$$

23,295 lbs H_2O_2 to regenerate 1000 lbs GAC

$$\frac{23{,}295lbsH_2O_2}{1000lbsGAC} = \frac{23.3lbsH_2O_2 / lbsGAC}{0.5} = \frac{46.6lbsH_2O_2}{lbsGAC}$$ for PCE-loaded GAC

and for MC,

$$0.30LH_2O_2 \times \left(\frac{1000lbs}{0.22lbs}\right) = 1364LH_2O_2 \times \frac{1.2kgH_2O_2}{LH_2O_2} \times \frac{2.2lbsH_2O_2}{kgH_2O_2} = 3600lbsH_2O_2$$

3600 lbs H_2O_2 to regenerate 1000 lbs GAC,

$$\frac{3600lbsH_2O_2}{1000lbsGAC} = \frac{3.6lbsH_2O_2 / lbsGAC}{0.85} = \frac{4.2lbsH_2O_2}{lbsGAC}$$ for MC-loaded GAC

Given the carbon wastage rate for PCE and MC (calculated above), the annual cost of H_2O_2 can be calculated for PCE at 10 and 100 cfm respectively,

$$\frac{46.6lbsH_2O_2}{lbsGAC} \times \frac{878lbsGAC}{yr} = \frac{40{,}915lbsH_2O_2}{yr} \times \frac{\$0.345}{lbH_2O_2} = \$14{,}116/yr$$

$$\frac{46.6lbsH_2O_2}{lbsGAC} \times \frac{8770lbsGAC}{yr} = \frac{408{,}682lbsH_2O_2}{yr} \times \frac{\$0.345}{lbH_2O_2} = \$140{,}995/yr$$

The annual cost of H_2O_2 for MC at 10 and 100 cfm

$$\frac{4.2lbsH_2O_2}{lbsGAC} \times \frac{405{,}961lbsGAC}{yr} = \frac{1{,}705{,}036lbsH_2O_2}{yr} \times \frac{\$0.345}{lbH_2O_2} = \$588{,}237/yr$$

$$\frac{4.2lbsH_2O_2}{lbsGAC} \times \frac{4{,}011{,}958lbsGAC}{yr} = \frac{16{,}850{,}224lbsH_2O_2}{yr} \times \frac{\$0.345}{lbH_2O_2} = \$5{,}813{,}327/yr$$

The H_2O_2 transportation cost is $3.50/mile -US Peroxide (1067 miles from Houston, TX to Tucson, AZ)

The cost of H_2O_2 depends on the requirements (e.g., H_2O_2 strength and grade, volume delivered per year, packaging, and distance to the production plant, etc.). Within the U.S., the list price for 50% Technical Grade, delivered in full tank trucks with a 40,000 lbs capacity, and shipment from the nearest production plant, is as follows:

Product: $0.345 per lb-50% (FOB Houston, TX)

Freight: $3.50 per mile (regardless of delivery volume)

Total H_2O_2 cost summary

Comp.	Annual H_2O_2 Cost ($/yr) $2m^3$ reservoir ($0.345/lb H_2O_2)		Transportation Cost ($/yr) ($3850/trip) 40,000 lbs truck load		Total H_2O_2 Cost ($/yr)	
	Q_{air} =10 cfm	Q_{air} =100 cfm	Q_{air} =10 cfm	Q_{air} =100 cfm	Q_{air} =10 cfm	Q_{air} =100 cfm
PCE	14,116 (40,915lbs H_2O_2 /yr)	140,995 (408,682 lbs H_2O_2/yr)	3,850	38,500	17,966	179,495
MC	588,237 (1.7Mlbs H_2O_2/yr)	5,813,327 (16.8M lbs H_2O_2/yr)	163,625	1,617,000	751,862	7,430,327

GAC Costs ($/yr) –Comparison

GAC Purchase Cost = $1.60/lb based on annual usage rate (Adams and Clark, 1989)

Cost index 1989 = 355

Cost index 2000 = 395.7

GAC disposal cost ($/yr) = $0.48/lb

Plus disposal transportation cost ($/yr) = $3000/8316 lbs GAC

Plus UT tax ($/yr) = $28/1000 kg = $12.73/1000lbs

Calculation of GAC cost – Option 1

Compound	GAC Purchase Cost ($/yr) – as of 2000		GAC Disposal Cost ($/yr)		Total GAC Cost ($/yr)	
	Q_{air} =10 cfm	Q_{air} =100 cfm	Q_{air} =10 cfm	Q_{air} =100 cfm	Q_{air} =10 cfm	Q_{air} =100 cfm
MC	0.72M	7.2M	0.35M	3.4M	1.1M	11M
PCE	1,566	15,641	749	7,485	2,315	23,126

Note: Costs of GAC include purchase ($1.60/lbs) and disposal (disposal + transportation + tax).

Calculation of GAC Cost – Option 2

Compound	GAC Cost ($/yr), ($1.60/lb) – 1989 (2000)		Total H_2O_2 Cost for GAC regeneration ($/yr)		Total GAC Cost ($/yr) as of 2000	
	Q_{air} =10 cfm	Q_{air} =100 cfm	Q_{air} =10 cfm	Q_{air} =100 cfm	Q_{air} =10 cfm	Q_{air} =100 cfm
PCE	140 (156)	1,403 (1,564)	17,966	179,495	18,122	180,898
MC	38,208 (42,588)	376,471 (419,633)	0.75M	7.4M	792,588	7,819,633

Note: Option 2 assumes 5% GAC loss/regeneration event. GAC Disposal Cost is $0/yr.

Additional GAC Cost for Option 2

Compound	Option 1 GAC Cost ($/yr), ($2.60/lb)		Option 2 GAC Cost ($/yr) ($H_2O_2$ + GAC Costs)		Option 2 Additional GAC Cost ($/yr)	
	Q_{air} =10 cfm	Q_{air} =100 cfm	Q_{air} =10 cfm	Q_{air} =100 cfm	Q_{air} =10 cfm	Q_{air} =100 cfm
PCE	2,545	25,416	18,122	180,898	15,577	155,482
MC	1.1M	11.1M	792,588	7,819,633	-307,412	-3,280,367

Note: Negative numbers indicate savings by using option 2.

Labor Costs ($/yr) - Comparison

Labor costs are comparable for both systems assuming breakthrough time and regeneration occur at the same time. Since, Methylene chloride can be degraded almost completely (86%) in-place, then the capacity of the GAC is a 100% for both systems. Hence, regeneration and breakthrough times coincide for both systems. For PCE on the

other hand, the GAC capacity is only 50% after regeneration. Thus, GAC regeneration events occur twice as often as the breakthrough times. Consequently, the labor costs are double for option 2 (In-place GAC regeneration).

Labor Cost -Option 1 (Assumes 8 hr/GAC replacement event)

Compound	GAC Replacement Events/yr		Labor Cost $/yr, ($40.00/hr)	
	Q_{air} =10 cfm	Q_{air} =100 cfm	Q_{air} =10 cfm	Q_{air} =100 cfm
PCE, 100% GAC capacity	1	9	320	2880
MC, 0.28 mg/g	406	4000	129,920	1.3M

Labor Cost -Option 2 (Assumes 8 hr/GAC regeneration event)

Compound	Regeneration Events/yr		Labor Cost $/yr, ($40.00/hr)	
	Q_{air} =10 cfm	Q_{air} =100 cfm	Q_{air} =10 cfm	Q_{air} =100 cfm
PCE, 50% GAC capacity	2	18	640	5,760
MC, 0.28 mg/g	406	4000	129,920	1.3M

Additional Labor Cost – Option 2

Compound	Regeneration Events/yr		Labor Cost $/yr, ($40.00/hr)	
	Q_{air} =10 cfm	Q_{air} =100 cfm	Q_{air} =10 cfm	Q_{air} =100 cfm
PCE, 50% GAC capacity	1	9	320	2,880

Pump selection and Process Energy Cost Calculations

Assuming that 1000 lbs of GAC will be regenerated at a time,

$\rho_{GAC} = 0.5$ g/cm^3

Then, Volume/regeneration is 0.9 m^3 ≈ 1 m^3

Storage tank estimation is 2 m^3

Detention time estimation is 10 min

Q = 0.1 m^3/min = 100 L/min = 26.5 gpm

Assuming a GAC column diameter of 1 m, the pump pressure head is:

$V_{GAC\ bed} = 0.9\ m^3$

$A_{GAC\ bed} = \Pi r^2 = \Pi(0.5m)^2 = 0.79\ m^2$

$h_{GAC\ bed} = V/A = 0.9\ m^3 / 0.79\ m^2 = 1.15\ m$

$d_{GAC\ bed} = 1\ m$ (h:d = 2.5:1)

Then, $h_{column} = 2.5\ m$

$h_{column} = 2.5\ m\ (8.2\ ft) = 3.55\ psi$ (1 foot head = 0.433527502 psi)

Based on the pump requirements of flowrate (26.5 gpm) and pressure head (3.55 psi),

Air-Powered Double Diaphragm Pump (Positive Displacement Pump)
High-Flow Double Diaphragm Pump with Air Filter Regulator

Max GPM	Max psi	Wetted parts	Price, $
44	120	PP/Teflon PTFE	935

Source: ColeParmer Catalog n(p.1562).

Pump Power requirements,

$P_{theoretical} = Q_l \rho_l g h$ where

$Q_l = 30$ gpm ($1.89x10^{-3}$ gps),

$\rho_l = 998\ kg/m^3$,

$g = 9.8\ m/s^2$ and

h(m) = height + 50% due to head loss = 2.5 m x 1.5 = 3.75 m

$$P_{theoretical} = Q_l \rho_l g h = \left(\frac{1.89x10^{-3} m^3}{\min}\right) \times \left(\frac{998kg}{m^3}\right) \times \left(\frac{9.8m}{s^2}\right) \times 3.75m = 69.3W$$

$P_{actual} = P_{theoretical} / n$

where n is the efficiency of the pump (assume n=0.7)

$P_{actual} = 69.3W / 0.7 = 99W$

$$PowerCost(\$) = P_{actual}(kW) \times \frac{\$0.11}{kw - hr} \times \frac{hrs}{year}$$

The pump usage (hr/year) depends on the regeneration events (see table below). For example, for the PCE-loaded GAC regeneration at 10 cfm air flowrate:

$$\frac{regenerationtime(hrs)}{year} = \left(48hrs \times \frac{1000lbs}{0.17lbs}\right) \times (2regenerations/\ yr) = 564{,}706hrs/\ yr$$

$$PowerCost(\$) = 99x10^{-3}\,kW \times \frac{\$0.11}{kw-hr} \times \frac{564{,}706hrs}{year} = \$6{,}149/\ yr$$

Additional Process Energy Cost – Option 2
Pump requirements for regeneration events

Target	Time/regen (hrs) – 0.2 lbs GAC	Time/regen (hrs)- 1000 lbs GAC	Regen/year		Hrs/year		Power Cost, $	
			10 cfm	100 cfm	10 cfm	100 cfm	10 cfm	100 cfm
PCE 0.17lbsGAC	48	282,353	2	18	564,706	$5x10^6$	6,150	55,347
MC 0.22lbsGAC	2	9,091	406	4000	$3.7x10^6$	$36.4x10^6$	40,194	396,004

Note: the regeneration time (hrs) and the number of regenerations required per year were calculated above.

Additional Capital Cost – Option 2

2 Chemical storage tanks[1], 2 m^3	1,014
2 Positive Displacement Pumps[2]	2,000
Incremental Labor (10% capital cost)	3,077
Additional Capital Cost, $	6,091

Note: Capital Cost for 2 GAC columns is $30,772.
Source: [1]www.watertanks.com, [2]Eng. estimate.

Summary annual costs – Option 2 (In-place GAC Regeneration)

PCE, Q_{air} = 10 cfm, Cs=250 mg/g	
Energy	6,150
Labor	320
GAC	18,122
O & M, $/yr	24,592
Present Worth (n=20 years, i=8%), $	241,448
Total Cost, $	247,539
Annual Cost, $	25,212

Note: Additional capital is $6,091.

PCE, Q_{air} = 100 cfm, Cs=250 mg/g	
Energy	55,347
Labor	2,880
GAC	180,898
O & M, $/yr	239,125
Present Worth (n=20 years, i=8%), $	2,347,764
Total Cost, $	2,353,855
Annual Cost, $	239,745

Note: Additional capital is $6,091.

MC, Q_{air} = 10 cfm, Cs=0.28mg/g	
Energy	40,194
Labor	0
GAC	792,588
O & M, $/yr	832,782
Present Worth (n=20 years, i=8%), $	8,176,376
Total Cost, $	8,182,467
Annual Cost, $	833,402

Note: Additional capital is $6,091.

MC, Q_{air} = 100 cfm, Cs=0.28mg/g	
Energy	396,004
Labor	0
GAC	7,819,633
O & M, $/yr	8,215,637
Present Worth (n=20 years, i=8%), $	80,662,335
Total Cost, $	80,668,426
Annual Cost, $	8,216,257

Note: Additional capital is $6,091.

Summary annual costs – Option 1 (GAC replacement/disposal)

Compound	Total GAC Cost ($/yr) as of 2000	
	Q_{air} =10 cfm	Q_{air} =100 cfm
PCE	2,315	23,126
MC	1.1M	11M

Note: Costs of GAC include purchase ($1.60/lbs) and disposal costs.

The annual cost analysis provided the following summary results (incremental cost only, or costs unique to the alternative).

SVE Flow	Target Contaminants	
	PCE	MC
10 cfm	#1: $2,315 #2: $25,212	#1: $1.1M #2: $0.83M
100 cfm	#1: $23,126 #2: $239,745	#1: $11 M #2: $8.2M

Note: Option 1: GAC cost = $1.60/lb + disposal costs (disposal, transportation and UT tax). Option 2: GAC cost = $1.60/lb (no disposal), H_2O_2 cost (purchase and transportation), additional process energy, labor, and capital (dosing pumps, chemical storage tanks).

Fraction of H_2O_2 of the total cost for option 2

The following table shows the estimate of the fraction of total cost that arises from H_2O_2 in our scenario #2:

Compound	Total H_2O_2 Cost for GAC regeneration ($/yr)		Total Annual Cost ($/yr)		Fraction of H_2O_2 Cost for GAC regeneration ($/yr)	
	Q_{air} =10 cfm	Q_{air} =100 cfm	Q_{air} =10 cfm	Q_{air} =100 cfm	Q_{air} =10 cfm	Q_{air} =100 cfm
PCE	17,966	179,495	25,212	239,745	71%	75%
MC	0.75M	7.4M	0.83M	8.2M	90%	90%

Note: All values were obtained from previous tables.

Some references for GAC costs:
Clark, Robert M. 1989. Granular Activated Carbon: Design, Operation and Cost. Lewis Publishers.

Activated carbon costs range from $1.40 to $2 per pound ($2,800 to $4,000 per ton) (U.S. EPA 1998). U.S. EPA. 1998. "Technical Bulletin: Zeolite, A Versatile Air Pollutant Adsorber." EPA 456/F-98-004. Office of Air Quality, Clean Air Technology Center. July.

Carbon cost is $2 to $3 per pound. http://www.frtr.gov/matrix2/section4/4-61.html
DOE, 1994. *Technology Catalogue*, First Edition. February.

EPA, 1991. *Granular Activated Carbon Treatment, Engineering Bulletin*, EPA, OERR, Washington, DC, EPA/540/2-91/024.

LaGrega, M., Buckingham, P., Evans, J. and Environmental Resources Management (2001). *Hazardous Waste Management*, 2nd edition. San Francisco: McGraw Hill.

REFERENCES

Arnold, S., Hickey, W. and Harris, R. (1995). Degradation of Atrazine by Fenton's Reagent: Condition Optimization and Product Quantification. *Environ. Sci. Technol*., *29*, 2083-2089.

ATSDR Information Center (last updated on June 22, 2001), ATSDR-Public Health Statements: Tetrachloroethylene, URL http://atsdr1.atsdr.cdc.gov/ToxProfiles/phs8822.html.

Bansal, R., Donnet J. and Stoeckli F. (1988). *Active Carbon,* New York: Marcel Dekker, Inc.

Bercik, L., (2003). "Heterogeneous Degradation of Chlorinated Solvents via Fenton's Reaction". Masters Thesis, University of Arizona.

Betterton, E., Hollan, N., Arnold, R., Gogosha, S., Mckim, K. and Liu, Z. (2000). Acetone-Photosensitized Reduction of Carbon Tetrachloride by 2-Propanol in Aqueous Solution. *Environ. Sci. Technol.*, *34*, 1229-1233.

Boltz, D. and Holwell, J. (1978). *Colorimetric Determination of Nonmetals,* 2nd. Edition, Chemical Analysis 8; John Wiley and Sons, Inc.: New York, p 543.

Burbano, A., Dionysiou, D., Suidan, M., and Richardson, T. (2005). Oxidation kinetics and effect of pH on the degradation of MTBE with Fenton reagent. *Water Research*, 39, 107-118.

Buxton, G., Greenstock, C., Helman, P. and Ross, A. (1988). Critical Review of Rate Constants for Reactions of Hydrated Electrons, Hydrogen Atoms and Hydroxyl Radicals (OH/O). *J. Phys. Chem. Ref. Data*, Vol. 17, No. 2, p 513.

Carmen, P., (1956). *Flow of Gases through Porous Media*, Academic Press, New York, N.Y.

Casero, I., Sicilia, D., Rubio, S. and Pérez-Bendito, D. (1997). Chemical Degradation of Aromatic Amines by Fenton's Reagent. *Wat. Res.* Vol. 31, No. 8, pp. 1985-1995.

Chen R. and Pignatello JJ. (1997). Role of quinone intermediate as electron shuttles in Fenton and Photoassisted Fenton Oxidations of Aromatic compounds. *Environ. Sci. Technol*., 31, 2399-2406.

Chen, G., Hoagb, G., Chedda, P., Nadim, F., Woody, B. and Dobbs, G.(2001). The mechanism and applicability of in situ oxidation of trichloroethylene with Fenton's reagent. *J. Haz. Mat*. 171-186.

Clark, J. (2002) (December, 2005). The Electrochemical Series, URL http://www.chemguide.co.uk/physical/redoxeqia/ecs.html#top.

Cotton, F., Wilkinson, G., Murillo, C. and Bochmann, M. (1999). *Advanced Inorganic Chemistry*, 6th Edition, John Wiley & Sons, Inc. New York.

Crank, J. (1975). *The Mathematics of Diffusion*, Oxford University Press, New York, N.Y.

Crittenden, J., Hutzler, N., Geyer, D., Oravitz, J. and Friedman, G. (March 1986). Transport of Organic Compounds with Saturated Groundwater Flow: Model Development and Parameter Sensitivity, *J. Water Resources Research*, Vol. 22, No. 3, pp. 271-284.

Crittenden, J.C., Hand, D.W., Arora, H. and Lykins, B.W. (1987). Design Considerations for GAC Treatment of Organic Chemicals. *J. AWWA*. *79*, No. 1, 74-82.

Crittenden, J.C., Cortright, R.D., Rick, B., Tang, S.R. and Perram, D. (1988). Using GAC to Remove VOCs From Air Stripper Off-Gas. *J. AWWA*. 80, 73-84.

De Laat, J. and Gallard, H. (1999). Catalytic Decomposition of Hydrogen Peroxide by Fe(III) in Homogeneous Aqueous Solution: Mechanism and Kinetic Modeling, *Environ. Sci. Technol.* 33, 2726-2732.

De Laat, J. and Giang Le, T. (2005). Kinetics and Modeling of the Fe(III)/H_2O_2 System in the Presence of Sulfate in Acidic Aqueous Solutions. *Environ. Sci. Technol*., *39*, 1811-1818.

De Laat, J. and Giang Le, T (2006). Effects of Chloride Ions on the Iron(III)-Catalyzed Decomposition of Hydrogen Peroxide and on the Efficiency of the Fenton-Like Oxidation Process. *Appl. Cat. B: Environ.*, 66, 137-146.

De Las Casas, C.L., Bishop, K.G., Bercik, L.M., Johnson, M., Potzler, M., Ela, W.P., Saez, A.E., Huling, S.G., and Arnold, R.G. (2006). "In- Place Regeneration of Granular Activated Carbon Using Fenton's Reagents", Chapter in book Innovative Approaches to the Remediation of Subsurface Contaminated Hazardous Waste Sites: Bridging Flask and Field Scales, American Chemical Society Symposium Series 940. p. 43- 65.

DiGiano, F.A. and Weber, W. J., Jr. (1973). Sorption Kinetics in Infinite-Batch Experiments. *JWPCF*, 45, 713-725.

Duesterberg, C., Cooper, W. and Waite, T. (2005). Fenton-Mediated Oxidation in the Presence and Absence of Oxygen. *Environ. Sci. Technol*., *39,* 5052-5058.

Eaton, A., Clesceri, L. and Greenberg, A. (1995). *Standard Methods for the Examination of Water and Wastewater*; 19th Edition, Publication Office, American Public Health Association: Maryland.

Environmental and Remediation Equipment (August, 2005). URL http://www.soiltherm.com/GAC_Comparison/gac_comparison.html.

EPA (2000). *Granular Activated Carbon Adsorption and Regeneration,*EPA-832-F-00-017.

Fredrickson, J. Kostandarithes H., Li S., Plymale A. and Daly, M. (2000). Reduction of Fe(III), Cr(VI), U(VI), and Tc(VII) by Deinococcus radiodurans R1., *Appl. Environ. Microbiol.*, 66, 2006-2011.

Furuya, E., Ikeda, H., and Takeuchi, Y. (1987). *Fundamentals of Adsorption*. Engineering Foundation, New York, N.Y., 235.

Furuya, E., Chang, H., Miura, Y., Yokomura, H., Tajima, S., Yamashita, S. and Noll, K. (1996). Intraparticle Mass Transport Mechanism in Activated Carbon Adsorption of Phenols. *J. Environ. Eng*., Vol. 122, No. 10, pp. 909-916.

Gallard, H., De Laat, J. and Legube, B. (1999). Spectrophotometric Study of the Formation of Iron (III)-Hydroperoxy Complexes in Homogeneous Aqueous Solutions, *Wat. Res.*, Vol. 33, No. 13, pp. 2929-2936.

Gallard, H. and De Laat, J. (2000). Kinetic Modeling of Fe(III)/H_2O_2 Oxidation Reactions in Dilute Aqueous Solution Using Atrazine as a Model Organic Compound, *Wat. Res*. Vol. 34, No. 12, pp. 3107-3116.

Glaze, W., Kenneke, J. and Ferry, J. (1993). Chlorinated byproducts from the titanium oxide-mediated photodegradation of trichloroethylene and tetrachloroethylene in water. *Environ. Sci. Technol*., *27*, 177-184.

Grigor'ev, A., Makarov, I. and Pikaev, A. (1987). Formation of Cl_2^- in the Bulk Solution During the Radiolysis of Concentrated Aqueous Solutions of Chlorides. *High Energy Chem*., *21*, 99-102.

Haag, W.R. and Yao, C.C.D. (1992). Rate constants for reaction of hydroxyl radicals with several drinking water contaminants. *Environ. Sci. Technol*., *26*,1005-1013.

Heslop, R. and Robinson, P. (1967). *Inorganic Chemistry. A Guide to Advanced Study*, 3rd Ed., Elsevier Publishing Company, Amsterdam.

Holleman, A. and Wiberg, E. (2001). *Inorganic Chemistry*, Academic Press, San Diego.

Huling, S., Arnold, R., Sierka, R. and Miller, M. (1998). Measurement of Hydroxyl Radical Activity in a Soil Slurry Using the Spin Trap -(4-Pyridyl-1-oxide)- *N-tert*-butylnitrone. *Environ. Sci. Technol*., *32*, 3436-3441.

Huling, S., Arnold, R., Jones, P. and Sierka, R. (2000a). Predicting Fenton-driven degradation using contaminant analog. *J. Environ. Eng*., pp. 348-353.

Huling, S., Arnold, R., Sierka, R., Jones, P. and Fine, D. (2000b). Contaminant Adsorption and Oxidation via Fenton Reaction, *J. Environ. Eng.*, pp. 595-600.

Huling, S. (2001). Environmental Protection Agency (EPA), Ada, Oklahoma.

Huling, S., Jones, P., Ela, W. and Arnold, R. (2005a). Fenton-driven chemical regeneration of MTBE-spent GAC, *Wat. Res*. Vol. 39, No. 10, pp. 2145-2153.

Huling, S.G., Jones, P.K., Ela, W.P., Arnold, R.G. (2005b). Repeated reductive and oxidative treatments on granular activated carbon. *J. Environ*. *Eng*. Vol. 131, No. 2, pp. 287–297.

Huling, S. and Jones, P. (In Review 2005c). Iron Optimization in Fenton-Driven Chemical Regeneration of Granular Activated Carbon. *Environ. Sci. Technol*.

King, RB. (2006). *Encyclopedia of Inorganic Chemistry,* 2nd. Edition, Copper: Inorganic and Coordination Chemistry; John Wiley and Sons, Inc.(online service); Chichester; Hoboken: New Jersey, p. 14.

Kommineni, S., Ela, W., Arnold, R., Huling, S., Hester, B. and Betterton, E. (2003). NDMA Treatment by Sequential GAC Adsorption and Fenton-Driven Destruction. *Environ. Eng. Sci.* Vol. 20, pp. 361-373.

LaGrega, M., Buckingham, P., Evans, J. and Environmental Resources Management (2001). *Hazardous Waste Management*, 2nd edition. San Francisco: McGraw Hill.

Letterman, RD. (1999). *Water Quality and Treatment. A Handbook of Community Water Supplies.* Fifth Edition, Adsorption of Organic Compounds; McGraw-Hill, Inc.:New York, p. 13.3.

Liu, Z., Betterton, E. and Arnold, R. (2000). Electrolytic Reduction of Low Molecular Weight Chlorinated Aliphatic Compounds: Structural and Thermodynamic Effects on Process Kinetics. *Environ. Sci. Technol*., *34*, 804-811.

Logan, B. (1999). *Environmental Transport Processes;* John Wiley & Sons, Inc.: New York, p 654.

Lowry, G. and Reinhard, M. (2000). Pd-Catalyzed TCE Dechlorination in Groundwater: Solute Effects, Biological Control, and Oxidative Catalyst Regeneration. *Environ. Sci. Technol.,* Vol. 34, pp. 3217-3223.

Ma Z., Whitley, R. D. and Wang, N.-H. L. (May 1996). Pore and surface diffusion in multicomponent adsorption and liquid chromatography systems. *AIChE J*., Vol. 42, No. 5, pp.1244-1262.

Masarwa, M., Cohen, H., Meyerstein, D., Hickman, DL., Bakac, A. and Espenson, JH (1988). Reactions of Low-Valent Transition-Metal Complexes with Hydrogen Peroxide, Are They "Fenton-like" or Not? 1. The Case of Cu^{+}_{aq} and Cr^{2+}_{aq}., *J. Am. Chem. Soc.110*, 2493-4297.

Miller Brooks Environmental Inc. (2004). *Final Draft Park-Euclid Remedial Investigation Report,* Arizona Department of Environmental Quality, Project No. 365-0011-01, Phoenix, AZ, 707.

National Research Council (1994). Alternatives for Ground Water Cleanup, National Academy Press, Washington, DC, 315.

Noll, K. E, Gounaris, V. and Hou, W. (1992). *Adsorption Technology for Air and Water Pollution Control*, Lewis Publishers, Michigan.

Petlicki, J. and van de Ven, T. (1998). The equilibrium between the oxidation of hydrogen peroxide by oxygen and the dismutation of peroxyl or superoxide radicals in aqueous solutions in contact with oxygen. *Faraday Trans.*, *94*, 2763-2767.

Peyton, G., Bell, O., Girin, E. and Lefaivre, M. (1995). Reductive Destruction of Water Contaminants during Treatment with Hydroxyl Radical Processes. *Environ. Sci. Technol*., *29*, 1710-1712.

Poppe, MA. (2001). Analysis of MTBE and MTBE By-product Degradation Using Fenton-Type Reactions in a Homogeneous System. Master Thesis, Unpublished. University of Arizona.

Prousek, J. (1995). Fenton Reaction after a Century, *Chem. Lisy,* Vol. 89, pp. 11-21.

Radiation Chemistry Data Center of the Notre Dame Radiation Laboratory (May, 2003). URL http://www.rcdc.nd.edu/.

Radiation Chemistry Data Center of the Notre Dame Radiation Laboratory (August, 2005). URL http://www.rcdc.nd.edu/.

Roberts, J. and Sawyer, D. (1981). Facile Degradation by Superoxide Ion of CarbonTetrachloride, Chloroform, Methylene Chloride, and p,p'-DDT in Aprotic Media. *J. Am. Chem. Soc*., *103*, 712-714.

Ruthven, D. M. (1984). *Principles of Adsorption and Adsorption Processes*, Wiley-Interscience, New York.

Sedlak, D. and Andren, A. (1991). Aqueous-phase oxidation of polychlorinated biphenyls by hydroxyl radicals. *Environ. Sci. Technol*., *25*, 1419-1427.

Smith, B., Teel, A. and Watts, J. (2004). Identification of the Reactive Oxygen Species Responsible for Carbon Tetrachloride Degradation in Modified Fenton's Systems. *Environ. Sci. Technol*., *38*, 5465-5469.

Snoeyink, V. L. (1990). Adsorption of Organic Compounds, *Water Quality and Treatment*, 4th Ed., McGraw Hill, New York, N.Y., 781-875.

Stark, J. and Rabani, J. (1999). Photocatalytic Dechlorination of Aqueous Carbon Tetrachloride Solutions in TiO2 Layer Systems: A Chain Reaction Mechanism. *J. Phys. Chem. B*, *103*, 8524-8531.

Stumm, W. and Morgan, J. (1981). *Aquatic Chemistry: An Introduction Emphasizing Chemical Equilibria in Natural Waters*. 2nd ed. Wiley-Inerscience, New York.

Sudo, Y., Misic, M., and Suzuki, M. (1978). Concentration dependence of effective surface diffusion coefficient in aqueous phase adsorption on activated carbon. *Chem. Engrg. Sci*., 33, 1287-1290.

Suzuki, M., and Fujii, T. (1982). Concentration dependence of surface diffusion coefficient of propionic acid in activated carbon particles. *AIChE J*., 28, 380-385.

Suzuki, M., (1990). *Adsorption Engineering*, Elsevier, Amsterdam.

Swarzenbach, R., Gschwend, P. and Imboden, D. (1993). *Environmental Organic Chemistry*, John Wiley & Sons, Inc., New York, p 681.

Teel, A., Warberg, C., Atkinson, D. and Watts, R. (2001). Comparison of Mineral and Soluble Iron Fenton's Catalysts for the Treatment of Trichloroethylene. *Wat. Res*., Vol. 35, No. 4, pp. 977-984.

Teel, A. and Watts, R. (2002). Degradation of carbon tetrachloride by modified Fenton's reagent. *J. Haz. Mat*. 179-189.

Toledo, L.C., Silva, A.C.B., Augusti, R., Lago, R.M., 2003. Application of Fenton reagent to regenerate activated carbon saturated with organochloro compounds. *Chemosphere*, Vol. 50, pp. 1049–1054.

Teruya, E. (2000). Potential Regeneration of Activated Carbon Using Fenton's Reaction after MTBE Adsorption, Master Thesis, Unpublished, University of Arizona.

U.S.EPA. Wastewater Technology Fact Sheet (2000). Granular Activated Carbon Absorption and Regeneration, U.S.EPA-Office of Water: Washington, DC, EPA 832-F-00-017.

Walling, C. (1975). Fenton's Reagent Revisited, *Acc. Chem. Res*., Vol. 8.

Walling C. and Kato S. (1971). The Oxidation of Alcohols, by Fenton's Reagent, The Effect of Copper Ion., *J. Am. Chem. Soc*., 93, pp. 4275-4280.

Watts, R., Bottenberg, B., Hess, T., Jensen, M. and Teel, A. (1999). Role of Reductants in the Enhanced Desorption and Transformation of Chloroaliphatic Compounds by Modified Fenton's Reactions. *Environ. Sci. Technol*., *33*, 3432-3437.

Weber, W. J. Jr., (1972). *Physiochemical Processes*, John Wiley, New York, N.Y., 199-259.

Yan, D. (2006). Factors That Affect Fenton-dependent Degradation of Chlorinated Volatile Organic Compounds and MTBE. M.S. Thesis, Department of Chemical and Environmental Engineering, The University of Arizona.

Yang, T. Ralph (1987). *Gas Separation by Adsorption Processes*, Massachusetts, Butterworth Publishers.

Yoshida, M., Lee, B-D. and Hosomi, M. (2000). Decomposition of aqueous tetrachloroethylene by Fenton oxidation treatment, *Wat. Sci. Technol*. Vol. 42, pp. 203-208.

Zoh, K. and Stenstrom, M. (2002). Fenton oxidation of hexahydro-1,3,5-trinitro-1,3,5-triazine (RDX) and octahydro-1,3,5,7-tetranitro-1,3,5,7-tetrazocoine (HMX), *Wat. Res*., Vol. 36, pp. 1331-1341.